CHALMERS

Wind integration into hydro dominant Power System

Master of Science Thesis

Jóhannes Porleiksson

Department of Energy & Environment
Division Electrical Power Engineering
Chalmers University of Technology
Göteborg, Sweden 2013

Wind integration into hydro dominant power systems

JÓHANNES ÞORLEIKSSON

Department of Energy and Environment
Division of Electric Power Engineering
CHALMERS UNIVERSITY OF TECHNOLOGY
Göteborg, Sweden 2013

Wind integration into hydro dominant power systems
JÓHANNES ÞORLEIKSSON

Department of Energy and Environment
Division of Electric Power Engineering
Chalmers University of Technology
SE–412 96 Göteborg
Sweden
Telephone +46 (0)31–772 1000

Cover: Picture of the first two Wind Turbines installed in Iceland taken by ©Þórdís Reynisdóttir.

Chalmers Bibliotek, Reproservice
Göteborg, Sweden 2013

Wind integration into hydro dominant power systems
JÓHANNES ÞORLEIKSSON
Department of Energy and Environment
Division of Electric Power Engineering
Chalmers University of Technology

Abstract

The Icelandic Power System is a hydro dominant system where approximately 75 % of the electricity generation is hydro based. However due to transmission constraints the potential of this mean of generation can not be fully utilised. In the eastern part of Iceland, in the last years, the consumption of electricity has been increasing. This has led to increased stress on the transient stability limits of the system. In recent years there has been a growing interest of wind power in Iceland. However the impact of wind generation on the system stability has not been assessed. In this thesis the impact of wind generation, in the east area, on the transient stability of the system is analysed and supplementary control based on wide area measurements is implemented to aid the transient stability of the system. This Master thesis was done in cooperation with Landsvirkjun, Landsnet and ABB Switzerland.

Index Terms: Power System Stability, Transient Stability, Oscillatory Stability, Aggregation of Power Systems, Wind Turbine, Wide Area Control.

Acknowledgements

The author would like to thank dr. Magni Þór Pálsson, at Landsnet, for his contribution to the initial idea behind the Master Thesis and contribution during the thesis. A special thanks to my supervisor dr. Mats Larsson, for creating the opportunity for me to carry out this work at ABB Corporate Research in Switzerland. Furthermore I would like to thank my supervisor at Chalmers Peiyuan Chen for the discussions during my thesis and ideas. Special thanks to my examiner Massimo Bongiorno for the input to this thesis. Furthermore the author would like to thank dr. Herwig Renner for discussions concerning power system aggregation during his stay at ABB. I would like to thank the employees at Landsnets who supported me during this thesis work with information and data. Special thanks to all my the interns and master thesis students at the C department for all the nice memories. I would like to thank Landsvirkjun, Landsnet and ABB Switzerland for support during this thesis. Finally I would like to thank my girlfriend, Elín, for her flexibility and patience during my studies and the work of this thesis.

The Author, Reykjavík , 2013

Contents

1

Introduction

1.1 Background

During the last decades generation companies in Iceland have had easy access to renewable energy sources such as geothermal and hydro. The government has however realized that the potential energy resources, which have not yet been harnessed, are limited. This has led to increased interests in other means of renewable generation such as wave and wind power. However, since wind power is not continuously available, hydroelectric plants can "store" energy in the reservoirs and release water to generate electricity when needed. Given that the Icelandic Power System is hydro dominated this is an intriguing solution. The Icelandic Power System is an islanded power system. Therefore, load demand has to be met with generation within the system which can be a challange when intermittency of wind power is considered. Preliminary studies in Iceland have shown that this combination could be economically feasible. However, it has yet to be fully explored since there have been more economical means available to generate electricity in the last decades. [1]

1.2 Problem Description

In the eastern part of Iceland there has been a growth in the consumption of electricity from various customers such as heavy industry and fishing industries. The fishing industries located in the eastern part of Iceland have shifted from generating their own electricity with oil to use electricity supplied via the transmission grid. However any new consumption of electricity in that area is a challenge since geographically available generation is located elsewhere. This requires more power exchange between the western and eastern part of Iceland. However, this will stress the transient stability limits of the transmission system even more, which are already stressed beyond their limits during certain periods of the year [2].

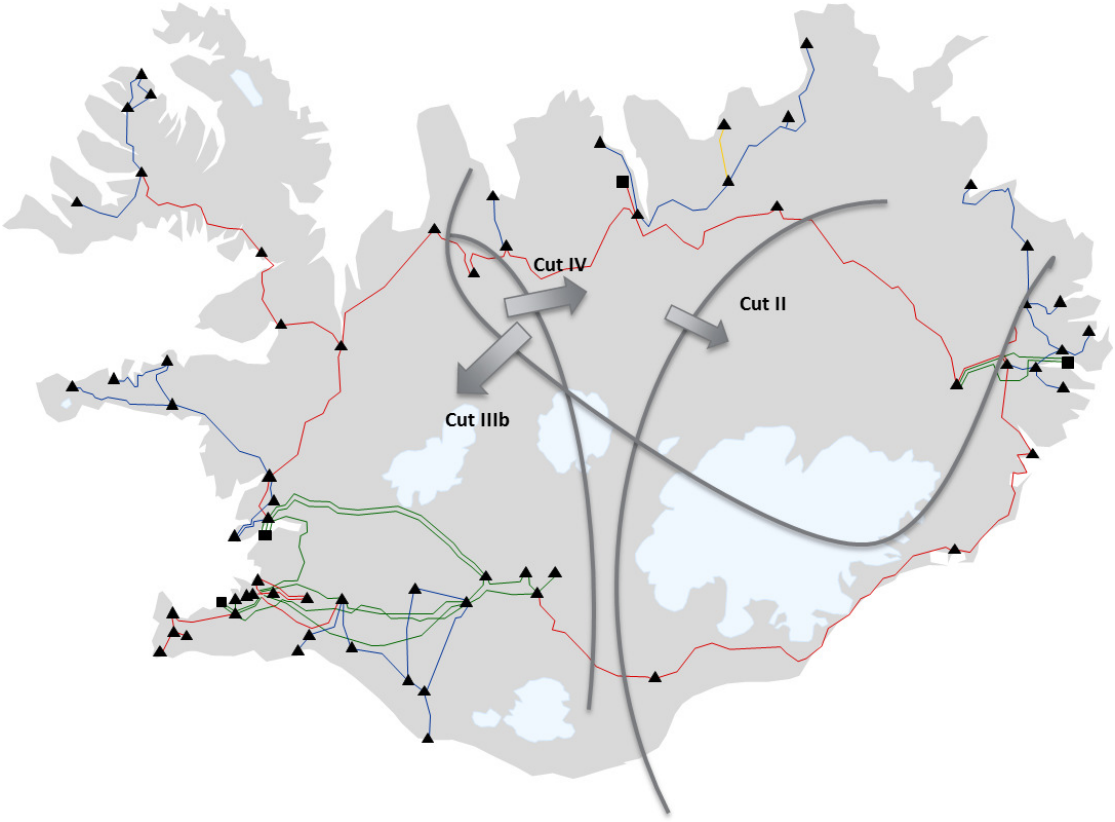

Figure 1.1: Transient stability limits in the Icelandic Transmission System

In fig. 1.1 the Icelandic Transmission System can be seen along with the transient stability limits. The most important transient stability limits are the following [2].

- Cut II: Through Kröflulina 2 and Sigöldulina 4, 100 MW.
- Cut IIIb: Through Blöndulína 1 and Fljótsdalslinu 2, 130 MW.
- Cut IV: Through Blöndulina 2 and Sigöldulina 4, 100 MW.

The transient stability limit cut IV is the most limiting one. That cut limits the transfer capacity from west to east dramatically and is one of the main constraints in the Icelandic Transmission System. The strongest part of the tranmission system is located in the southwest area, which is a 220 kV network. Approximately two thirds of the generation is located in that area. In the east part there exists another strong 220 kV tranmission system which connects a hydro power plant and an aluminum smelter.

In order to increase the power exchange between the areas, new transmission lines from the west to the east have been planned [2] at 220 kV voltage level. An alternative solution would be to install wind generation in the east area, and meet increased of power demand with the synergy of wind and hydro generation. This may be advantageous since studies have shown that the efficiency for onshore wind farms in Iceland is in general high.

This is an interesting option since in that area a hydro power plant with a large reservoir is located and can be used to facilitate the intermittent generation of wind power. However this is only an option if the transient stability limits of the system are not negatively affected by the wind integration.

1.3 Objective

The main objective of this thesis is to investigate the impact of wind integration on the transient stability limits of the power system. This is of great interest, as the possibility of the integration of wind generation depends on the impact it will have on the power system and wether it will lead to decreased or increased utilization of the transmission network.

1.4 Scope

The main scope of this master thesis is to investigate transient stability limits when transporting electrical power between the eastern and western part of Iceland. In particular, the goal of this work will be to study the impact of the added wind generation, that will have on those limits and to propose improvements in case of undesired system behavior due to wind integration. Furthermore, a wide-area control strategy is designed in order to improve the transient stability of the system.

2

Overview of Rotor Angle Stability and Power System Modelling

In this chapter, the theory used in this thesis will be laid out. First Rotor Angle stability is explained and how different parameters in the transmission system affect the frequency of angle oscillations, stability limits and damping of these oscillations. Secondly aggregation techniques of power systems will be described. Finally a model of a full converter wind turbine for transient stability studies is displayed.

2.1 Introduction to Power System Stability

The proposed definition of power system stability according to [3] is: "*Power system stability is the ability of an electric power system, for a given initial operating condition, to regain a state of operating equilibrium after being subjected to a physical disturbance, with most system variables bounded so that practically the entire system remains intact*". Subcategories of power system stability can be seen in fig. 2.1.

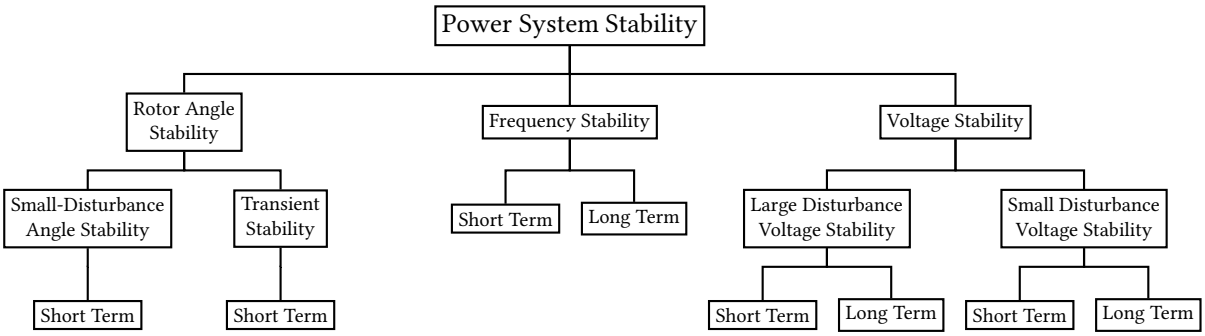

Figure 2.1: Classification of Power System Stability [3]

In the case of the Icelandic power system the main stability problems are related to Rotor Angle Stability [2]. The thesis will mainly work with angular stability. Angular stability is subcategorised into Small-Disturbance Angle Stability and Transient Stability. Small disturbances can be for example when changing the operation point of generators or small voltage dips. Transient stability may be an issue in case of larger disturbances such as disconnection of a line or faults where the voltage drops close to zero at the fault location.

2.2 Rotor Angle Stability

Consider a two generator system connected by a lossless line, as seen in fig. 2.2.

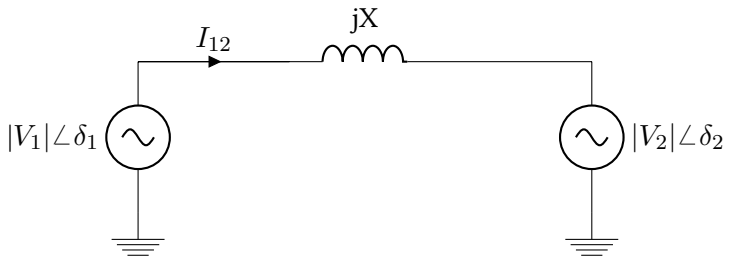

Figure 2.2: Two generator network with reactance between them

The current I_{12} can be calculated as follows

$$I_{12} = \frac{|V_1|\angle\delta_1 - |V_2|\angle\delta_2}{jX}. \tag{2.1}$$

The active power transferred between the generators is then

$$\begin{aligned} P_{12} &= \Re(V_1 I_{12}^*) && (2.2)\\ &= \frac{|V_1||V_2|}{X}\sin(\delta_1 - \delta_2) && (2.3)\\ &= \frac{|V_1||V_2|}{X}\sin(\delta_{12}). && (2.4) \end{aligned}$$

The power transferred between the two generators depends mainly on the angle difference between them as seen in (2.4). If (2.4) is plotted as a function of angle it can be seen how the maximum power transfer between the two generators occurs when the angle difference is 90° as seen in fig. 2.3.

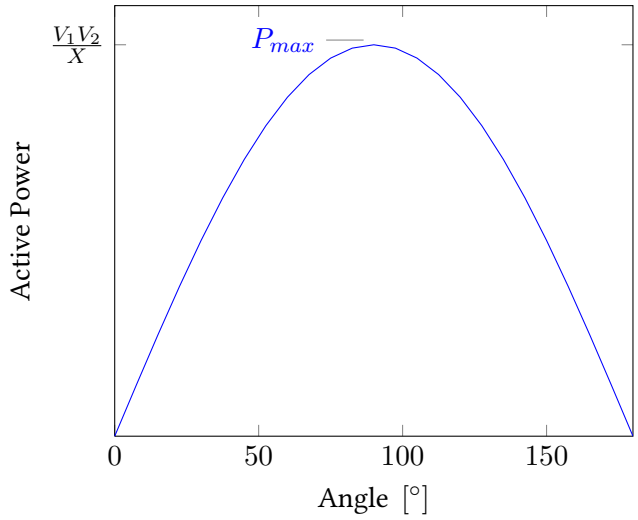

Figure 2.3: Power flow between two buses based on the angle difference between them

Although the maximum power interchange is at $90°$ a power system is rarely operated at that point. The main reason is that the power system in general is dynamic and quantities are constantly varying. Small disturbances could then lead to a system collapse, since small angle variations would reduce the air gap power of the generators and the initial angle could not be restored. As stated before Rotor Angle Stability is classified into two categories depending on the significance of the fault, Small-Disturbance Angular Stability or Transient stability.

2.3 Small-Disturbance Angular Stability

Let us consider a single machine connected to an infinite bus (SMIB). An infinite bus has a phase and a angle which do not vary, so only the phase and angle of the single machine varies. The dynamic behaviour of a SMIB can be described by the swing equation [4]

$$M\frac{d^2\delta}{dt^2} = P_m - P_e - D\frac{d\delta}{dt} \tag{2.5}$$

$$\frac{d\delta}{dt} = \Delta\omega \tag{2.6}$$

where $M = 2H$ is the angular momentum at synchronous speed, P_m is the mechanical power applied to the rotor of the generator, P_e is the electrical power produced in the air gap(i.e. between rotor and stator) as described by (2.4), D is the damping coefficient at synchronous speed and δ is the angle of the rotor relative to the voltage stiff system. In order to analyse the small signal stability, (2.5) is linearized around an angle $\delta = \delta_0$

$$M\frac{d^2\Delta\delta}{dt^2} + D\frac{d\Delta\delta}{dt} + K_e \cdot \Delta\delta = 0 \tag{2.7}$$

where

$$M = 2H \tag{2.8}$$

$$K_e = \frac{|V_1| \cdot |V_2|}{X} \cdot \cos(\delta_0). \tag{2.9}$$

The initial conditions are

$$\Delta\delta(t=0) = \delta_0 \tag{2.10}$$

$$\Delta\omega(t=0) = 0 \tag{2.11}$$

The characteristic equation of (2.5) then becomes

$$\lambda^2 + \frac{D}{M}\lambda + \frac{K_e}{M} = 0 \tag{2.12}$$

which has the solutions

$$\lambda_{1,2} = -\frac{D}{2M} \pm \sqrt{\left(\frac{D}{2M}\right)^2 - \frac{K_e}{M}} \tag{2.13}$$

Then there are three cases possible

1. The roots are real and not equal
2. The roots are real and equal
3. The roots form a complex conjugate pair.

In general for a Power Systems the roots form a complex conjugate pair where solutions are

$$\lambda_{1,2} = -\frac{D}{2M} \pm j\sqrt{\frac{K_e}{M} - \left(\frac{D}{2M}\right)^2}. \tag{2.14}$$

Denoting

$$\alpha = -\frac{D}{2M} \tag{2.15}$$

$$\Omega = \sqrt{\frac{K_e}{M} - \left(\frac{D}{2M}\right)^2} \tag{2.16}$$

where α is the damping coefficient and Ω is the frequency of oscillations (in rad/s). The coefficient

$$\xi = \frac{-\alpha}{\sqrt{\alpha^2 + \Omega^2}} \tag{2.17}$$

is referred to as the damping ratio. The damping ratio is used to determine weather responding modes are sufficiently damped or not. If (2.7) is compared with a standard-second order differential equation

$$\frac{d^2\Delta\delta_m}{dt^2} + 2\xi\Omega_{nat}\frac{d\Delta\delta}{dt} + \Omega_{nat}^2\Delta\delta = 0 \tag{2.18}$$

with the roots

$$\lambda_{1,2} = -\xi\Omega_{nat} \pm j\Omega \tag{2.19}$$

$$\tag{2.20}$$

where Ω_{nat} is the undamped natural frequency of rotor swings for small oscillations, ξ is the damping ratio and $\Omega = \Omega_{nat}\sqrt{1-\xi^2}$ is the frequency of oscillations. Comparing (2.18) with (2.7) gives

$$\Omega_{nat} = \sqrt{\frac{K_e}{M}} \tag{2.21}$$

$$\xi = \frac{D/2}{\sqrt{K_e M}}. \tag{2.22}$$

The frequency and damping of small signal oscillations is directly connected to the damping, inertia and the electrical properties of the network. Lets consider a case where the response of a single generator connected to an infinite bus is simulated. It has been shown, that the variation in K_e will cause changes to frequency and damping.

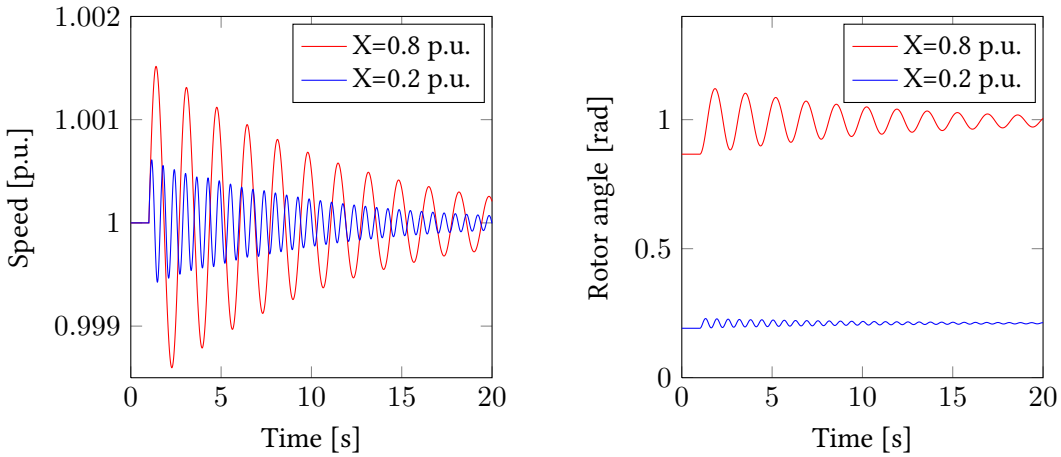

Figure 2.4: Small signal response of a SMIB with different reactance

From fig. 2.4 it is easy to see the change in frequency of the oscillations due to change reactance. Lower reactance leads to increase in the oscillation frequency. With higher reactance the initial speed variation are higher than when comparing the low reactance case. The reduction in amplitude of oscillations is greater for the case where we have higher reactance. For the small signal case the damping of the oscillations is greater for the case with high reactance.

2.4 Transient stability

Let's consider the case where a single machine is connected to an infinite bus (SMIB), as seen in fig. 2.5, is subjected to a fault.

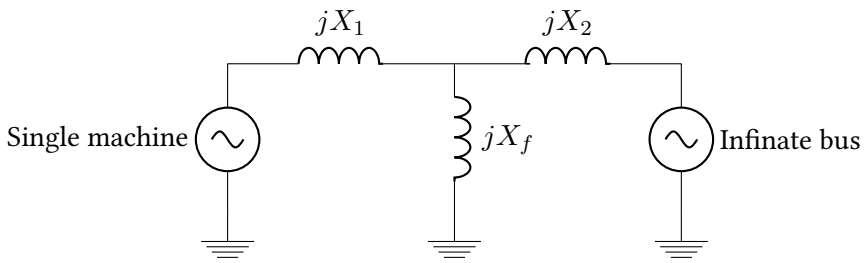

Figure 2.5: Single machine connected to a infinite bus

Where X_f is the fault reactance and the sum of X_1 and X_2 is the total reactance that connects the single machine to the infinite bus. The magnitude of X_1 and X_2 will depend on the fault location. The dynamics of this single generator can be described by (2.5) and to simplify the discussion, damping will be neglected so the equation becomes

$$M\frac{d^2\delta}{dt^2} = P_m - P_e. \tag{2.23}$$

Furthermore, it will be assumed that changes in rotor speed, following a fault, are too small to activate the governor control system, therefore P_m can be considered to be constant. P_e is then equal to the power transferred between the single machine and the infinite bus as described by (2.4) and P_m is assumed to be $P_m = P_{emax}/2$.
Pre fault, the impedance between the machine and the infinite bus is

$$X_{Pre} = X_1 + X_2. \tag{2.24}$$

Using star-delta transformation the reactance between the generators during the fault is

$$X_{During} = X_1 + X_2 + \frac{X_1 X_2}{X_f} \tag{2.25}$$

For a three phase fault where $X_f = 0$, the power transfer from the single machine is blocked completely as seen by (2.25) as $X_{During} = \inf$ and the fault current is purely inductive. After the fault it is assumed that $X_{post} = X_{pre}$. In fig. 2.6 the active power transfer as a function of angle can be seen. Where P_m is represented by a straight line at half the maximum power transfer, and the parabola is the electric power curve before and after the fault. During the fault the power transferred is zero.

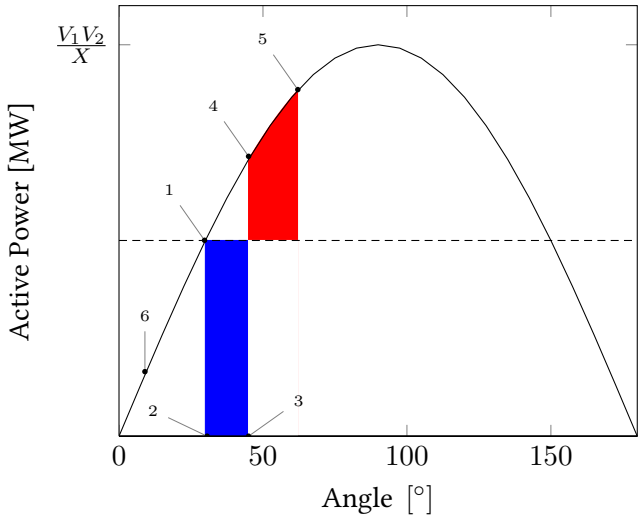

Figure 2.6: Change in angle due to fault

If (2.23) is reviewed, then at point 1 (pre fault), P_m is equal to P_e. Due to the fault, the power transferred from the single machine is blocked and $P_e = 0$ represented by point 2. As the machine is subjected to this fault the generator starts to accelerate at $\frac{P_m}{M}$ and the angle of the machine relative to the infinite bus increases. At point 3 the fault is cleared and the pre fault power curve is restored.

Now the generator is operating at point 4 and the angle difference is greater than before the fault so $P_e > P_m$. During the fault the machine has accumulated kinetic energy and the speed of the generator is above the synchronous speed. The angle of the machine therefore continues to increase until the kinetic energy gained during the period of acceleration is expended. So the generator will deaccelerate from point 4 to point 5 where it reaches synchronous speed.

Since P_e > P_m at point 5, the machine will deaccelerate and the angle starts to decrease until operating point 1 is reached. At point 1 we have equilibrium between the mechanical and the electrical power. However the speed of the machine is below the synchronous speed so the machine will accelerates until it reaches synchronous speed at point 6. At point 6 P_e<P_m so the generator starts to accelerate again. If no damping is apparent the generator will oscillate from point 5 to point 6.

The acceleration of the generator during a fault depends on how much P_e drops during the fault

$$\epsilon = \frac{d\delta^2}{dt^2} = \frac{P_m - P_e}{M} = constant. \tag{2.26}$$

The highest rate of acceleration will occur when the voltage drops to zero and $P_e = 0$ as seen in 2.26.

How much the angle increases during a disturbance depends on the time that the fault is sustained. If 2.5 is integrated twice and the damping neglected the angle increase with respect

to time can be obtained

$$\delta(t) = \frac{P_m - P_e}{M} t^2 + \delta_{init}. \tag{2.27}$$

Obviously if synchronism of the generator is to be kept, the generator may not accelerate infinitely. During the fault the generator accumulates kinetic energy A_1 as seen in fig. 2.7.

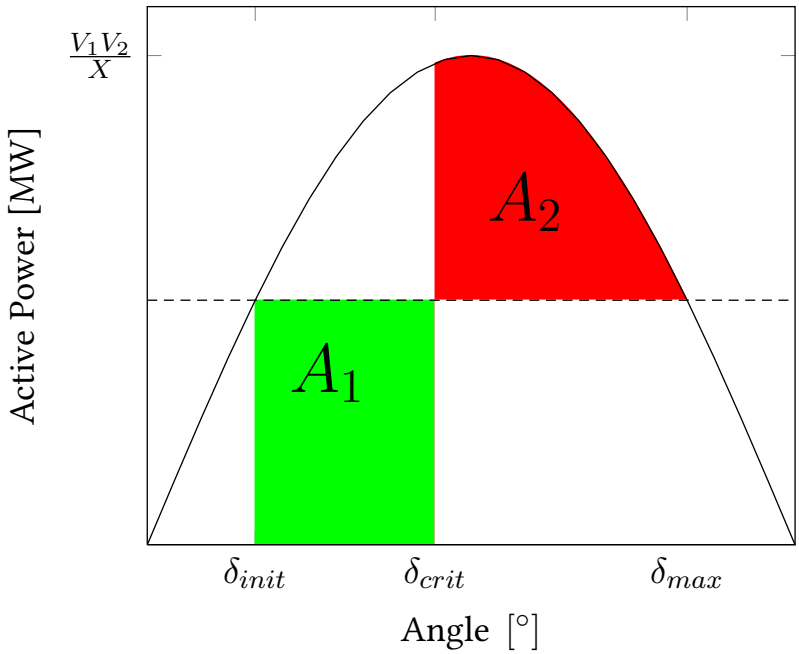

Figure 2.7: Acceleration and deacceleration areas during fault

During it's deacceleration period the area available to release that energy is denoted at A_2 in fig. 2.7. For the case when $A_1 < A_2$ the system is transiently stable and when $A_1 > A_2$ the system is transiently unstable. When $A_1 = A_2$, the angle, which the fault is cleared at, is called the critical clearing angle and denoted as δ_{crit}. Integration of the areas when $A_1 = A_2$ gives

$$\int_{\delta_{init}}^{\delta_{crit}} (P_m - P_{e_{fault}}) d\delta = \int_{\delta_{crit}}^{\delta_{max}} (P_{e_{afterfault}} - P_m) d\delta \tag{2.28}$$

Where P_m is the mechanical power , $P_{e_{fault}}$ is the characteristic power curve during the fault and $P_{e_{afterfault}}$ is the characteristic power curve after the fault. If the assumption is made

that the power transfer drops to zero during the fault $P_{efault} = 0$. Then the equation becomes

$$\int_{\delta_{init}}^{\delta_{crit}} (P_m) d\delta = \int_{\delta_{crit}}^{\delta_{max}} (\frac{EV}{X_{eq}} \sin(\delta) - P_m) d\delta \tag{2.29}$$

$$\Rightarrow P_m(\delta_{crit} - \delta_{init}) = \frac{\cos(\delta_{crit}) - \cos(\delta_{max})}{X_{eq}} - P_m(\delta_{max} - \delta_{crit}) \tag{2.30}$$

$$\Rightarrow \cos(\delta_{crit}) - \cos(\delta_{max}) = \frac{P_m X_{eq}}{EV}(\delta_{max} - \delta_{init}) \tag{2.31}$$

Since δ_{max} and δ_{init} are known, δ_{crit} can be obtained from (2.31). The critical clearing time can then be calculated from (2.27)

$$t_{crit} = \sqrt{\frac{2M}{P_m - P_e}(\delta_{crit} - \delta_1)} \tag{2.32}$$

2.5 Damping power

If there is no way to dissipate the energy, the generator accumulates during the fault the generator will oscillate infinitely. The main source of damping in the synchronous generator is provided by the damper or amortisseur windings, which are located on the rotor of the generator. In transient state the air-gap flux which rotates at synchronous speed will penetrate these windings and create a torque in opposite direction, according to Lenz's Law of induction. Derivation of this damping power is complicated but if following assumptions are made the damping power can be derived using the induction motor equivalent [4] connected to an infinite bus:

- armature and field winding resistance neglected
- damping only produced by damper windings
- leakage reactance neglected
- damping independent of excitation.

Then the circuit for the synchronous generator can be simplified as seen in fig. 2.8 when the leakage reactance is neglected.

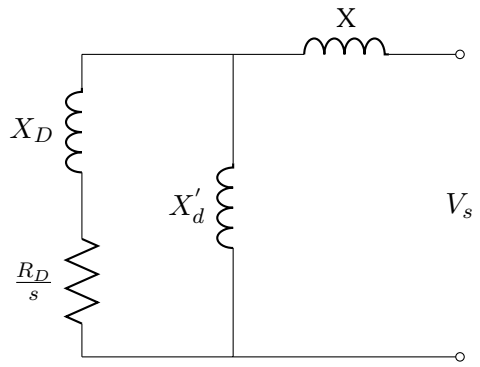

Figure 2.8: Equivalent of circuit for synchronous generator connected to inifinate bus

An expression for the damping power can be derived from the circuit assuming that the rotor is not salient

$$P_D = V_s^2 \frac{X'_d - X''_d}{(X + X'_d)^2} \frac{X'_d}{X''_d} \frac{T''_d \Delta\omega}{1 + (T''_d \Delta\omega)^2}. \tag{2.33}$$

In the case of saliency the equation can be written as follows

$$P_D = V_s^2 \left[\frac{X'_d - X''_d}{(X + X'_d)^2} \frac{X'_d}{X''_d} \frac{T''_d \Delta\omega}{1 + (T''_d \Delta\omega)^2} \sin^2(\delta) + \frac{X'_q - X''_q}{(X + X'_q)^2} \frac{X'_q}{X''_q} \frac{T''_q \Delta\omega}{1 + (T''_q \Delta\omega)^2} \cos^2(\delta) \right] \tag{2.34}$$

For small changes in $\Delta\omega$ 2.34 becomes

$$P_D = V_s^2 \left[\frac{X'_d - X''_d}{(X + X'_d)^2} \frac{X'_d}{X''_d} T''_d \sin^2(\delta) + \frac{X'_q - X''_q}{(X + X'_q)^2} \frac{X'_q}{X''_q} T''_q \cos^2(\delta) \right] \omega \tag{2.35}$$

or on a more common form

$$P_d = \Big[D_d \sin^2(\delta) + D_q \cos^2(\delta) \Big] = D(\delta) \Delta\omega. \tag{2.36}$$

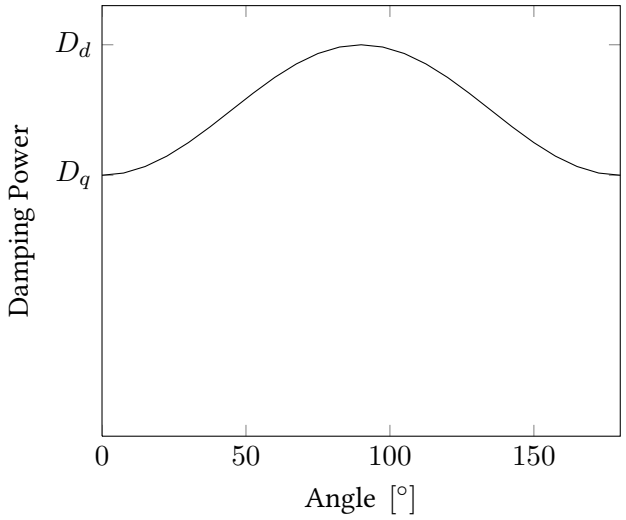

Figure 2.9: Damping Power as a function of rotor angle for small oscillations

2.6 Synchronous generator and control systems

The synchronous machine model in this analysis is modelled using the following differential equations [4]

$$T_{d0}^{''}\dot{E}_{q}^{''} = E_{q}^{'} - E_{q}^{''} + I_d(X_{d}^{'} - X_{d}^{''}) \tag{2.37}$$

$$T_{q0}^{''}\dot{E}_{d}^{''} = E_{d}^{'} - E_{d}^{''} - I_q(X_{q}^{'} - X_{q}^{''}) \tag{2.38}$$

$$T_{d0}^{'}\dot{E}_{q}^{'} = E_f - E_{q}^{'} + I_d(X_d - X_{d}^{'}) \tag{2.39}$$

$$T_{q0}^{'}\dot{E}_{d}^{'} = -E_{d}^{'} - I_q(X_q - X_{q}^{'}) \tag{2.40}$$

where $^{''}$ denotes subtransient, $^{'}$ transient and no prime denotes steady state.

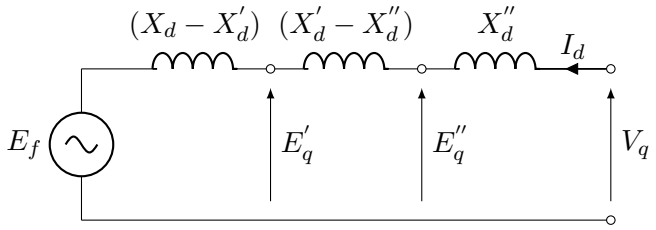

(a) d-axis

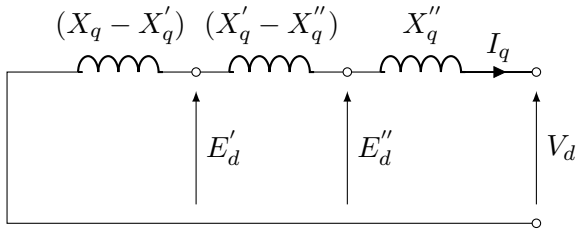

(b) q-axis

Figure 2.10: Generator equivalent circuit with resistance neglected[4]

The differential equations allow different models of the synchronous machine to be developed. In this thesis a model of the synchronous machine, the rotor body eddy-currents in the q-axis are neglected, so $X_q^{'} = X_q$ and $E^{'} = 0$ which eliminates (2.40). To complete the generator model the generator is represented by the subtransient emfs $E_d^{''}$ and $E_q^{''}$ behind the reactances $X_d^{''}$ and $X_q^{''}$ describe the armature voltages [4]

$$V_d = E_d^{''} - RI_d - X_q^{''} I_q \tag{2.41}$$

$$V_q = E_q^{''} + X_q^{''} I_d - RI_q. \tag{2.42}$$

Since the differential equations include the influence of the damper windings mechanical damping due to windings and friction which is usually small can be neglected in the swing equation. The air gap power of the generator is [4]

$$P_e = (E_d^{''} I_d + E_q^{''} I_q) + (X_q^{''} - X_q^{''}) I_d I_q. \tag{2.43}$$

In previous sections the classical synchronous generator model was used

$$M\frac{d^2\delta}{dt^2} = P_m - P_e - D\frac{d\delta}{dt} \tag{2.44}$$

$$\frac{d\delta}{dt} = \Delta\omega \tag{2.45}$$

to describe in a simple way the impact that faults have on the synchronous generator. However this model makes the assumption that d-axis armature current I_d does not change and the excitation voltage is constant during the transient state. This only holds for faults electrically far away from the generator and is therefore not suitable as a representation for the synchronous generator in this thesis.

2.6.1 Excitation system

The excitation system controls the voltage fed to the excitation winding. The excitation control is necessary for the security of interconnected system and a fast responding automatic voltage control is used to increase the synchronising torque of power systems following a fault. However, fast regulators can cause electromechanical modes to become unstable. In addition the exciter itself maybe unstable when the generator is running in islanded operation. To improve the stability of the exciters an external control loop is added which can have input such as the variation in rotor speed as an input which will compensate for this undesirable behaviour of the excitation system. In fig. 2.11 the IEEE ST1A model can be seen. The voltage is controlled by a PI regulator which compares V_{ref} with the measured voltage.

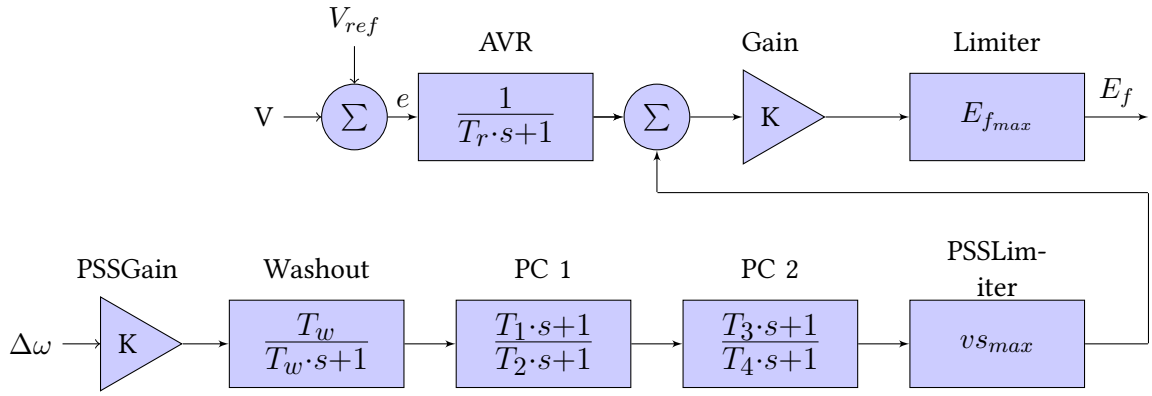

Figure 2.11: Block diagram of IEEE (1992/2005) ST1A Model [5]

This AVR system is very simple and many other control systems exist in the literature. The stabiliser is the lower control loop which uses variations in speed as input signal. The idea of the stabiliser is to produce an electrical torque at the generator proportional to the speed. This input signal goes through a washout filter which is a high pass filter so the steady state value is eliminated. The signal is then passed through phase compensators which are adjusted to the input signal to give the correct phase.

2.6.2 Governor control

The governors main purpose is to control the speed of the generator. When a generator is connected to an interconnected system, the governor plays an important role in controlling the synchronous speed of the network. When generators are interconnected they rotate at a synchronous speed. Initially the power demand is distributed between the generators by the economic dispatch. The additional power needed for each generator is controlled by the governor system of the generator. If a load is lost from a system the generator will accelerate to a new steady state determined by all the steady state gain of the governor. In fig. 2.12 a block diagram of a governor for a generator can be seen.

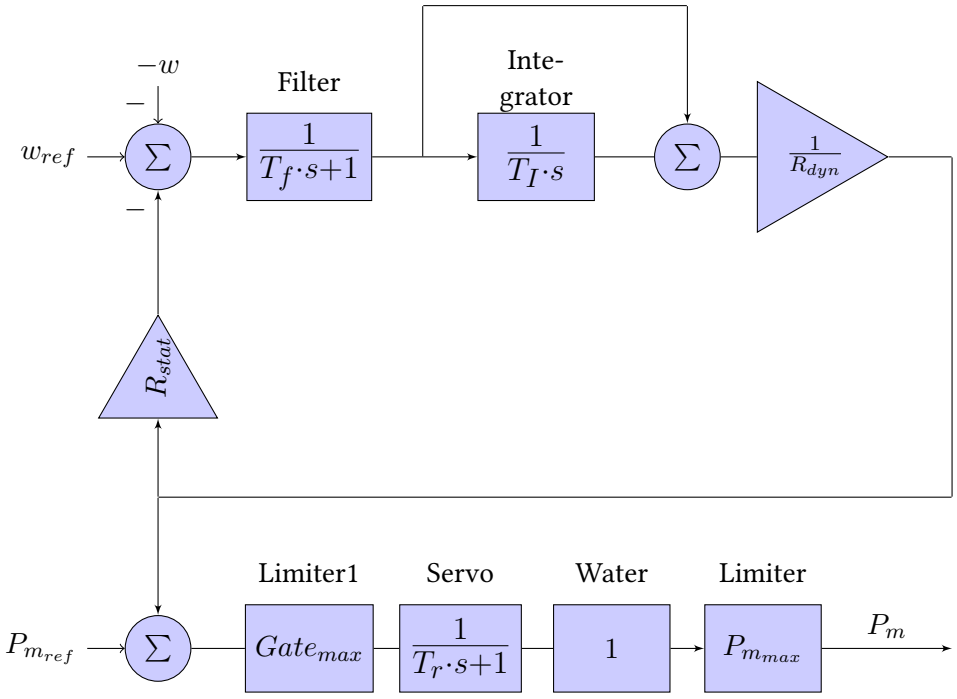

Figure 2.12: Block diagram of a Governor [6]

The lower cascaded blocks control the prime mover which in this diagram is water. A reference value is fed to the system and then the gate of the hydro power plant are changed so it give the desirable output. The upper control loop is the droop control which tells the generator how it should change it's generation following a change in the system frequency.

2.7 Load models

One of the simplest load models used in power system analysis is the ZIP model which describes a load model which has the following features:

- a constant power demand (P)
- a constant current demand (I)
- a constant impedance (Z)

The constant power model is voltage invariant and presents a stiff load, the constant current model represents a model which varies linearly with the voltage and a constant impedance

model varies with the voltage squared. The ZIP model can be represented by the polynomal

$$P = P_0 \left[a_1 \left(\frac{V}{V_0} \right)^2 + a_2 \left(\frac{V}{V_0} \right) + a_3 \right] \tag{2.46}$$

$$Q = Q_0 \left[a_4 \left(\frac{V}{V_0} \right)^2 + a_5 \left(\frac{V}{V_0} \right) + a_6 \right] \tag{2.47}$$

where V_0, P_0 and Q_0 are normally taken as the values at the initial operating conditions and the parameters a_1 to a_2 represent how much share of the active and the reactive belong to each part of the ZIP model.

2.8 Power System Aggregation

When simulating large power systems it is often desirable to derive an equivalent network to study a certain phenomena. Aggregation of power systems is a complex task and to derive a dynamic equivalent is even more difficult as there is always some information lost during the aggregation. However, aggregation can give a rough approximation of the system that is to be studied. Many methods deal with for example aggregation of transmission lines and nodes, however in this thesis the power system aggregation will mainly be used to derive a dynamic equivalent in order to study the interarea modes. The method used is based on [7] and is not meant to be a comprehensive approach to aggregation, but rather to give one a simple way to derive an equivalent. First the lets describe the notation used

1. k: vector of indices of all generators contained in a given external network
2. f: index of the border bus at which one wants to compute the REI equivalent
3. c: vector of indices of load buses contained in the external network
4. r; vector obtained from the union of k and f

First contribution for each generator to the network is calculated from the so called REI (radial, equivalent, independent) equivalent from bus i to bus f.

$$\bar{s}_{if} = \bar{v}_j \frac{(\bar{v}_j - \bar{v}_f)^*}{\bar{z}_{if}} \quad \forall j \epsilon k \tag{2.48}$$

where j is the index for a generator in the generator group k which should be aggregated. Then the distribution power factor can be calculated

$$PF_{jf} = \frac{\Re \hat{s}_{jf}}{p_j} \tag{2.49}$$

where p_j is the total active generator power of each generator. The equivalent base power is then

$$S_{N_g} = \sum_j PF_{if} S_{N_j}. \tag{2.50}$$

Where S_{N_j} is the base power of each machine. The equivalent inertia is then

$$H_g = \frac{1}{S_{N_g}} \sum_j PF_{if} H_j S_{N_j} \tag{2.51}$$

In a similar way the resistances, reactance and time constants can be obtained using an inertia weighted mean. For example the sub transient reactance is then

$$x''_{dg} = \frac{1}{Hg} \sum_j H_j x''_{dj} \tag{2.52}$$

2.9 Wind Turbine modelling

The wind generation literature focuses mainly on four different types of wind generation topologies [8].

- Type 1: Fixed speed wind turbines
- Type 2: Limited variable speed
- Type 3: Variable speed with partial scale frequency converter
- Type 4: Variable speed with full-scale frequency converter

Type 1 refers to asynchronous squirrel cage induction generator (SCIG) connected to the grid via a transformer. Since the SCIG always draws reactive power this configuration uses a capacitor bank for reactive compensation. Type 2 uses wound rotor induction with a variable generator rotor resistance and capacitor bank for reactive power compensation. By utilising the variable additional rotor resistance the speed of the generator generator can be varied by $\pm 10\,\%$. Type 3 is commonly known as doubly fed induction generator (DFIG). It consist of a wound rotor induction generator and a partial scale frequency converter on the rotor circuit. The speed range comprises $60\,\%$ to $130\,\%$ of synchronous speed. The main drawbacks are the use of slip rings and protection against of grid faults. For the Type 4 configuration the wind generator is connected to the grid through a full-scale frequency converter. The frequency converter provides a reactive compensation and smoother grid connection. This topology usually uses wound rotor synchronous generator or a permanent magnet synchronous generator. Types 3-4 all have fault ride through capabilities. However the main advantage of Type 4 compared to the other toplogies is smooth grid connection and any grid code can be applied as the generator is decoupled from the grid [9]. Due to the fact of fault ride through capabilities and grid code compliance of variable speed wind generators with full converter they will be as a base for the wind turbine model used in this thesis.

2.10 Modelling of type 4 Wind Turbine

Variable speed generation with a full-scale frequency converter offers many advantage compared to other toplogies such as, energy optimal operation, soft drive train, gearless option,

controllability and improved stability. The main disadvantage of this topology is the cost of the frequency converter.

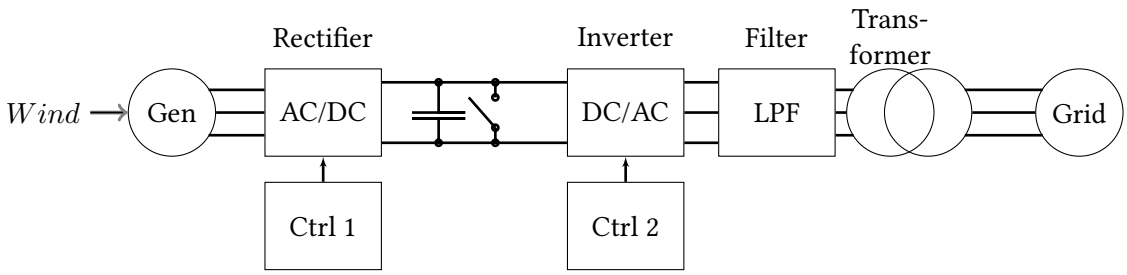

Figure 2.13: Diagram of full converter wind turbine

A diagram of the topology of a full converter wind turbine can be seen in fig. 2.13. The wind acts as a prime mover on a generator which can be either a permanent synchronous generator (PMSG) or a wound rotor synchronous generator (WRSG). The electric power generated is then rectified from AC to DC. The rectifying can be done either by a diode rectifier or a rectifier based on insulated gate polar transistors (IGBT). On the DC side there is a capacitor whose main purpose is to act as a temporary energy storage for switching of the valves in the converter and a DC chopper whose main purpose is to protect the DC circuit from overvoltages. The DC voltage is then inverted to AC using an inverter based on IGBT. The output of the inverter is then filtered to get rid of undesirable harmonics and then finally transformed up to the voltage level of the system. The conventional control strategy is that the generator side converter controls the active power P_{grid} and the stator voltage U_s. The grid side converter controls the voltage of the DC-link U_{DC} as well as the reactive power flow to the grid Q_{grid} [9]. A newer control strategy switches the control of the active power to the grid side. In this case, the generator side converter controls the dc voltage and the inverter control the P_{grid}. In principle since the generator is decoupled from the network there is only a need to model the inverter side and the grid interface for system studies [10] [11].

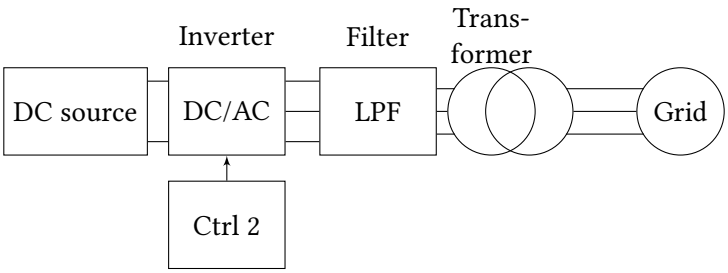

Figure 2.14: Simplified diagram of full converter wind turbine

In fig. 2.14 The simplified model of the variable speed wind turbine can be seen. The generator and rectifier have now been replaced by an ideal DC source. The Low pass filter is simply modeled as LC-circuit and the transformer as a reactance.

2.10.1 Converter Model

For the converter model a fundamental frequency model is used as described in [12]. The real and imaginary voltage vectors at the grid side of the converter can be described as

$$U_{AC,R} = K_0 M_r U_{DC} \tag{2.53}$$
$$U_{AC,I} = K_0 M_i U_{DC}. \tag{2.54}$$

Where the equations are completed by power conversion between AC and DC side

$$P_{AC} = \Re(U_{AC} I_{AC}^*) = U_{DC} I_{DC} = P_{DC}. \tag{2.55}$$

The variables in 2.54 are defined as follows

- $U_{AC,R}$: Real part of AC-voltage (RMS)
- $U_{AC,I}$: Real part of AC-voltage (RMS)
- K_0: Constant based on the modulation method ($\frac{\sqrt{2}\sqrt{3}}{\pi}$ for no modulation, $\frac{\sqrt{3}}{2\sqrt{2}}$ for sinusoidal modulation or determined by a fixed on-off ratio of the pulse if using rectangular method).
- M_r: Real part of modulation ratio
- M_i: Imaginary part of modulation ratio
- U_{DC}: DC-voltage.

The variables of 2.55 can be defined as follows

- U_{AC}: The AC-voltage phasor (RMS-value)
- I_{AC} the AC-current phasor
- U_{DC}: The DC voltage
- I_{DC}: The DC-Current
- P_{DC}: The DC-Power.

Furthermore the converter is assumed to be ideal and lossless PWM-converter.

2.10.2 Controller

The control of the converter consists of three cascaded controllers.

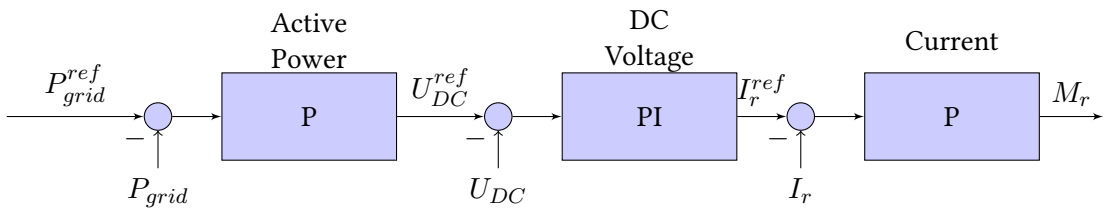

Figure 2.15: Active Power control

The layout for the active power controller can be seen in fig. 2.15. The most inner control loop is the current control. It is assumed to be really fast compared to the second stage, therefore only a P controller is used for that step denoted K_{pI} and is used to control the real part of the modulation ratio. It compares the real part of the current to the reference value from the DC voltage control. The DC voltage is slower and controls the DC source voltage with a PI controller, where the integral gain is denoted as K_{iD} and the proportional gain is K_{pD}. Finally, the active power reference is set, at the last stage of the cascaded controller. For that stage, a proportional gain used denoted as K_{pP}. It is used to give the DC voltage source a reference to what the set point should be to achieve the desired active power output at the PCC.

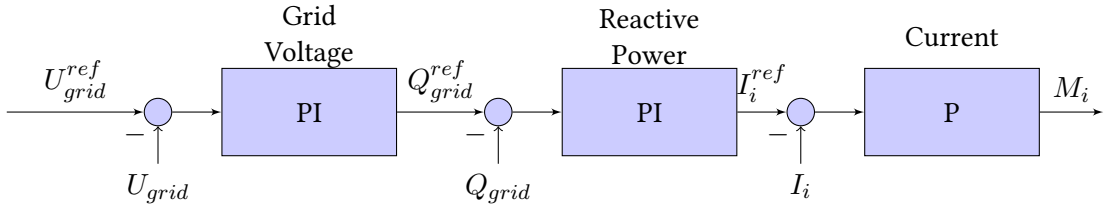

Figure 2.16: Voltage control

The block diagram for the voltage control can be seen in fig. 2.16. As for the active power controller, the most inner stage, is assumed to be a fast current controller with a gain K_{pI} which calculates the imaginary part of the modulation ratio that is desired, based on the error between the imaginary current reference and the measured value. The imaginary current reference is set by the reactive power controller which is assumed to be slower and is represented by a PI controller with a proportional gain as K_{pQ} and integral gain as K_{iQ}. The reactive power is measured at the point of PCC and compared to the reference calculated by the grid voltage controller. The grid voltage is also measured at the PCC and compared to a desired voltage and then fed to a PI controller, slower than the reactive power controller, with a proportional gain as K_{pU} and a integral gain as K_{iU}. In this thesis, when the term voltage control is used the structure displayed in 2.16 is used and when reactive power control is used it is the same structure but without the voltage controller.

2.10.3 Capability curve of the converter

In general converters have no thermal inertia meaning that they can not exceed their operating limits even for short period without risking a damage. Therefore strict limits are enforced in

order to protect the converter. In this thesis four limits are considered.

The first is the maximal current of the converter

$$U_s \cdot I_{eq}^{max} = \sqrt{P_{grid}^2 + Q_{grid}^2} \tag{2.56}$$

where U_s is the voltage at the point of common connection. The locus of maximal current in the PQ diagram is a circle at the origin, and radius $U_s \cdot I_{eq}^{max}$. Which gives a locus of the maximal current in the PQ diagram. The voltage at the terminals of the converters is also limited to the maximum voltage U_C [13] which gives the second limit

$$P_{grid} = \frac{U_s U_c}{X_{eq}} \sin(\delta) \tag{2.57}$$

$$Q_{grid} = -\frac{U_s^2}{X_{eq}} + \frac{U_s U_c}{X_{eq}} \tag{2.58}$$

After eliminating δ we get a circle which projects onto the PQ diagram with a center in $(0, -U_s^2/X_{eq})$ and a radius $(U_s U_c/X_{eq})$ as shown in fig. 2.17.

$$\left(\frac{U_s U_c}{X_{eq}}\right)^2 = P^2 + \left(Q + \frac{U_s^2}{X_{eq}}\right) \tag{2.59}$$

The third limit is is the maximum current through the conductors and is vertical in the PQ diagram at the rated DC voltage which is represented in fig. 2.17 as two vertical lines.

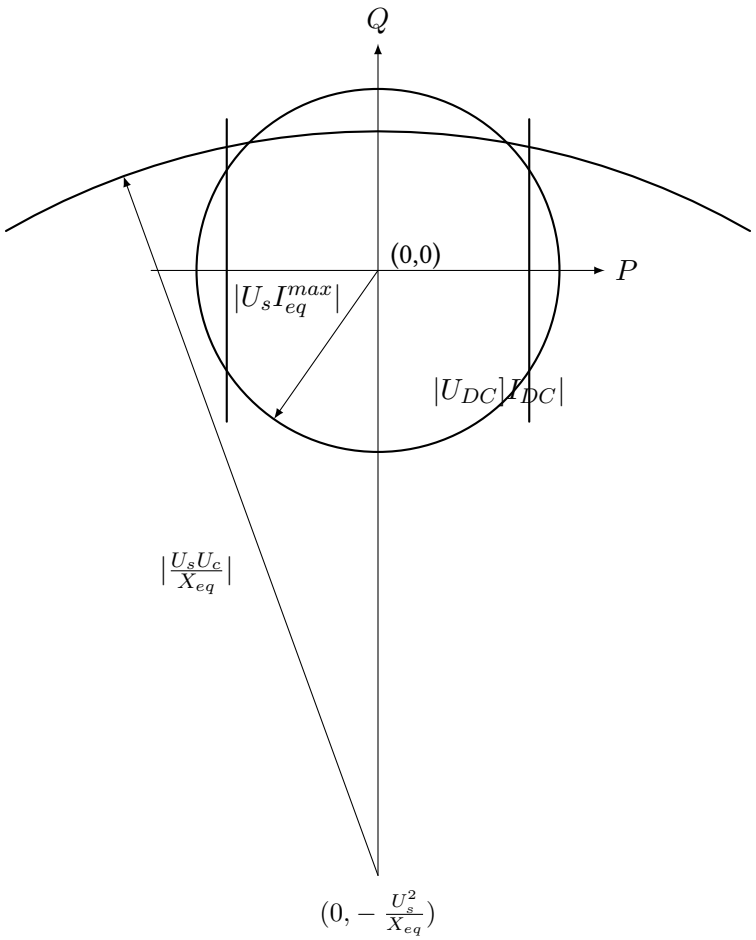

Figure 2.17: Capability curve of VSC converter

3

Transient and small disturbance stability in the Icelandic grid

In this chapter the transient stability limits and small disturbance stability in the Icelandic system will be investigated. Simulations will be done with a full system in PSS/E and the dynamic response of the system will be observed when subjected to various faults.

3.1 Introduction

In the Icelandic Power System three transient stability cuts have been defined as seen in fig. 3.1 in order to operate the system in a safe and reliable manner. Of the three stability cuts in the Icelandic power system the cut IV is the most limiting of these stability cuts [2]. The stability cut covers the flow in the transmission lines Sigöldulina 4 and Blöndulina 2.

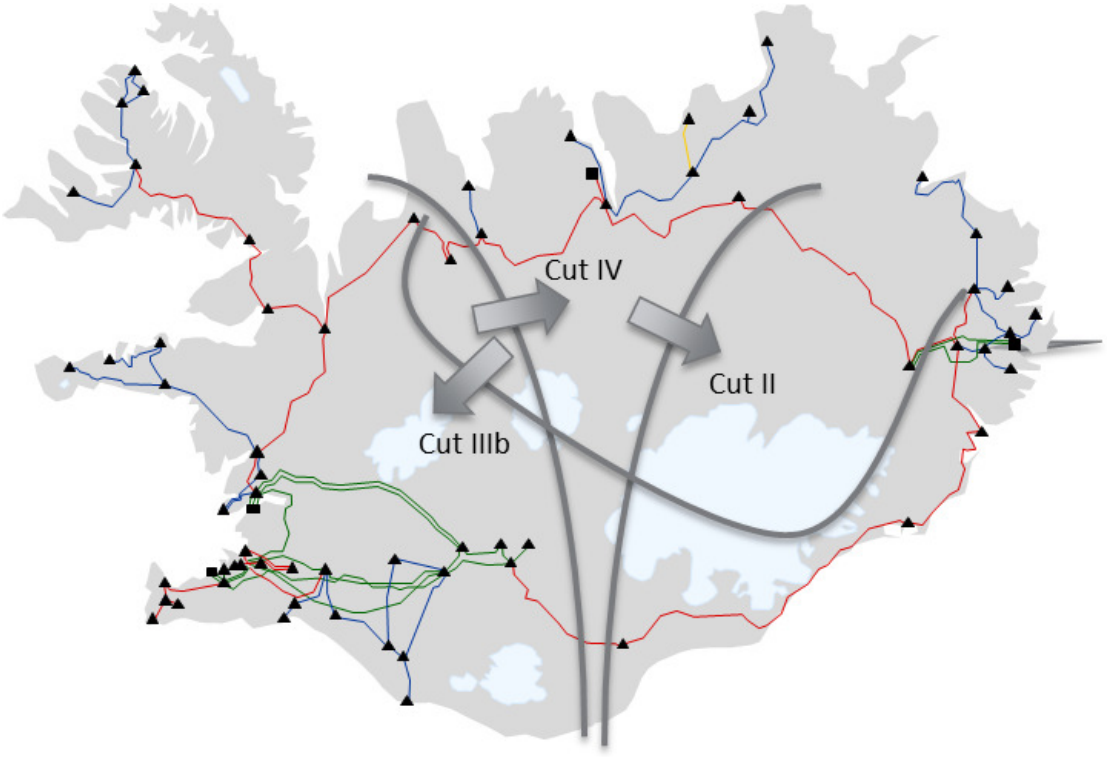

Figure 3.1: Transient stability cuts in the Icelandic Power System

To analyse the stability limit denoted as cut IV, four fault cases are simulated in PSS/E and the inter-area oscillations observed. The faults that are applied are the following and are illustrated by corresponding circles in fig. 3.2:

1. 100 ms three phase fault on bus Búrfell in southwest Iceland and clearing of the fault.
2. 100 ms three phase fault on Sigöldulína 4 and disconnection of the line.
3. 100 ms three phase fault on bus Fljótsdalur in the east part of Iceland and clearing of the fault.
4. 100 ms three phase fault on bus Kröflulína 2 and disconnection of the line.

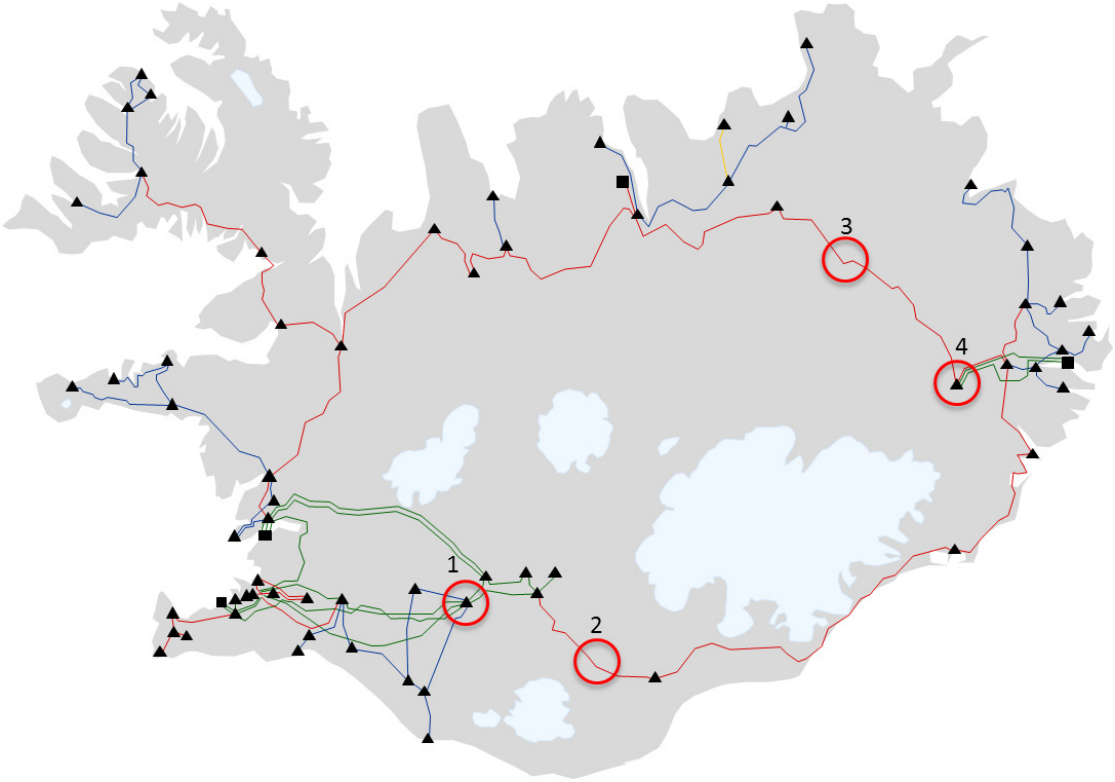

Figure 3.2: Location of three phase fault

In the east area six different load scenarios of an industrial load were observed and for each load scenario five different generation profiles for the hydro power plant Kárahnjúkar which is located close to the fourth fault in fig. 3.2 are simulated. The specific loading and generation scenarios can be seen in table 3.1. There is no change in the dispatch of the generators during the faults. Only their production set points are varied from case to case. First the basecase from the system plan is analysed without PSS's active and then the PSS's are added and their effect is analysed.

Table 3.1: Load profiles observed and generation associated with each case.

Load [MW]	Gen [MW]
560	610
540	570
520	520
500	470
480	420
460	420

3.2 Base Scenario

The base case is based on the 2013 system plan case [2]. The power generation associated with the base case can be seen in table 3.2.

Table 3.2: Generation connected to the 2013 basecase.

Type	No.	Name of Power Plant	Abbrevation	Capacity [MW]
Hydro	1	Búrfellstöð	Búr	270
	2	Sigöldustöð	Sig	150
	3	Hrauneyjafosstöð	Hra	210
	4	Vatnsfellsstöð	Vat	90
	5	Sultartangastöð	Sul	120
	6	Fljótsdalsstöð \ Kárahnjúkar	Kára	690
	7	Írafosstöð	Íra	48
	8	Steingrímsstöð	Ste	27
	9	Ljósafossstöð	Ljó	15
	10	Mjólkárvirkjun	Mjó	8.1
	11	Blöndustöð	Blö	150
	12	Lagarfossstöð	Lag	28
	13	Laxárstöðvar	Lax	27.5
	14	Andakílsárvirkjun	And	8
Geothermal	15	Kröflustöð	Krö	60
	16	Hellisheiðarvirkjun	Hel	300
	17	Reykjanesvirkjun	Rey	100
	18	Svartsengisvirkjun	Sva	75
	19	Nesjavallavirkjun	Nes	120
Total				2498

In the base case the power produced is 2178.2 MW while the load is 2122.5 MW. The short circuit power for a three phase fault in the south west region is 3984 MVA which is the strongest part of the system. The location of the generators can be seen in fig. 3.3 From the short circuit power the Icelandic power system can be classified as a weak system where during faults the system is not voltage stiff.

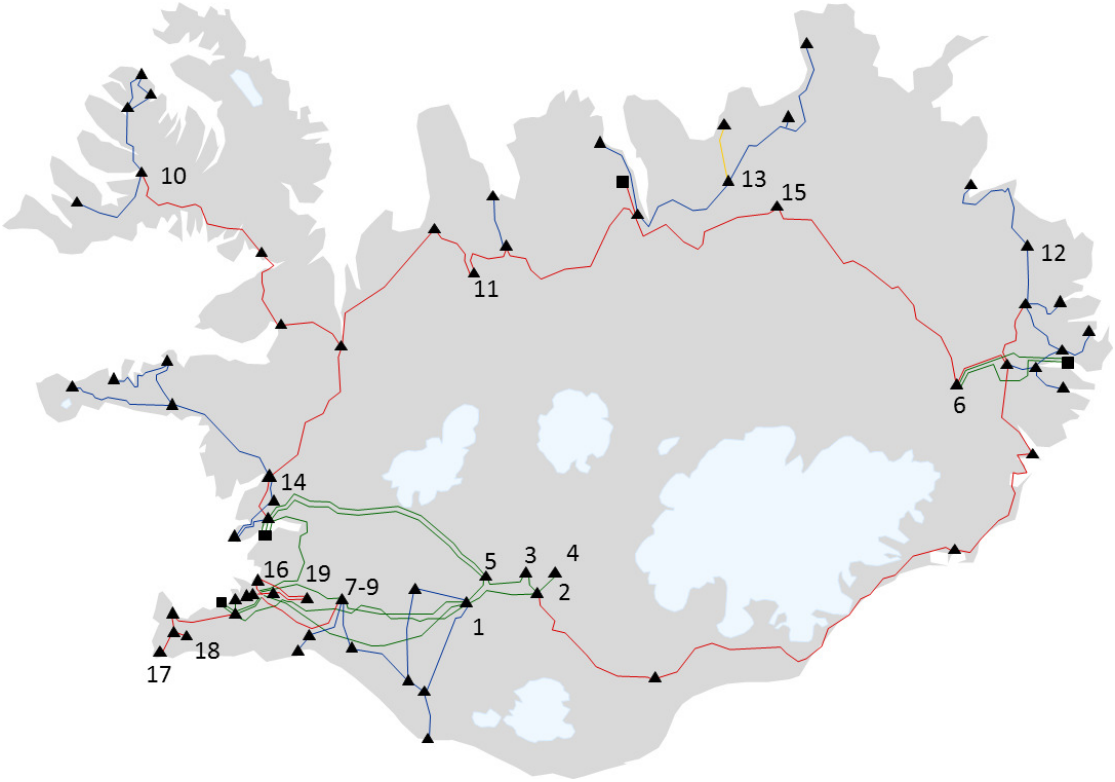

Figure 3.3: Power stations associated with the base case

3.3 Fault at Búrfell

In the simulation, a fault is applied at the 220 kV bus close to Búrfell at 1 s for 100 ms. The fault was cleared after and the variation of speed of the generators and power flow through the cut observed for 30 seconds. The modes of the speed variation of the generators and damping were then calculated using prony analysis [14] from 5 seconds to 15 seconds. The power transfer over the stability cut IV can be seen in figure 3.4 for the cases described in table 3.1.

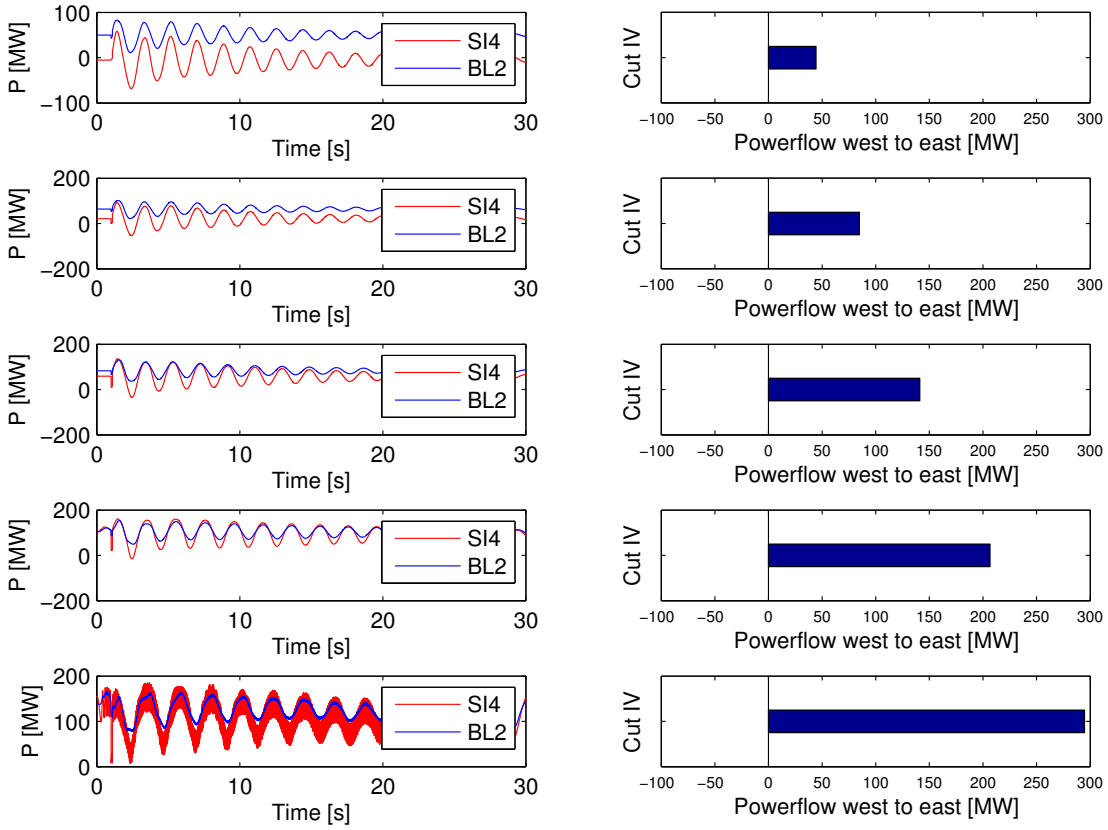

Figure 3.4: Real power flow over the stability cut IV, Load 560 MW and generation varied

On the right side power flow through cut IV can be seen before the fault. To the left the power flow through the transmission lines which cross cut IV can be seen as a function of time. For the first three cases the system starts in steady state and after the fault is applied and cleared we can see how the power flow through those lines oscillate. In the fourth case there are initalization problems in the beginning, since the power flow does not start at a steady state value as seen in fig. 3.4, but appears otherwise stable. The fifth case seems to suffer from a numerical oscillation due to limited precision of the numerical solver since the power flow through Sigöldulína 4 shows a high frequency ripple. In fig. 3.5 the speed of 7 generators are displayed. Búrfell, Sigalda, Hrauneyjar and Hellisheiði which are generators located in the southwest area.

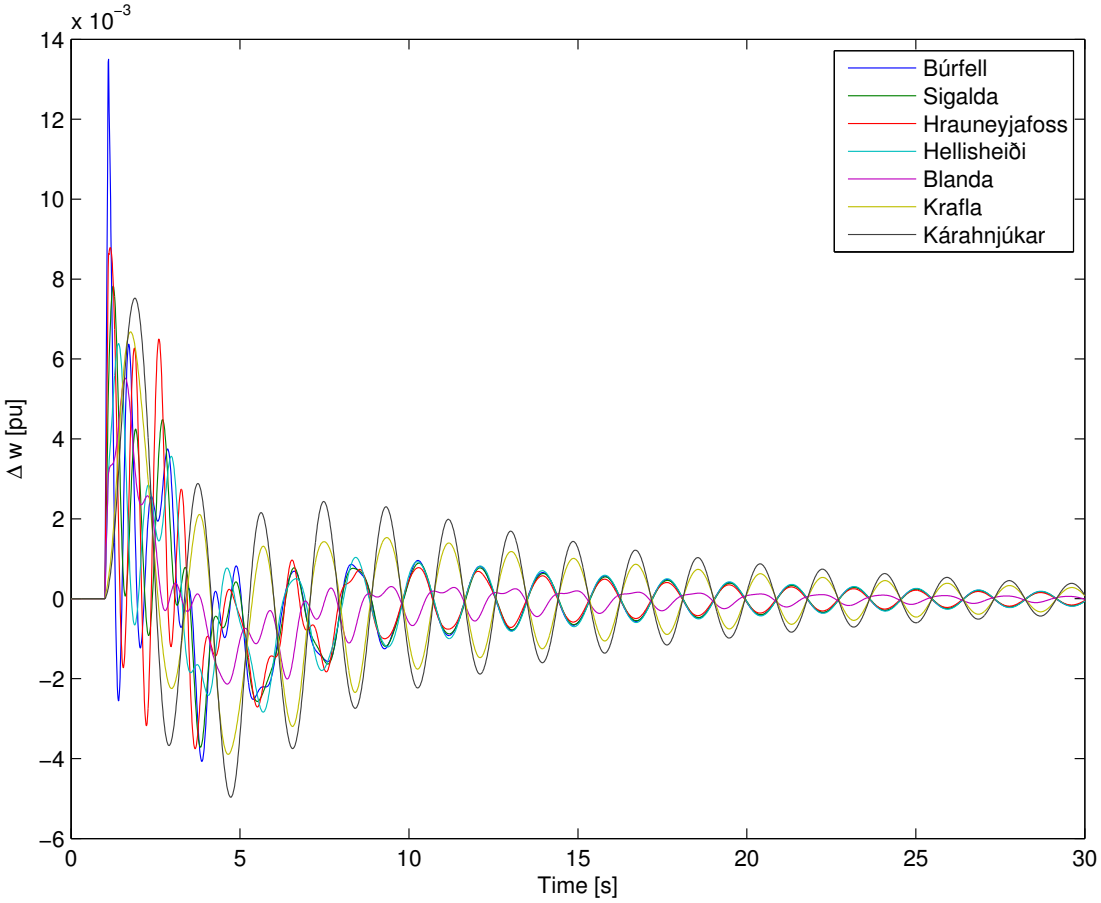

Figure 3.5: Change in speed of generators due to fault at 560 MW load and 610 MW generation

Blanda and Krafla are connected to the power system on the 132 kV tie connection and Kárahnjúkar is a big hydro power plant connected to the 220 kV system in the East. The generators in the southwest system increase their speed the most as seen in fig. 3.5, as they are closest to the fault bus which the fault is applied at. This is coherent with (2.26) since the air gap power drops most where the voltage drop is the higher. Initially there are some local modes in the south west area but after around 4 seconds the interarea modes become dominant and it can be seen that the south west area oscillates against the east generator. Blanda, which is situated close to the middle of the oscillation path, does not become coherent with either group in the speed oscillations. In fig. 3.6 the angle difference between a big hydro power plant Búrfell in the southwest is and between the powerplant Kárahnjúkar in the east.

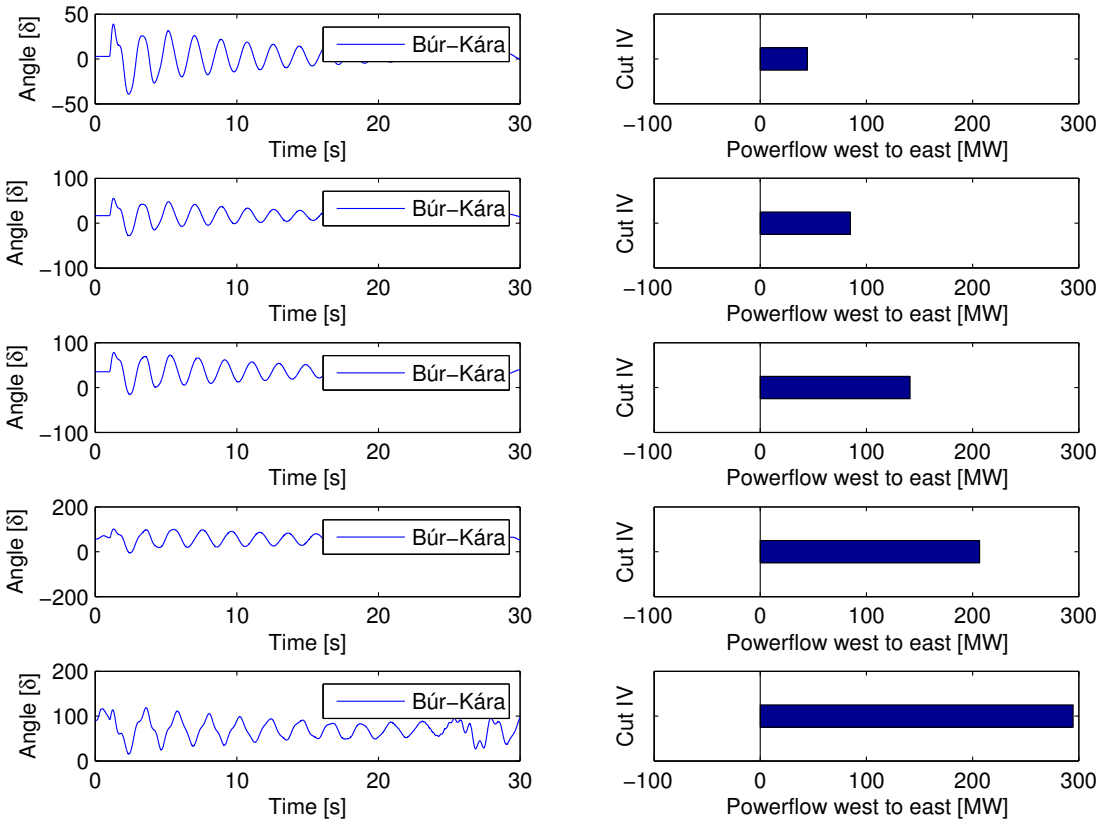

Figure 3.6: Change in angle due to fault 560 MW load and varying generation

As the angle difference changes it will impact the power exchange between the areas. As the power exchange is increased, which leads to increased angle difference, it is observed how the damping of the oscillations decreases. When comparing fig. 3.5 and fig. 3.6 it can be seen how angle oscillations and power oscillations are connected. Equation (2.22) states that the damping ratio is inversely proportional to the syncrhonizing torque, which is linked to the initial angle. As the power exchange increases the angle difference moves closer to the maximum value of 90 degrees, and it can be seen that the 5th case that was computationally unstable starts in 90 degrees as seen in fig. 3.6. During the fault generators in the south-west system increase their angle so the initial angle deviation is positive. For the stable cases the dominant mode of oscillation was analysed with prony analysis using the PSS/E package [15]. The magnitude and phase of each generator was plotted as seen in figure 3.7.

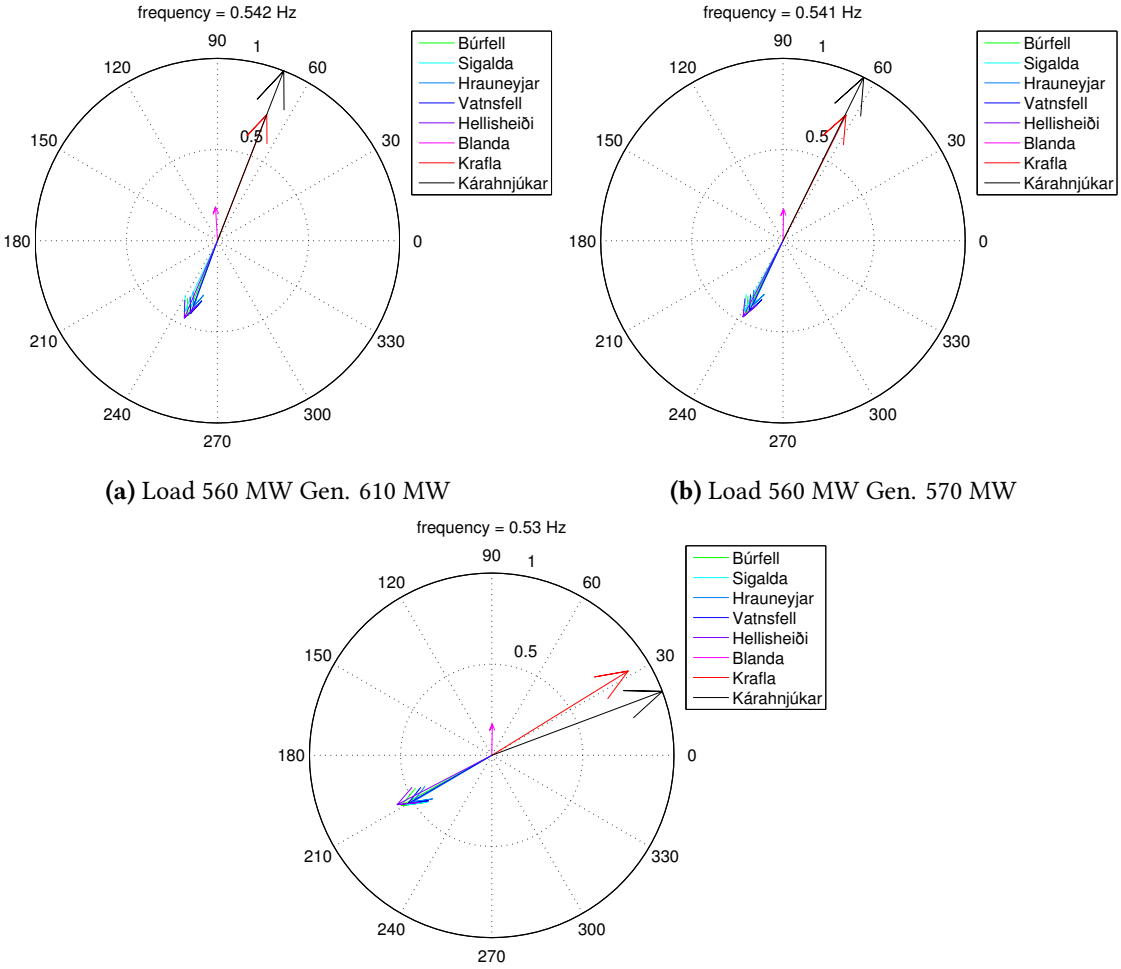

(a) Load 560 MW Gen. 610 MW

(b) Load 560 MW Gen. 570 MW

(c) Load 560 MW Gen. 520 MW

Figure 3.7: Magnitude and phase of generator speed

In general the generators in the southwest oscillate against the generators in the east region. The generators in Blanda are always a little bit out of phase with the east system, however they are oscillating against the southwest and the participation in the mode is very low compared to the other modes. It can also be noted that as the power exchange increases the phasor in Blanda moves away from the east group. Equation (2.21) states that the frequency is proportional to the synchronizing torque, furthermore the synchronizing torque depends on the angle. As the angle difference increases that the frequency of the dominant mode decreases.

After analysing all the different cases the damping of the oscillations over the transfer cut was calculated using the prony method [14] and can be seen in fig. 3.8.

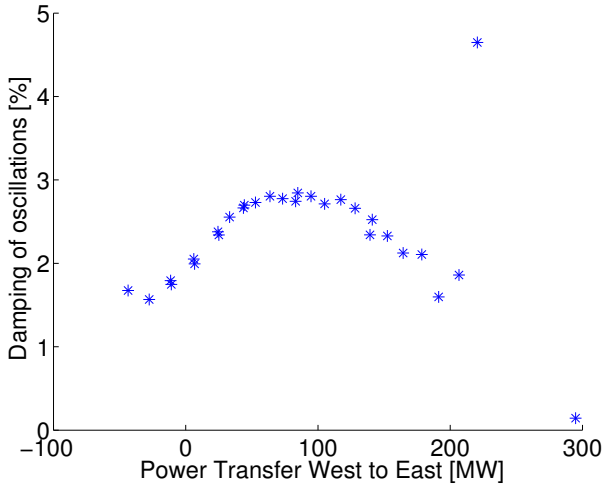

Figure 3.8: Damping of the dominant mode when power transfer is varied.

The dominant mode of oscillations was around 0.540 Hz. The highest damping ratio is when the power flow through cut IV is around 75 MW as seen in fig. 3.8. The peak of the damping curve is around 3 %. The damping declines as the power is transfer is varied around this point. At 75 MW the angle difference between Búrfell and Kárahnjúkar is close to zero as seen in fig. 3.6. As the power transfer is varied the angle is increased or decreased which affects the damping constant and the synchronzing torque as seen in (2.9) and (2.36). That is the reason for why the damping declines. Close to the maximum transfer between the areas, as seen in fig. 3.8, we get damping points that do not follow the hyperbola curve and it is because of numerical instability in extreme loading conditions of the simulations. Fig. 3.9 shows how the critical clearing time of the fault also varies as the power transfer is varied.

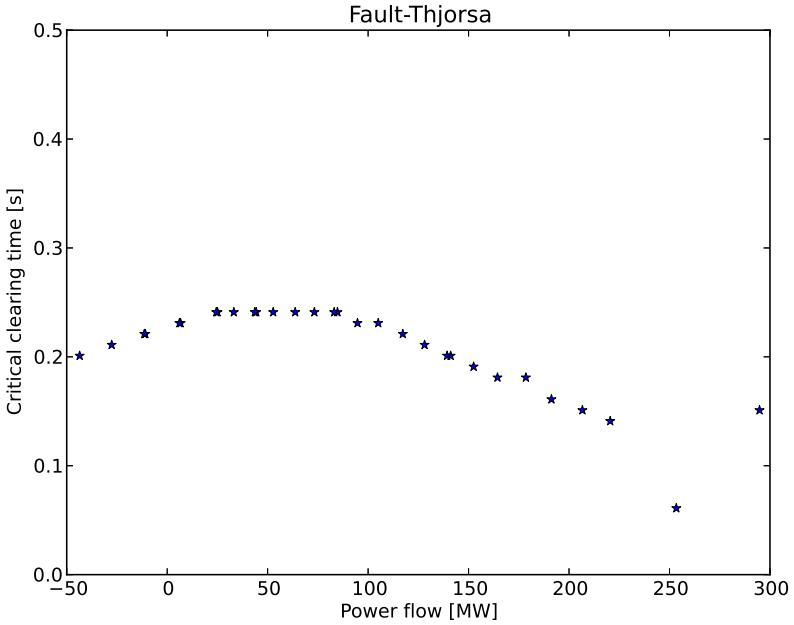

Figure 3.9: Critical clearing time of the fault with respect to power transfer.

Analytically the critical clearing clearing time can be calculated from (2.32). So as the initial angle difference is closer to zero, i.e. there is no power exchange between the areas, then the deacceleration area is the biggest for the equal area criterion as stated in (2.31). As expected the critical clearing time becomes lower when power exchange is increased into the east part of the network. It can be observed that the profile gets flat in the area around 25 MW to 75 MW power exchange and there is not a peak as expected. The reason is not fully understood but it is expected that the complexity of a multi machine system plays an important role in this behaviour. For example Svenska Kraftnät demands that a power plant survives a 0.25 s fault on the collector bus [16] which the Icelandic grid does not fulfill. In fig. 3.9 and 3.8 the max value of damping and critical clearing time is when the angle difference between the generators chosen is around 10 degree is zero as seen in 3.6. The reason is that the system has the biggest deacceleration area when the initial angle difference is zero. Note that since the system is not completely symmetrical in terms of load and generation distribution, this does not necessarily correspond to the case with zero power transfer, as otherwise would be expected.

3.3.1 Effect of varying impedance

As stated in the overview chapter the equivalent reactance will influence the damping and the frequency of oscillations. The system impedance was first halved and then varied to analyze the impact of change in reactance. Halving or varying the impedance of all transmission lines in the system will mostly impact the inter-area modes in the dynamic simulations, since the reactance in the 132 kV interconnection is the one that determines the frequency of oscillations.

As can be seen in fig. 3.10 the peak damping of the system has now changed.

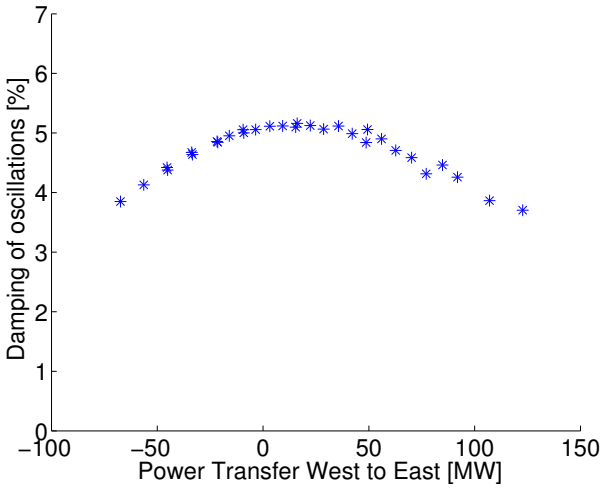

Figure 3.10: Damping of the dominant mode when power transfer is varied with half reactance.

The damping has increased with lower reactance and also the peak has changed from 75 MW to around 25 MW. The dominant frequency has also increased from 0.54 Hz to around 0.671 Hz. The impedance was then scaled in order to see the changes in frequency and damping with respect to reactance. As seen in fig. 3.11 the damping increases as the reactance of the system is decreased.

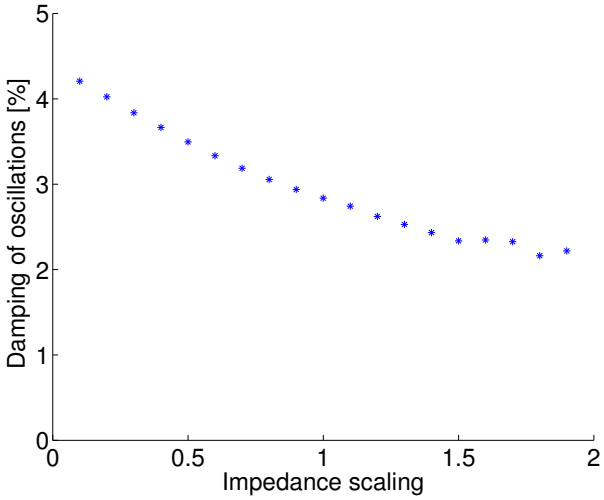

Figure 3.11: Damping of the dominant mode when reactance is varied.

The frequency of the modes between the regions also depends on the reactance as seen in fig. 3.12. It should be noted that the power exchange between areas is kept constant so for a certain power exchange the damping increases but does not necessarly display the maximum

damping following variance of the reactance.

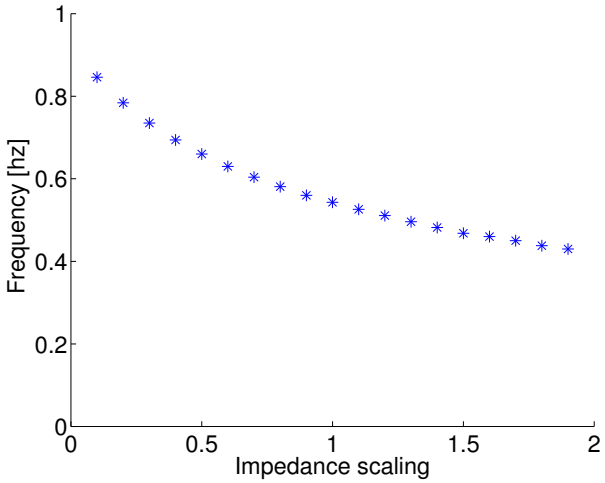

Figure 3.12: Frequency of the dominant mode when reactance is varied.

It is evident that damping and frequency of power oscillations depends on reactance between the generators as shown by (2.35) and (2.21). When the reactance in the network decreases, it can be said that the electrical distances in the network are reduced. A low reactance leads to a high short circuit power in the system. Thus, the voltage stiffness of the network is improved and the strength of the network increases.

3.4 Fault at tranmission line Sigöldulína 4

Sigöldulína 4 is a transmission line in south Iceland. It is close to the hydro mass in the south west area. 100 ms fault is applied at the 132 kV bus close to the hydro mass and the transmission line is disconnected following the fault. The power transfer over the cut can be seen in fig. 3.13 for the cases described in table 3.1.

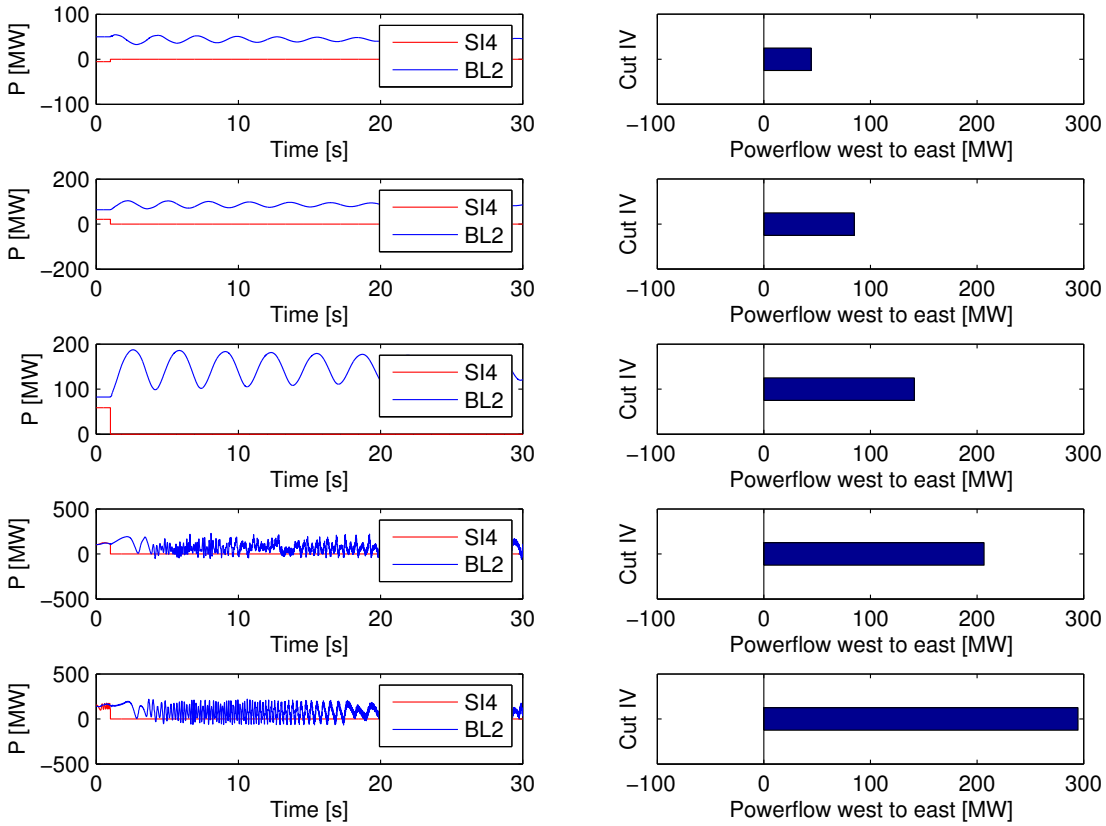

Figure 3.13: Real power flow over the stability cut IV,Load 560 MW

On the right we see the inital power exchange between the areas and on the right we see the power flow through the transmission line that cross the stability cut when exposed to a fault. For the first three cases the system is stable, however for the last two cases the Southwest and Eastern part lose synchronism following the disturbance so it said to be transiently unstable. From fig. 3.13 it is quite obvious that the frequency of oscillation is lower than in the fault at the bus Búrfell and the system damping has decreased. Another interesting phenomena is that for around 50 MW transfer the oscillations have quite poor damping although the magnitude of the oscillations is not that high. However the magnitude of the oscillations increases rapidly as the power transfer is inreased. For the third case this is quite evident so at that point we expect to be getting quite close to the stability limits of the system for a 100 ms fault. In the last two cases the system become transiently unstable and the areas lose synchronism. A single case of speed response following the fault can be seen in fig. 3.14.

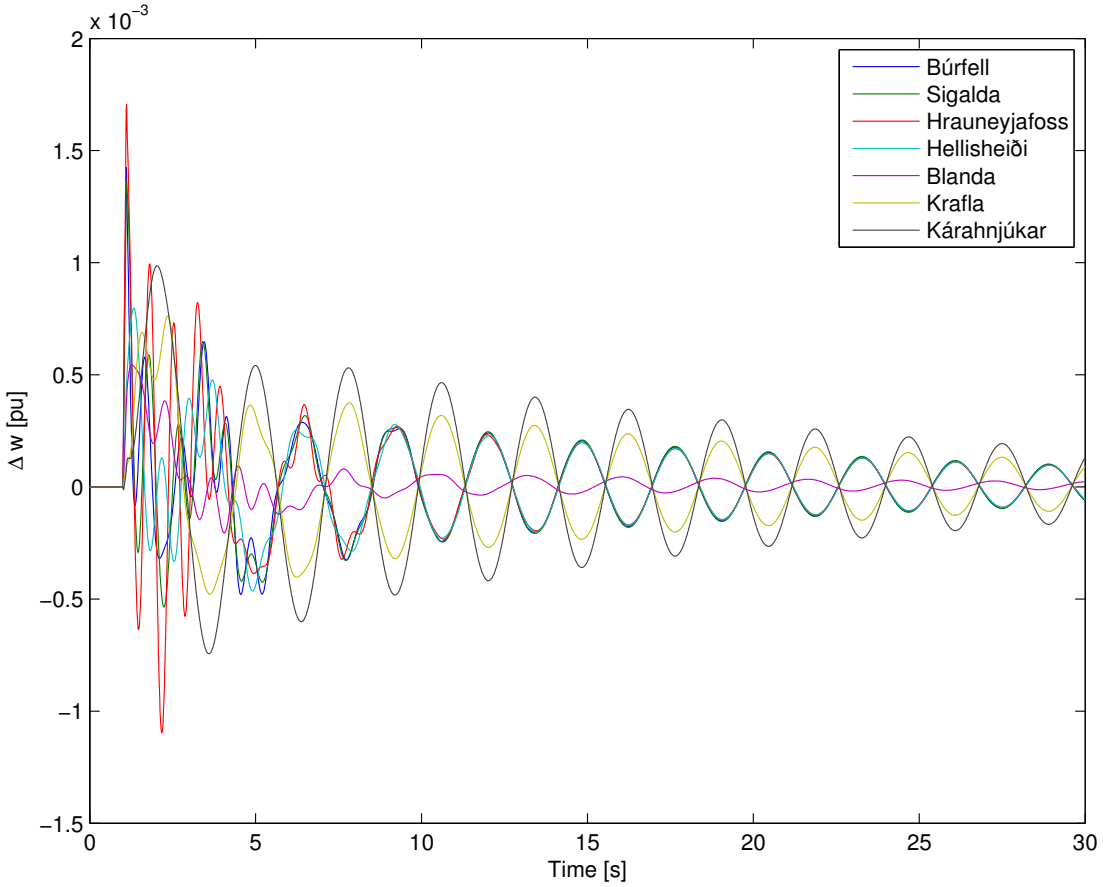

Figure 3.14: Change in speed of generators due to fault, Load 560 MW

The generators closest to the fault increase their speed the most as can be seen in fig. 3.14. The generators in Sigalda should increase their speed the most since the fault is closest to them. If (2.26) is viewed it is noted that the inertia also plays a big role in the acceleration, since the initial angle increase following a fault is inveresly proportional to the inertia constant and proportional to the power. As the inertia constant at Hrauneyjafoss is 3.51 p.u. while the inertia constant at Sigalda is 4 p.u. and the power generated by Hrauneyjafoss is 60 MW while the power generated by Sigalda is 38 MW. The maximum speed increase is around $1.5 \cdot 10^{-3}$ p.u. compared to $14 \cdot 10^{-3}$ p.u. as seen in fig. 3.5 for the fault case at Búrfell. The reason is that the reactance that the generators see during the fault is much higher when there is a fault in the 132 kV system then in the 220 kV system. This is because there is a transformer between the 220 kV and the 132 kV voltage levels which increases the reactance. In other words the voltage drop at the generator terminals is smaller than for a fault within the strong system so the electric power curve does not drop that far down. This leads to less acceleration of the generators in this case. In fig. 3.15 the angle difference following the fault and clearing of the line can be seen.

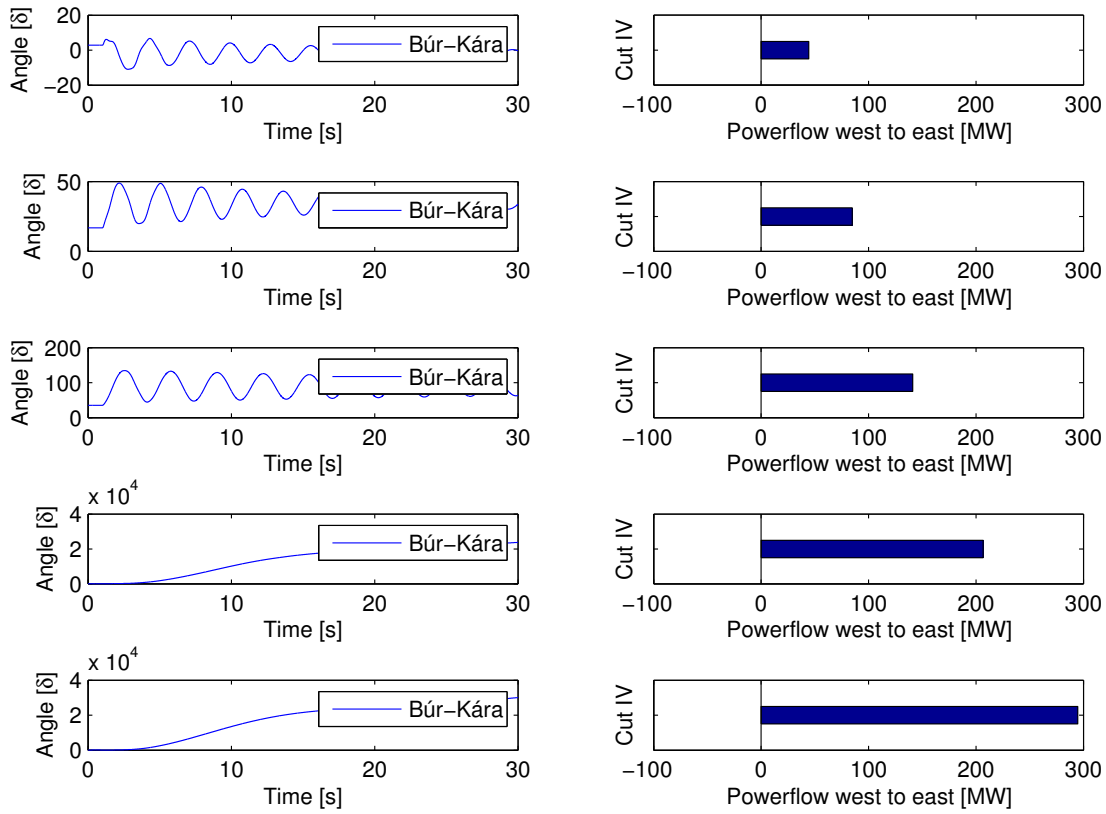

Figure 3.15: Change in angle difference of generators due to fault, Load 560 MW

When comparing the first three cases it is quite interesting that angle difference immediately after the fault for the first case is very little. As the power transfer is increased over the cut, the fault has greater impact on the angle difference due to higher operating point on the power curve. The frequency also decreases as more power is transferred over the transient stability limit. When the swing equation is linearised it can be seen from (2.21) how it effects the natural frequency of those oscillations as the angle increases. In the third case the change of the reactance after the fault since one line is disconnected, clearly moves the operating angle difference between the generators. The fourth and fifth case can be classified as transiently unstable since there angle is an angle seperation. Fig. 3.16 shows analysis of the dominant mode and also how the frequency has changed from the first fault case.

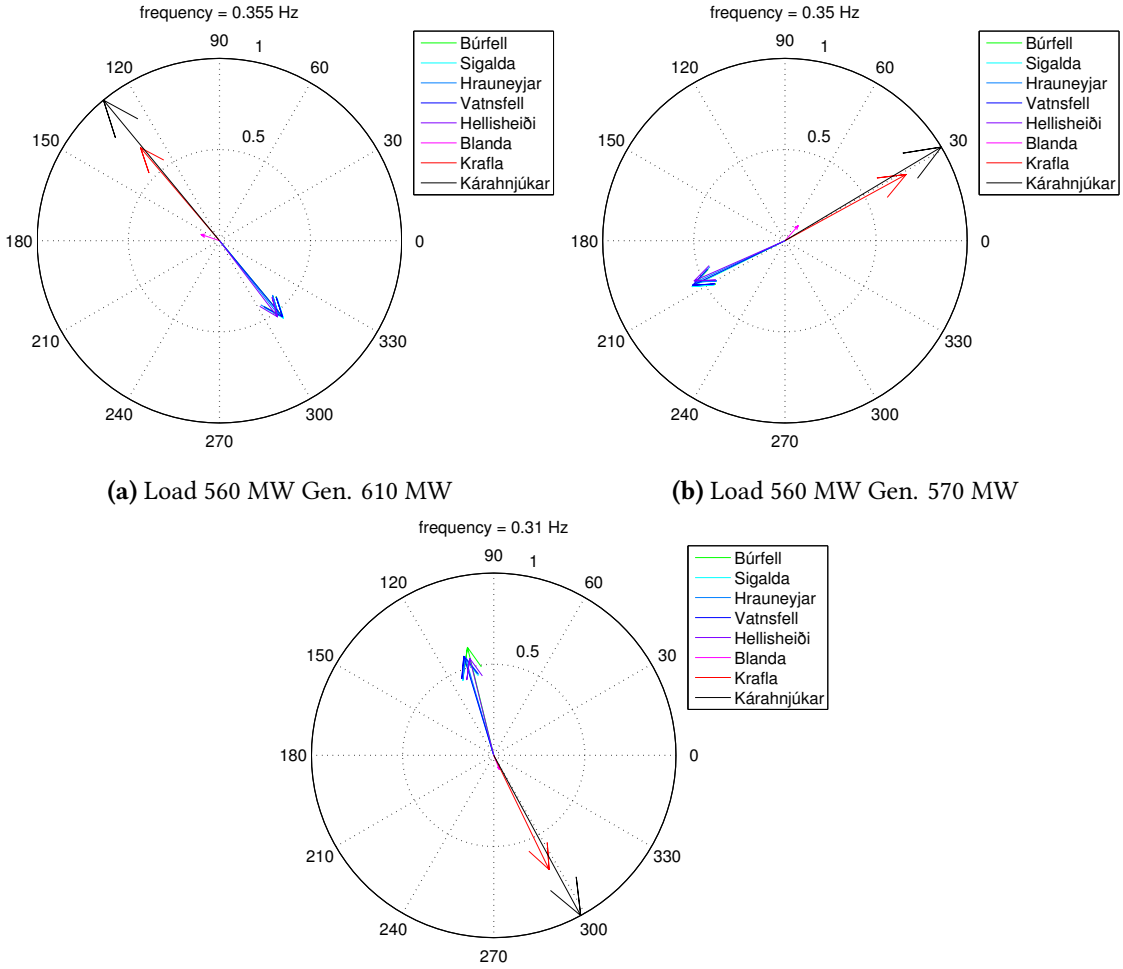

(a) Load 560 MW Gen. 610 MW

(b) Load 560 MW Gen. 570 MW

(c) Load 560 MW Gen. 520 MW

Figure 3.16: Magnitude and phase of generator speed

Following the loss of the line there is only a single 132 kV line connecting the power system. It is easier to see also how the angle between the areas affects the frequency of the oscillations. As the transmission is increased between the areas the frequency of oscillations varies. So the slope of the linearisation of the power curve becomes less step as the power transfer is varied. When Sigöldulína 4 is disconnected Blanda participates less in the dominant mode of the system than before. A probable explanation is that it is moved closer to the ”middle” of the transmission system and therefore does not align with either generating group in the inter area oscillations. For the last figure the phasors of oscillations are somewhat out of phase which means that are some units the should counter balance these generating groups. The peak of the damping is, as for the case when we had a fault within the strong system, when the transfer is 75 MW as seen in fig. 3.17.

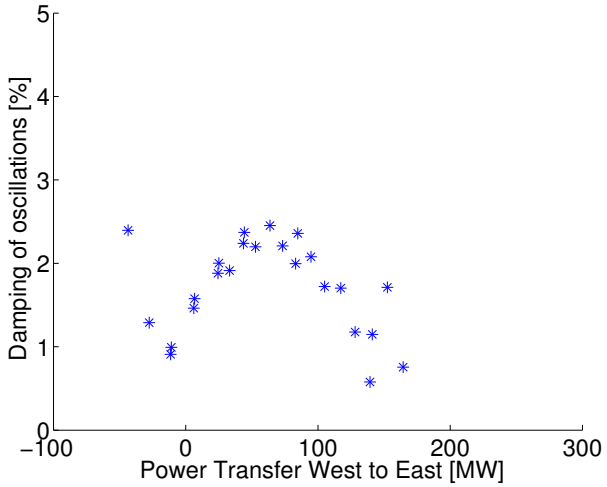

Figure 3.17: Damping of the dominant mode when power transfer is varied.

The maximum damping curve is around 2.5 % and the maximum power transfer is lower than compared to the case when you have both lines in operation as in fig. 3.8.

In fig. 3.18 the calculated critical clearing time for faults at transmission line Sigöldulína 4 can be seen.

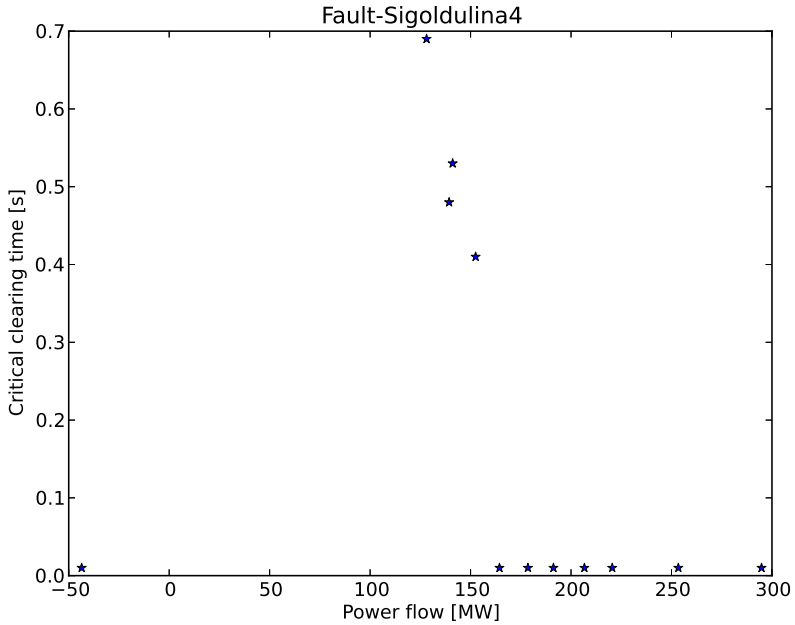

Figure 3.18: Critical clearing time of the fault with respect to power transfer.

When the critical clearing time was calculated, there was not found a critical clearing time

that gave reasonable value unless it was close to the transient stability limits of the system. since the fault was located in the electrical middle between them, they accelerated both and quite slowely since the voltage drop was not significant as in the cases when we have a fault in the strong parts of the system.

3.5 Fault at Fljótsdalur

Fault was applied at the substation Fljótsdalur in the east 220 kV system. Fljótsdalur is a bus in the east which connectes the hydro power plant Kárahnjúkar to the transmission system.

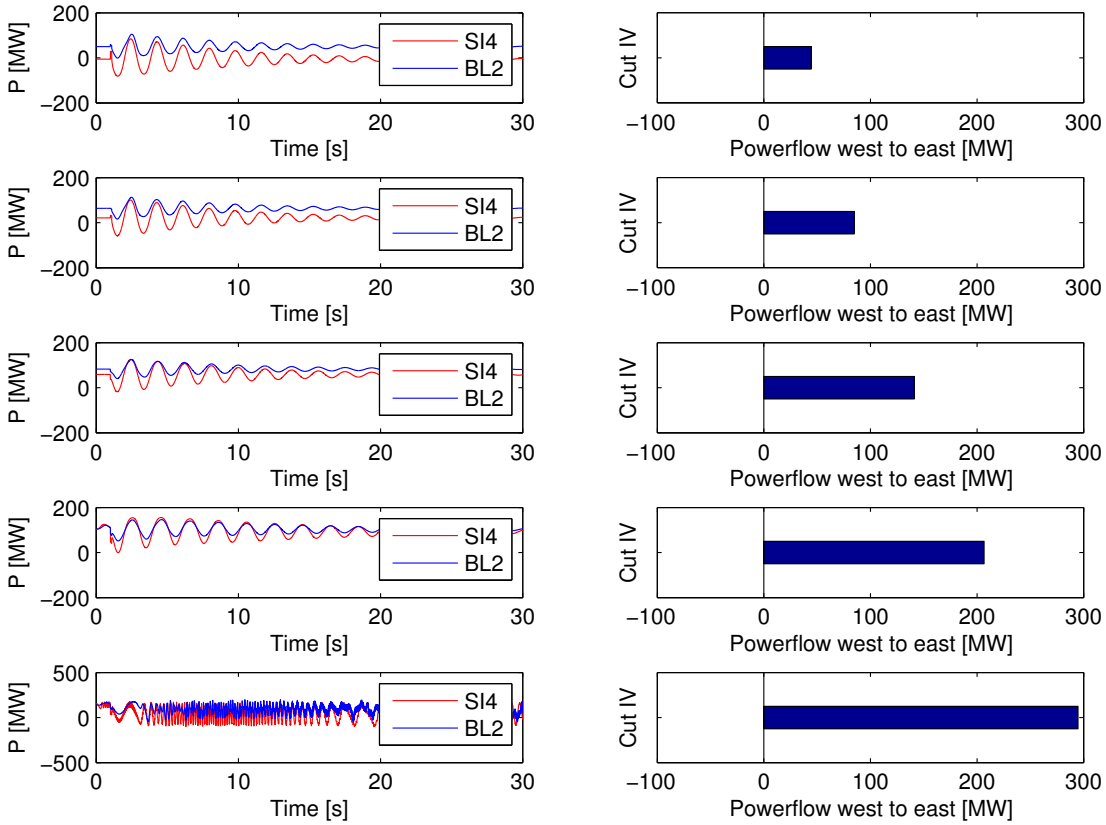

Figure 3.19: Real power flow over the stability cut IV, Load 560 MW

The power transfer over the cut can be seen in figure 3.19 for the cases described in table 3.1. On the right we have the initial power exchange over the stability cut IV and on the left we have the power flow in the lines which cross this stability cuts. For fault at Fljótsdalur there is similar behaviour as for a fault in the other end of the system. The first four cases are stable but in the fifth case the two strong areas lose synchronism following this fault. The first swing after the fault decreases the power flow. The reason for that is that now the angle in the east end is increasing so the angle difference between the areas is reduced. In fig. 3.20 the speed of

7 generators are shown as described before.

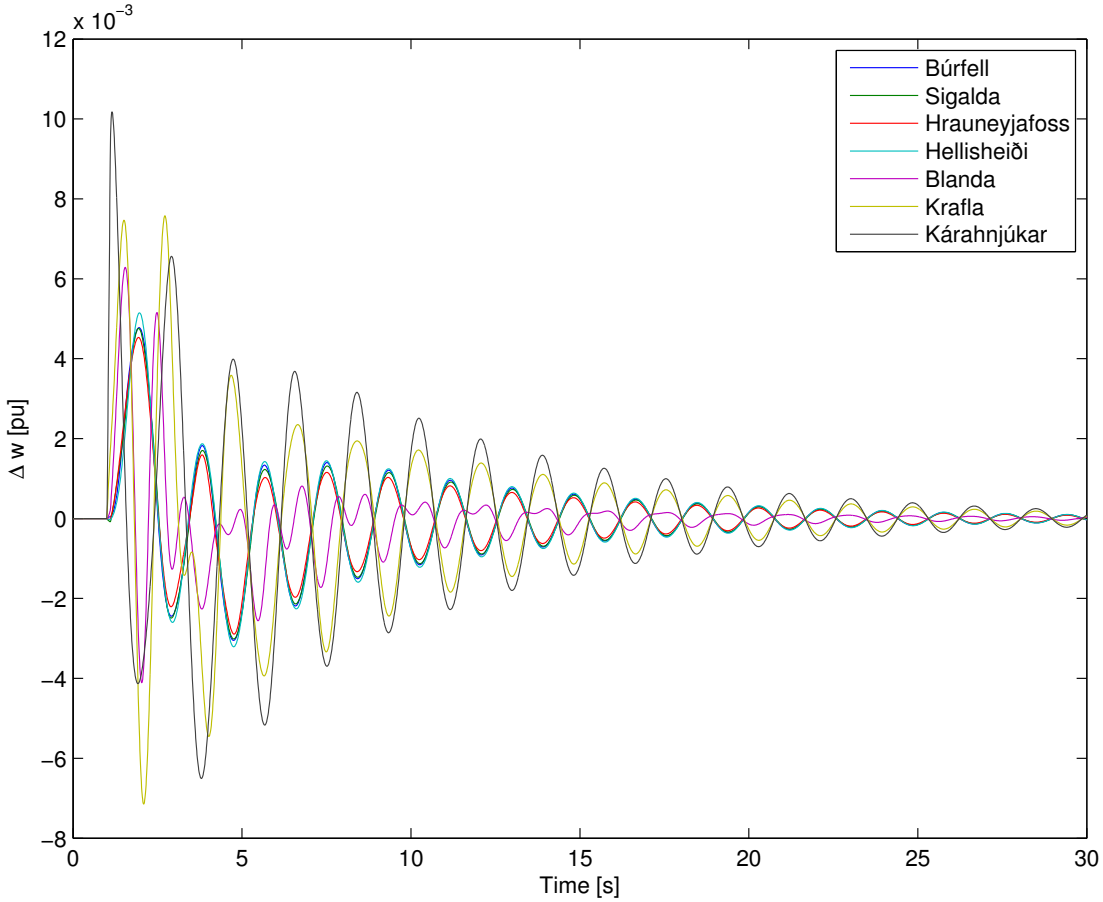

Figure 3.20: Change in speed of generators due to fault, Load 560 MW

It can be observed that the generators closest to the fault increase their speed the most during the fault. In this case these are Kárahnjúkar and then the generators in Blanda and Krafla. From the time when the fault is applied the oscillations between the areas are quite coherent. Blanda is as before not aligning with the east or west part system but oscillates as the system voltage is oscillating. The speed increase of Kárahnjúkar is less for this fault compared to the speed increase of the generators in the Southwest when a fault was applied at the bus in Búrfell. In fig. 3.21 the angle difference between a hydro power plant Búrfell in the southwest and the powerplant Kárahnjúkar in the east is displayed.

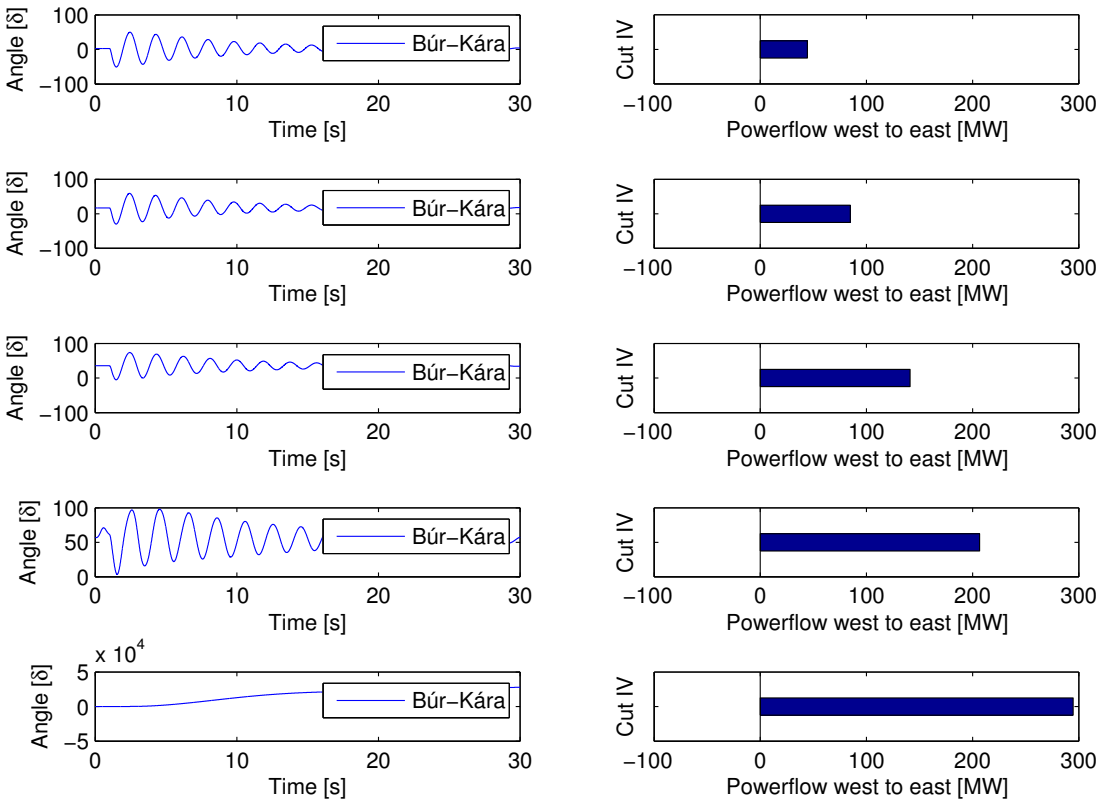

Figure 3.21: Change in angle of generators due to fault, Load 560 MW

As the angle difference increases the power exchange between the areas is increased. Also as the angle increases the oscillation become more severe following a fault. In the last case the areas lose synchronism so it is transiently unstable. It is noted that during the fault the generator in the east increases its angle so the angle difference becomes negative which explains the that the first power swing is decreasing the power flow between the areas.
In fig. 3.22 it can been seen that the Kárahnjúkar is the most dominant generator in these oscillations. Furthermore, it is more dominant than in the other cases where the fault was applied in the south west system, since the voltage drop is greatest closest to Kárahnjúkar so the initial swing is because of that generator.

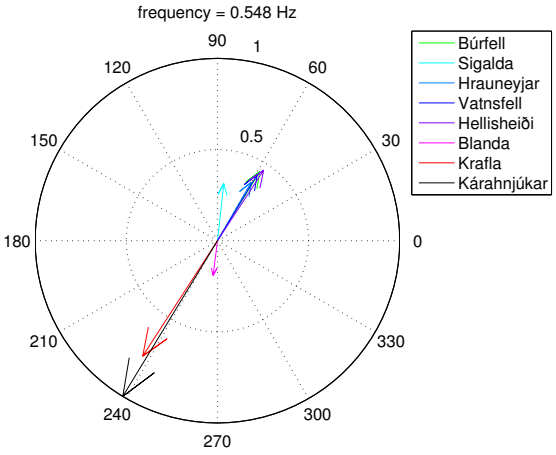

(a) Load 560 MW Gen. 610 MW

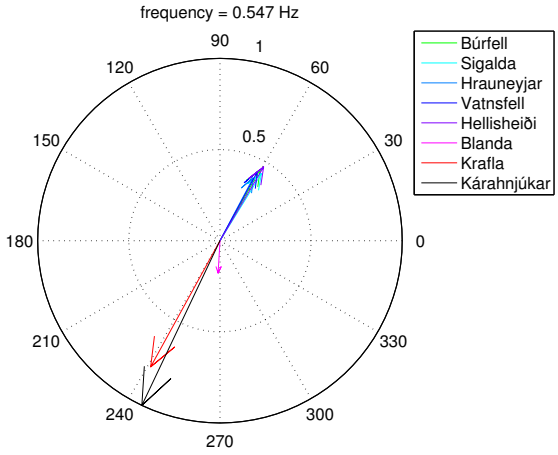

(b) Load 560 MW Gen. 570 MW

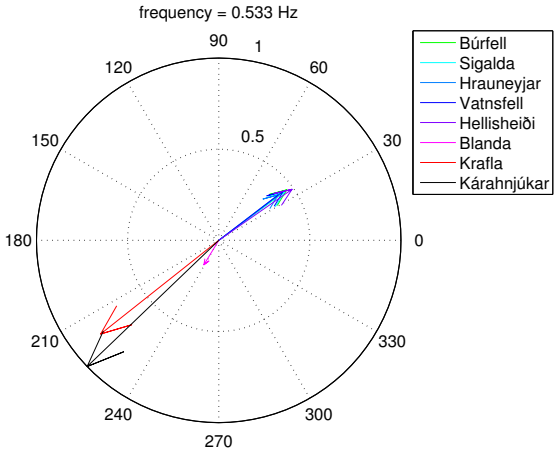

(c) Load 560 MW Gen. 520 MW

Figure 3.22: Magnitude and phase of generator speed

The dominant mode of oscillations was around 0.540 Hz. This is the same frequency as when a fault in the south west part of the system was modelled. From this we can draw the conclusions that the properties of the network determine the frequency of power oscillations but not the location of the fault itself which is coherent with (2.21). Blanda shows similar behaviour as for the fault in the south west system. As the power transfer increases it aligns more and more with the generators in the east. However the participation of that generator is small in the most dominant mode.
In fig. 3.23 the damping of the dominant mode can be seen for the fault at Fljótsdalur.

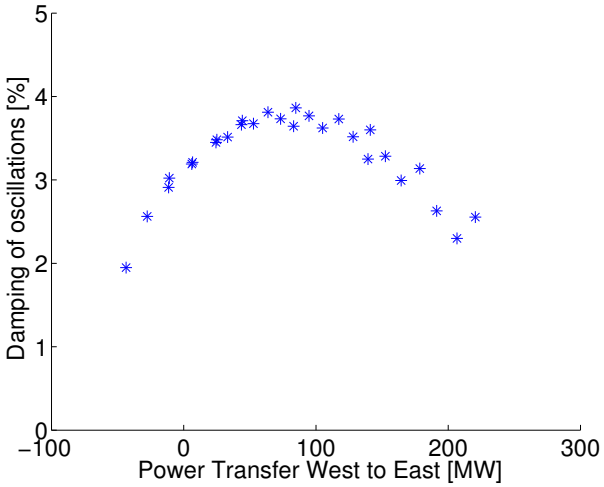

Figure 3.23: Damping of the dominant mode when power transfer is varied.

The peak of the damping curve is around 75 MW as seen before at approximately 3.8 %. The damping declines as the power transfer varies around that point. The peak of the damping curve is now higher than when a fault was applied in the south west of the system. The first swing after the fault is caused by the acceleration of the generation units in the east part of the system. The south west area has a much larger inertia than the east so that seems to have an impact on the damping in the system. In fig. 3.24 the critical clearing time for the fault is seen to vary with power flow.

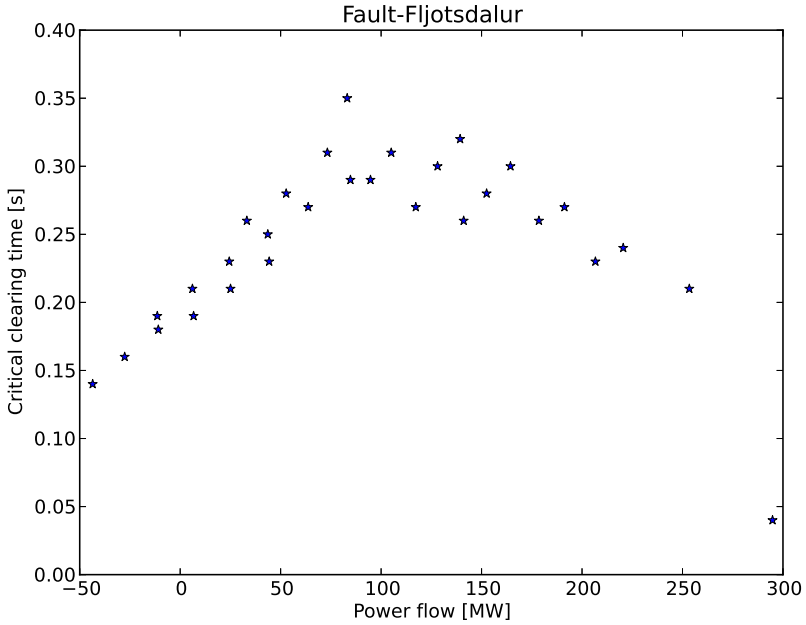

Figure 3.24: Critical clearing time of the fault with respect to power transfer.

The distribution of the critical clearing time here is more scattered than before. The reason is that since the generation in Kárahjúkar is varied the acceleration constant defined by (2.26) varies, therefore variation of the acceleration constant will affect the critical clearing time for faults close to the varying generation. It is interesting to note that the critical clearing time is higher for fault at Fljótsdalur than for the first fault case. If the case of the single machine infinite bus is considered, the strength of the system that the generators are oscillating against will define the critical clearing time of the system. This can be seen when the second swing is observed as it is bigger than the initial swing between the generator groups.

3.6 Fault at Kröflulina 2

Kröflulína 2 is a transmission line in the northern connection between the areas located close to the bus Fljótsdalur as seen in fig. 3.2. 100 ms fault is applied at the 132 kV bus in Fljótsdalur and the transmission line is cleared following the fault. The power transfer over the cut can be seen in figure 3.25 for the cases described in table 3.1.

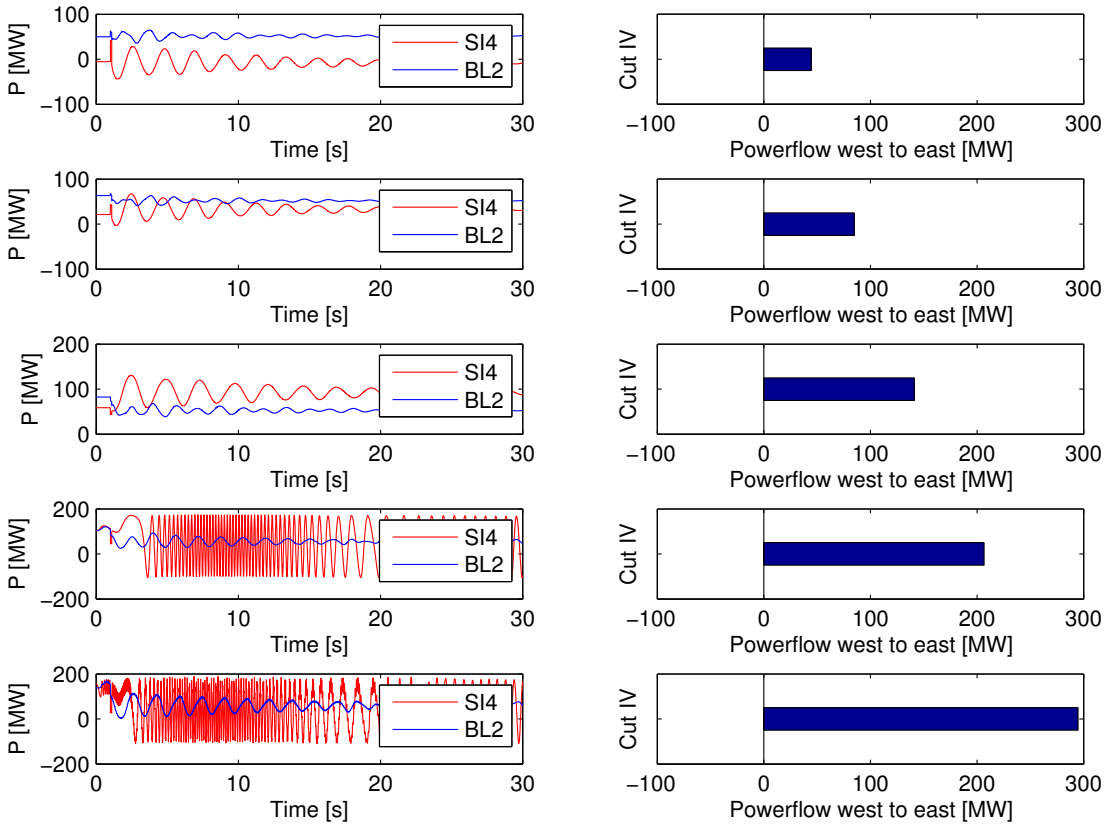

Figure 3.25: Real power flow over cut IV, Load 560 MW

For the first three cases the system is stable, however for the last two cases the system loses synchronism following the disturbance. What might seem quite odd is that for the first case after disconnecting the transmission line Kröflulína 2 the power flow through Blöndulína 2 stays at a similar level as before. The reason is that there is a large load located to the right of the stability cut. So when the transmission line is disconnected there still flows a lot of active power towards that load. When transmission is increased for cases 2 and 3 in fig. 3.25 then the power drop becomes more clear since as the line is loaded more. The power flow through Sigöldulína 4 displays the power oscillations between the areas now. In fig. 3.26 the speed variation following a fault on Kröflulína 2 can be seen.

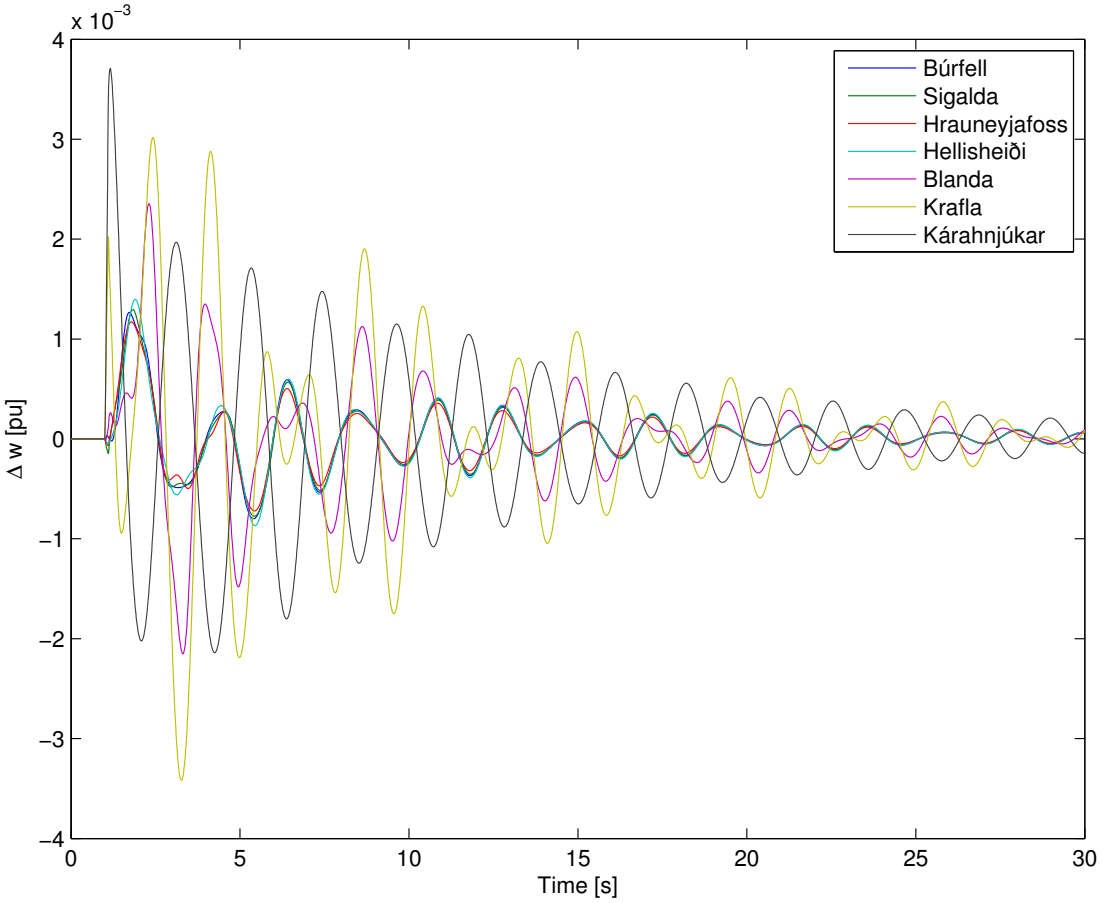

Figure 3.26: Change in speed of generators due to fault, Load 560 MW

As in the other fault cases the generators closest to the fault accelerate the most. However when the line between the power plants Krafla and Kárahnjúkar is disconnected they are on the ”opposite” end of the system. So in fig. 3.26 it can be seen how Kárahnjúkar oscillate against blanda and Krafla. The speed of the generators in the southwest system which is in the ”middle” between these generator groups also parcticipates in these oscillations but with a smaller magnitude. In fig. 3.27 the angle difference between a hydro power plant Búrfell in the southwest and the powerplant Kárahnjúkar in the east is displayed.

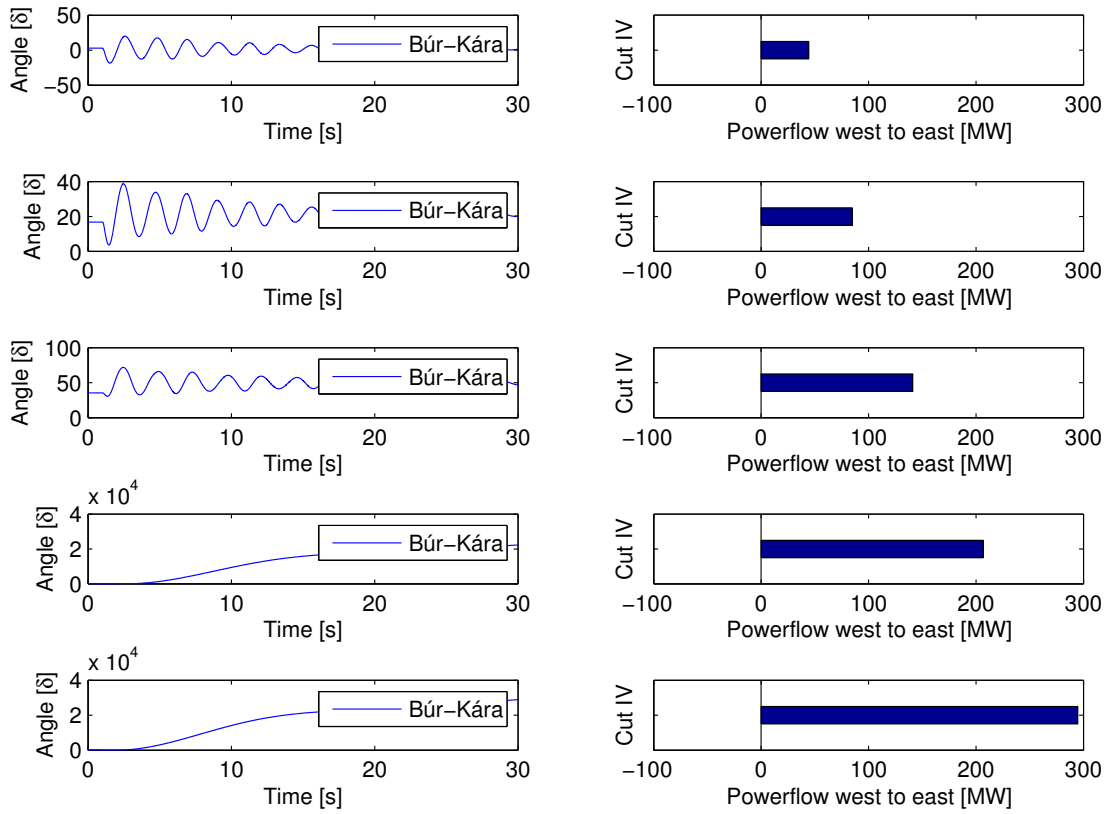

Figure 3.27: Change in angle of generators due to fault, Load 560 MW

As the angle difference changes the power exchange between the areas is altered. For this certain fault the angle variation between the southwest and the east is not large. The major angle difference would be between the generators Krafla, Blanda and Kárahnjúkar. In the last two cases the areas lose synchronism so it is transiently unstable. It is noted that during the fault the generator in the east increases its angle so the angle difference becomes negative which explains the that the first power swing is deacresing the power flow between the areas. In the third case we do not even exceed 90 degree angle difference between the south and the east so it is quite obvious that for this fault case that the angle difference between Búrfell and Kárahnjúkar is not a major impact on the Power System Stability. In figure 3.28 the participation of the generators in the most dominant mode can be seen.

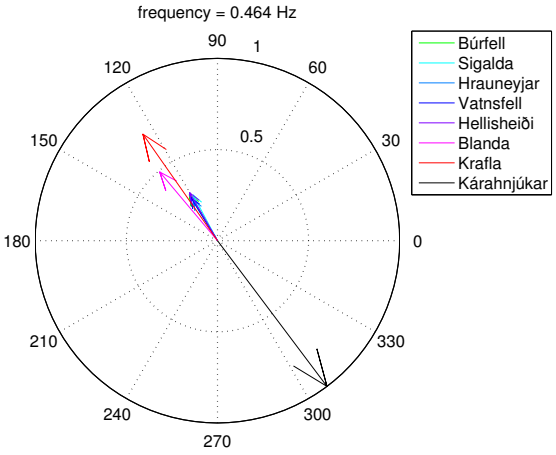

(a) Load 560 MW Gen. 610 MW

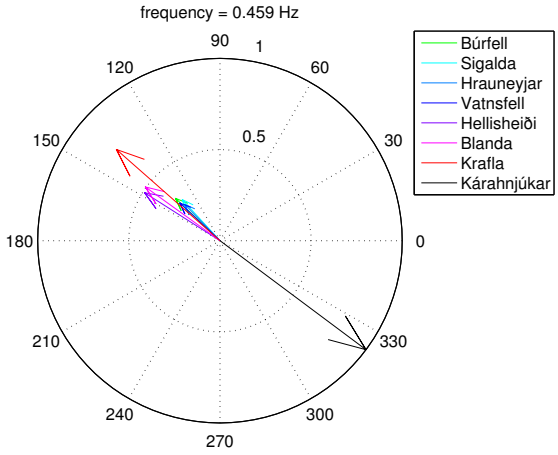

(b) Load 560 MW Gen. 570 MW

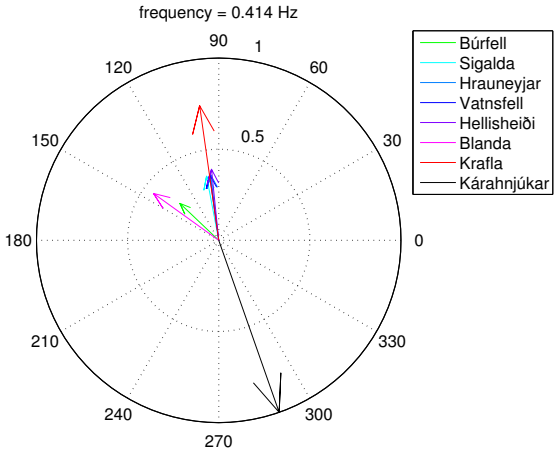

(c) Load 560 MW Gen. 520 MW

Figure 3.28: Magnitude and phase of generator speed

As seen from the speed curves in fig. 3.26 the generators on the opposite end of the system after the fault are the most dominant. What is quite interesting to observe here is that the frequency of the most dominant mode is around 0.46 Hz which is higher than when the areas were only connected with the northern transmission line and the southwest and the east on each side of the system. The electrical distance from the oscillating generators to the strong network seem to be a major influence on the frequency. Electrically the distance between the generators Kárahnjúkar on one side and Krafla and Blanda on the other side is much longer than between the two areas. So the frequency of the oscillations is much higher than expected and as stated before it is believed that having that strong network between them influences the dominant frequency of oscillations.
The peak of the damping curve is as before when the transfer is 75 MW between the areas as seen in fig. 3.17.

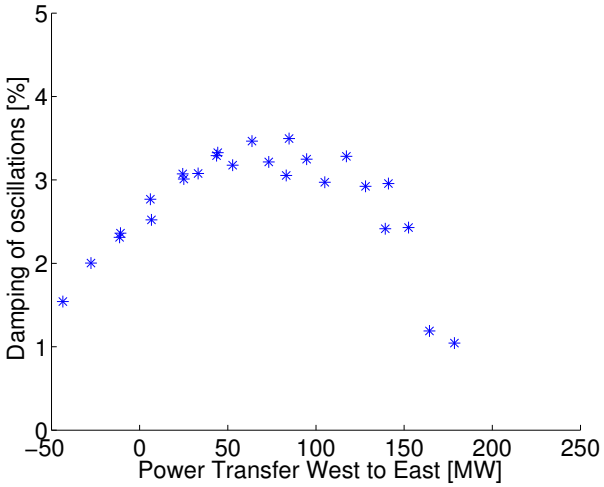

Figure 3.29: Damping of the dominant mode when power transfer is varied.

The maximum damping is around 3.5 % and the maximum power transfer is lower than compared to the case when you the fault is located in the east and have both lines in operation as in fig. 3.8. The damping declines as the power transfer is varied around the point with maximum damping. However it is observed that the damping declines faster when increasing the power transfer west to east. When compared with the case when Sigöldulína 4 was disconnected the damping is higher for this case.

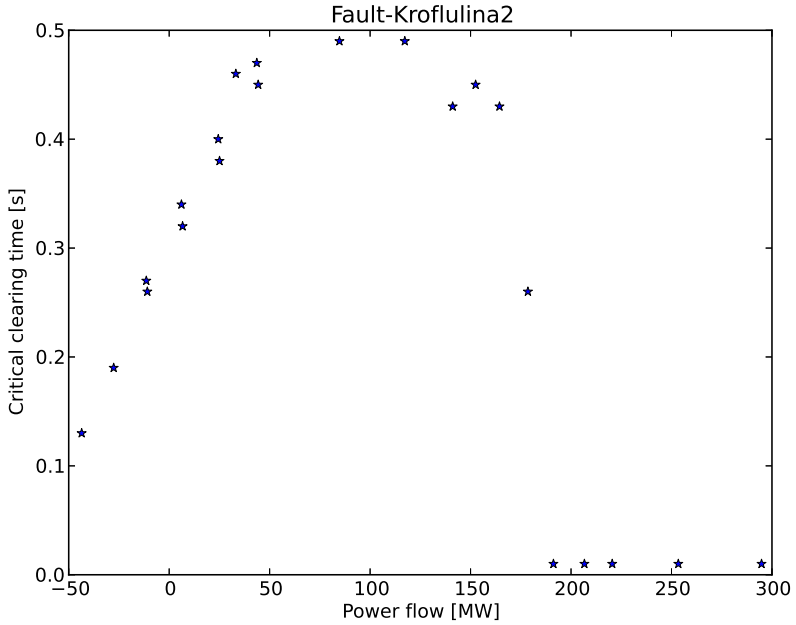

Figure 3.30: Critical clearing time of the faul with respect to power transfer.

The critical clearing time is now higher than when the fault was applied at the 220 kV bus close the east generation. Since the fault is located in the 132 kV network the generators closes to the fault specially Kárahnjúkar do not see the same voltage drop as before. This is because the reactance towards the fault is higher than when the fault is located within the 220 kV network. Therefore the generator Kárahnjúkar does not accelerate as fast as before and the critical clearing time has a higher peak than before. However the critical clearing time falls rapidly due to the fact there is a line disconnected and the power curve is lowered because of change in reactance.

3.7 PSS active

In the Icelandic Power system there are four power system stabilizers active at the following power plants: Hrauneyjar, Karahnjúkar, Krafla and Blanda. The main objective of those stabilizers is to damp the modes around 0.5 Hz. The Power System Stabilizers were implemented in PSS/E using the predefined models [15], the models that were chosen can be seen in table 3.3 and the parameters were obtained from Landsnet. In this chapter the effect of the PSS will be briefly analysed. The location for a PSS at Blanda is quite interesting since that generator does not even participate that much in the most dominant mode.

Table 3.3: Power system stabilzer models.

Plant	PSS model
Hrauneyjar	PSS2A
Kárahnjúkar	STAB2
Krafla	STAB4
Blanda	IVOST

To confirm the effectiveness of the PSS's on the damping of the oscillations two faults were analysed, a fault in the south west area at Búrfell and a fault on the transmission line Sigöldulína 4 will be studied in the next sections.

3.7.1 Fault at Búrfell

A fault is applied as before on the bus Búrfell for 100 ms in the southwest area and the dynamic response of the system observed. The power transfer over the cut can be seen in figure 3.31 for the cases described in table 3.1.

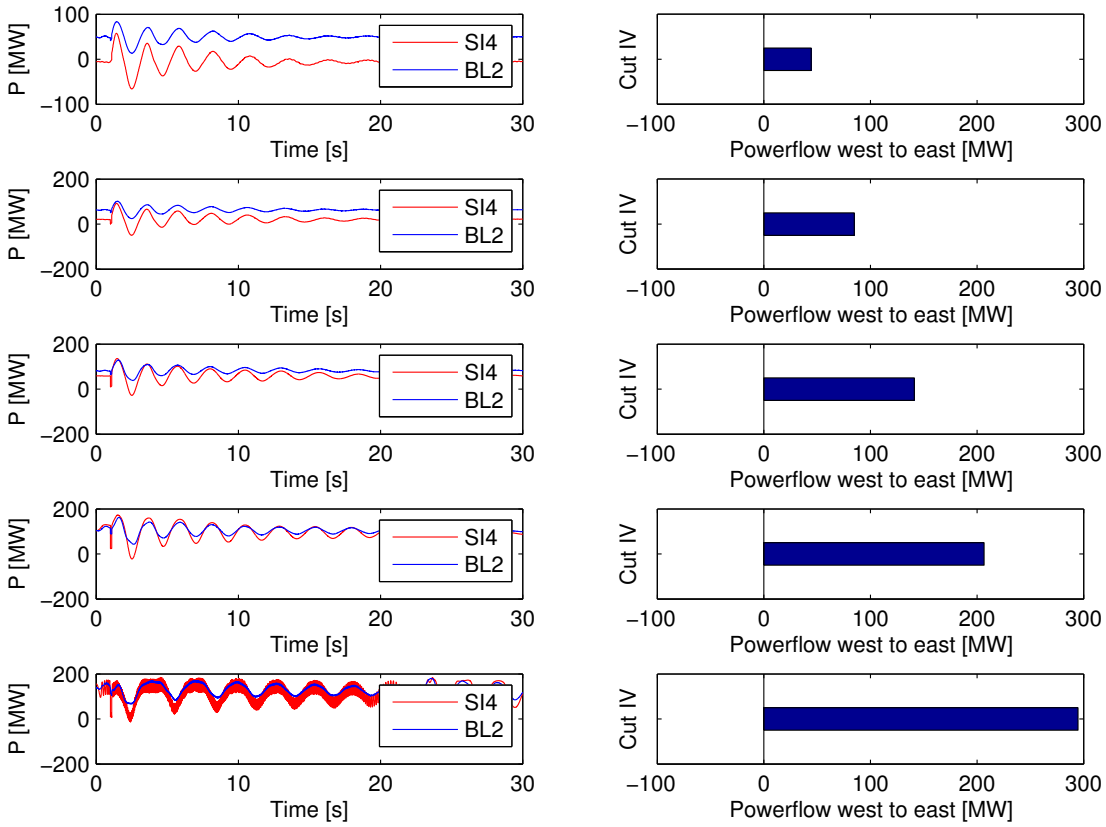

Figure 3.31: Real power transfer over cut IV, Load 560 MW

For the first three cases the system is stable, for the fourth case we have similar initialization problems as before and in the fifth case there seems to be a numerical oscillations due to limited step size in the solver. This is the same as for the case without pss, as the pss manipulates the voltage on the terminal to damp the speed of the machine following the fault. That increases the small signal stability and the damping in the system. However the factor most determining to the transient stability is the synchronizing torque which the pss has minimal effect on in a multi machine system except in special cases. In fig. 3.31 for the first case that there seem to be initialization problems of the power flow when the PSS's have been added which were not without the PSS's as seen in fig. 3.31. In the beginning an abnormal behaviour of the speed of Blanda can be seen in fig. 3.32.

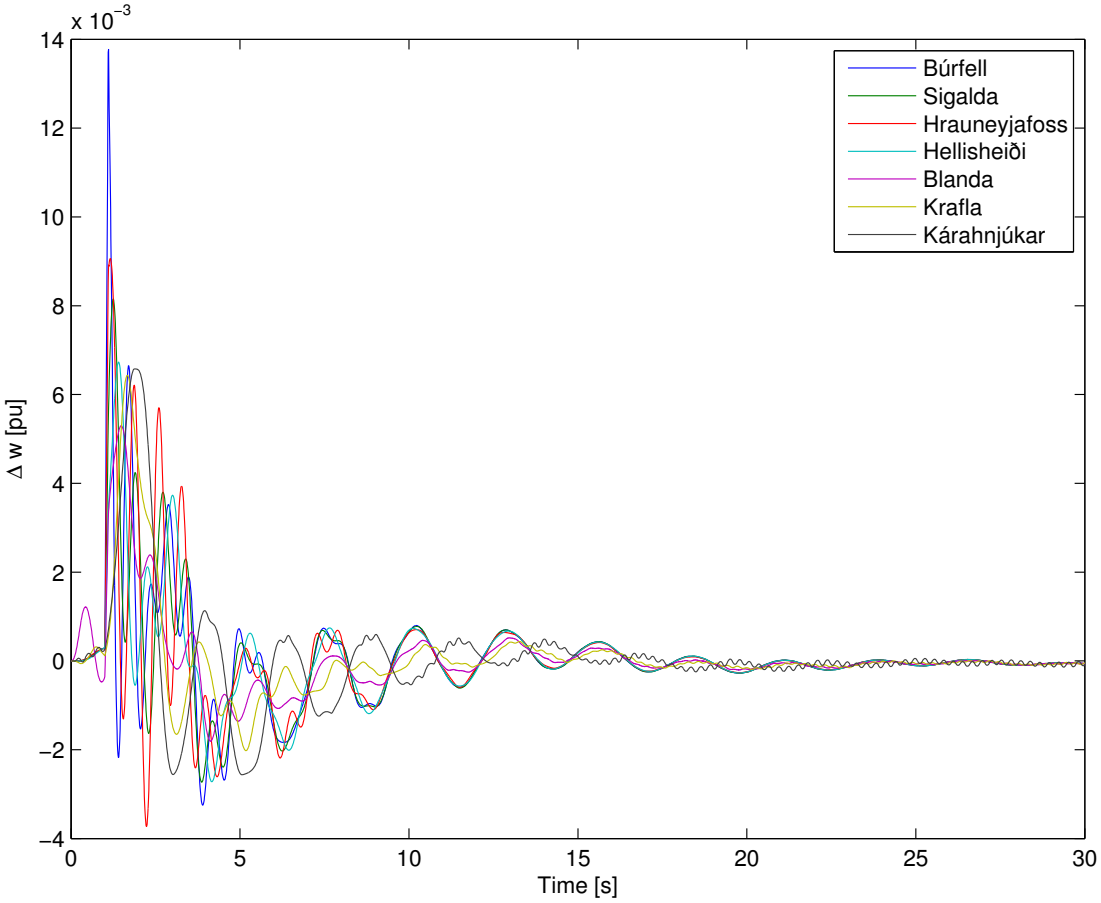

Figure 3.32: Change in speed of generators due to fault, Load 560 MW

So it is very likely that it is not tuned properly as the speed response of the generators as there is a ripple present in the speed response of the generators following a fault. Since PSS tuning is outside the scope of this thesis this will not be investigated further. The damping of the speed variation is much better than in the one without the PSS as seen in fig. 3.32. However a ripple can be seen in the speed response of Kárahnjúkar which is another indicator that something has to be retuned. However it is important to note that the initial speed variation of the generators is the same for the case without and with the pss active. This confirms what has been stated that the pss does not increase the transient stability of the system.
In fig. 3.33 the angle deviation following the fault can be seen with the pss active.

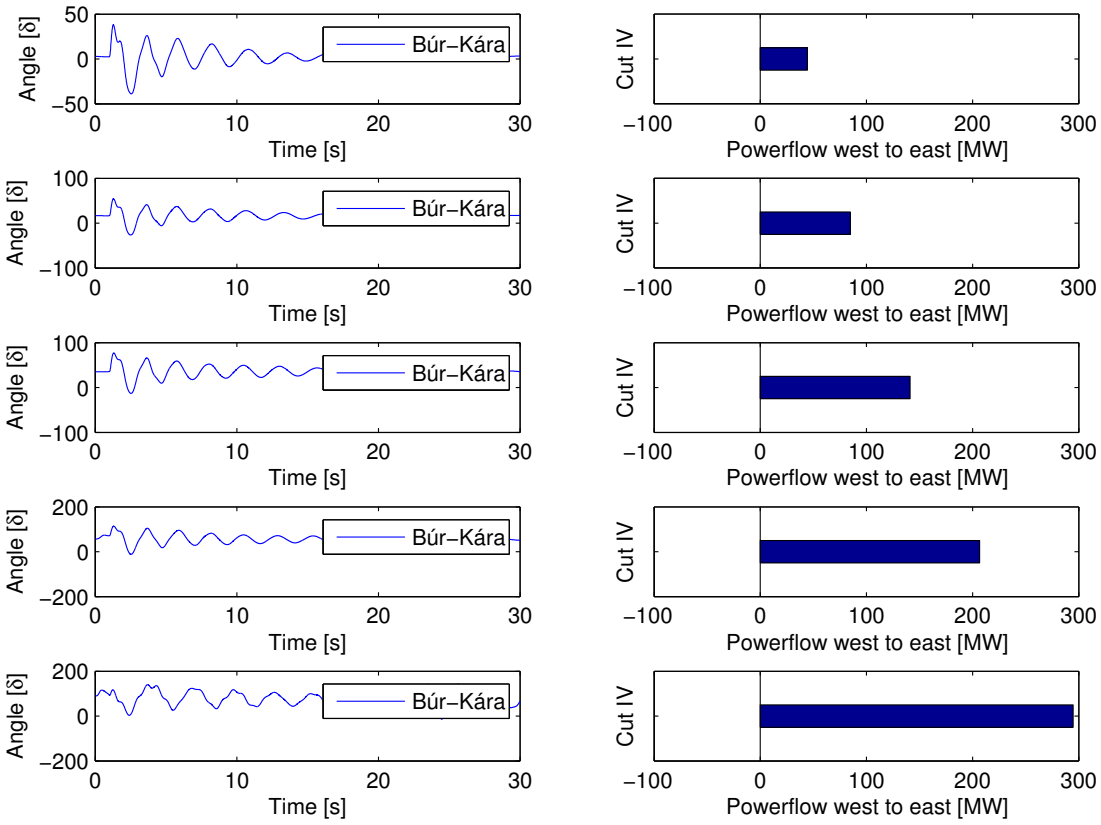

Figure 3.33: Change in angle of generators due to fault, Load 560

The angle difference between the east and the west can be seen in fig. 3.33. The improvement compared to fig. 3.6 is quite evident, in other words the damping is improved of the angle variation following a fault.

3.7.2 Fault at Sigöldulína 4

100 ms fault was applied at 132 kV bus in Sigalda and then the transmission line Sigöldulina 4 disconnected which is a part of the southwest ring. The power transfer over the stability cut can be seen in fig. 3.34 for the cases described in table 3.1.

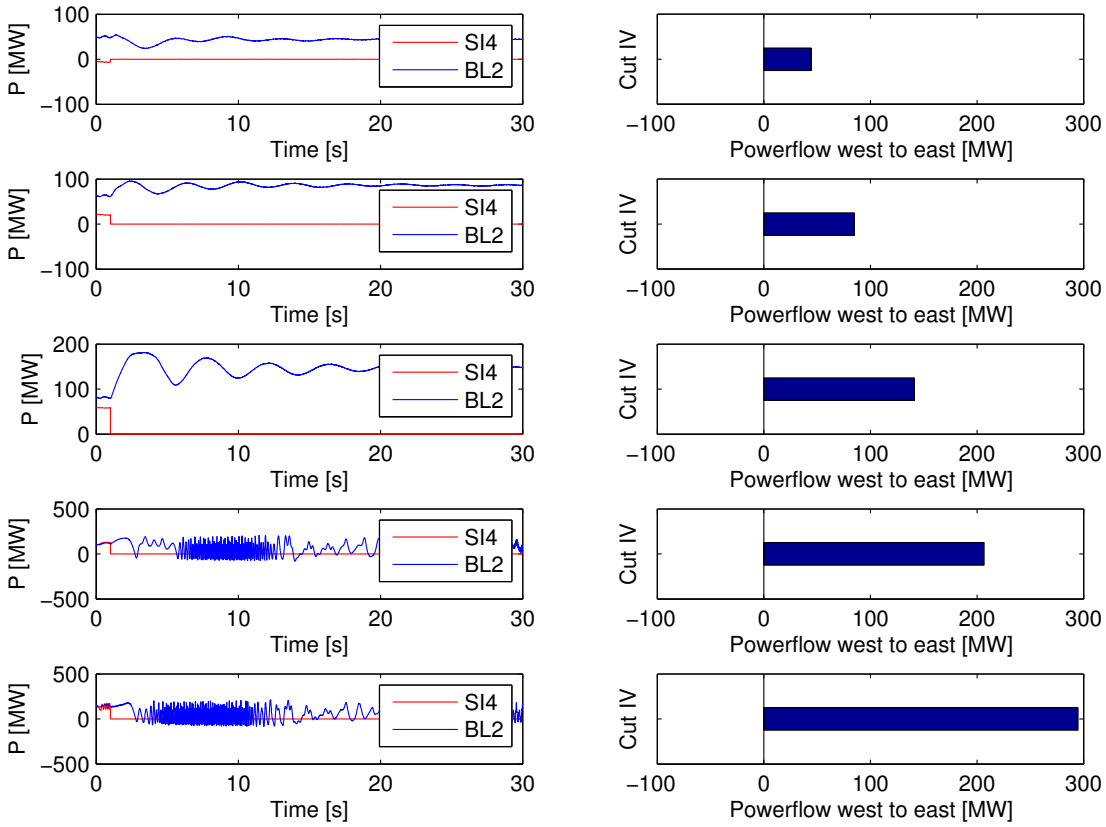

Figure 3.34: Real power transfer over stability cut iv, Load 560 MW

For the first three cases the system is stable, however for the last two cases the system loses synchronism following the disturbance. As stated before the PSS's does not increase the transfer limits between the areas however it improves the damping significantly. It is also quite clear in fig. 3.34 that the frequency of the oscillations between the areas has changed if compared to 3.13.

When fig. 3.35 is compared with fig. 3.33 it is observed that the variation in speed is less when the fault is applied at the 132 kV than at 220 kV.

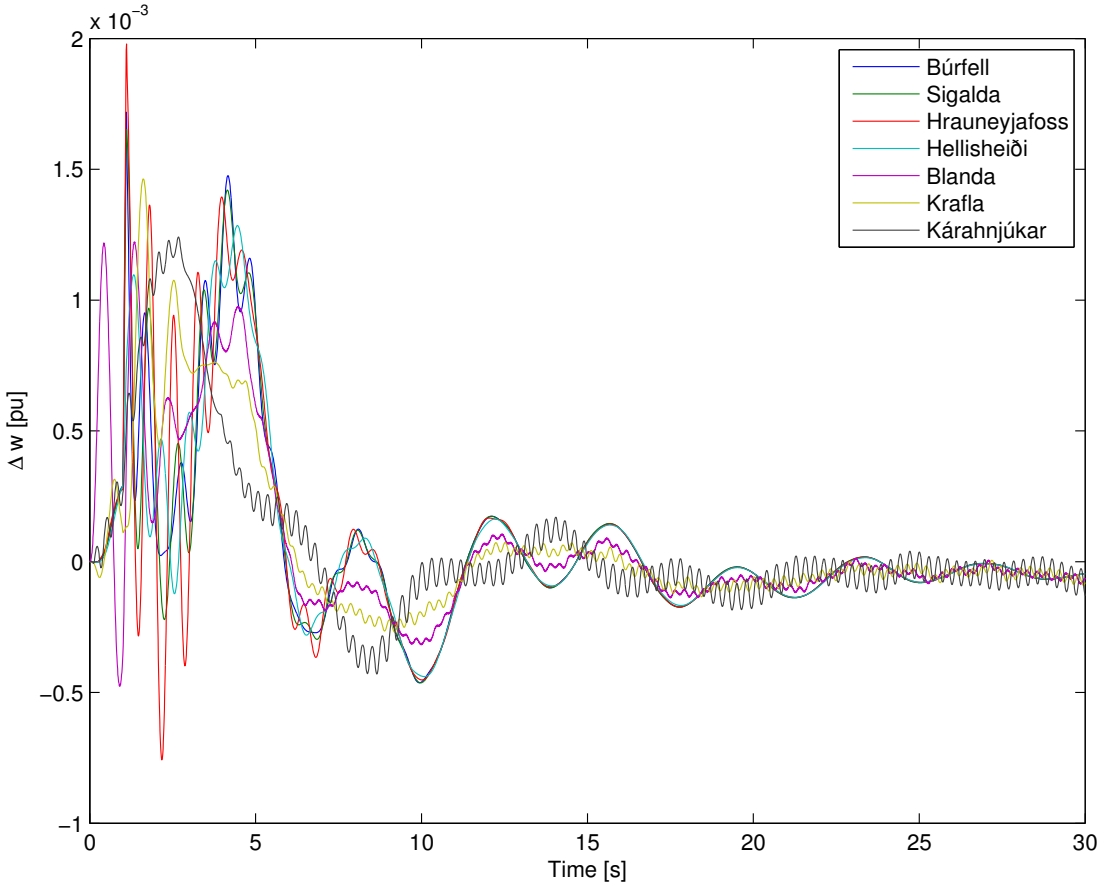

Figure 3.35: Change in speed of generators due to fault, Load 560 MW

There is however apparent a ripple in the speed response of the generator Kárahnjúkar and as before there is an initalization problem with Blanda. The PSS's are tuned around 0.5 Hz so there is a possibility that their tuning is not optimal for the dominant frequency when a line is disconnected.
In fig. 3.36 the angle deviation following a fault can be seen.

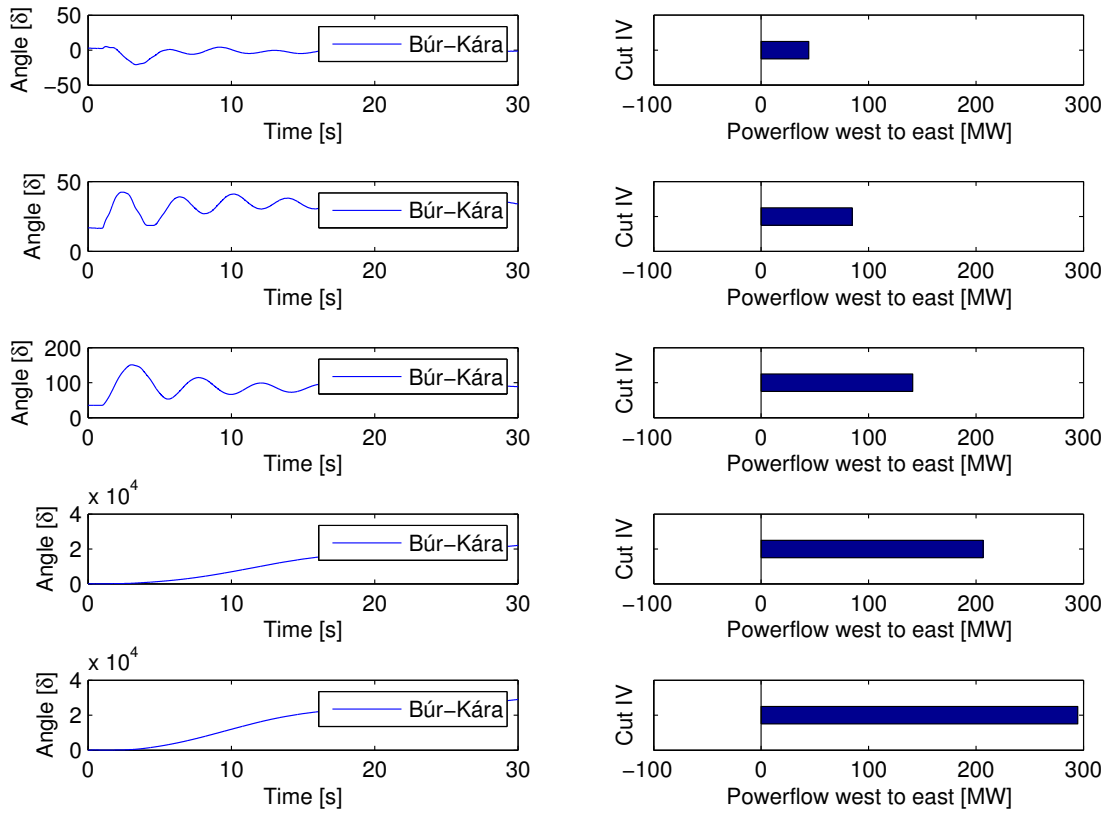

Figure 3.36: Load 560 MW Angle difference between generators in the soutwest and the east area

The frequency of the oscillations have lowered to around 0.2 Hz compared with around 0.3 Hz without the pss's active. As stated before the pss will aid the damping of the system but in general does not aid the transient stability limits due to the fact that the synchronizing torque is the determining factor.

3.8 Summary

As shown in this chapter the power transfer between areas is limited by transient stability. The fault location determined the acceleration of the generators following a fault. Faults within the 220 kV areas of the Iceland grid caused the most acceleration while faults in the interconnection between the areas, made the generators accelerate less due to the difference in voltage drop at the terminals of the generators. This has the effect that the critical clearing time was different for different faults. However faults in the 132 kV interconnection with a loss of a transmission line were the faults that limited the power exchange between the areas due to the change of reactance following a loss of a transmission line. It was also shown how frequency of oscillations in the system and damping are affected by the reactance in the system. For the full system the frequency of oscillations between the area was around 0.5 Hz but when a transmission line was lost the frequency was lower. The damping in the system was also increased with higher

reactance. The peak of damping and cricital clearing time seemed to be around 75 MW for the full system. However altering the reactance did move this peak around as was seen for the damping. When the PSS's were implemented in the PSS/E model it showed improvement of the damping of inter-area oscillations, however it did not influence the transient stability as expected. A PSS's is located in Blanda although Blanda does not participate in the inter-area oscillations. Initialization problems were encountered when implementing the PSS's in the the full model of the system and a ripple was seen in the speed response following a fault. The parameters of the PSS's in the full system and the parameters of the generators do need further investigation.

4

Simplification of the Icelandic Power System

In this chapter the model of the Icelandic transmission system is aggregated in order to study the inter-area oscillations between the east and the west. The simplified model is modelled in Dymola [17] using the ObjectStab library [18].

4.1 Power system simplification

Power systems in general are large and complex systems. When working with power systems, detailed modelling can be quite cumbersome and they can become computationally heavier than needed. Because of this, the system model is quite often simplified depending on the phenomena of interest. When calculating the critical clearing time for different faults an iterative process is used find each value, therefore in this thesis simplification is needed to shorten the computational time. Furthermore, developing custom models for PSS/E is tricky as knowledge of Fortran is needed for writing such models. However when simplifying a dynamic model some assumptions are made and it is necessary to be aware of the limitations of the model following simplification. In the literature there have been published quite a few papers concerning power system equivalents as Zhukov's method and Dimo's method [4] for aggregation of nodes. In order to aggregate generators for power system reduction, the practice is to aggregate machines who show the same speed characteristic and are said to be electromechanically coherent. In fig. 3.4 the oscillations between the two areas area can be observed. If the speed of the machines in fig. 3.5 are observed, it can be seen that immediately after the fault that the machine's in the south-west part of the system are oscillating against each other until they become electromechanically coherent and oscillate as a group against the east of the system. Since local modes are of no interest here this is enough justification that they can be grouped to together as a one equivalent generator.

Since the focus of this thesis is mainly on the inter-area oscillations between the south

west system and the east part, the generator inertia connected to the 132 kV ring connection, that participate in the dominant mode, are summed up to become part of two big generators. As has been shown the generator in Blanda usually does not participate in these oscillations. However due to voltage stability issues the generator Blanda is kept in the system to improve the power exchange between areas. The load flow into radial connections is observed and they are modelled as ZIP loads as described in (2.46) and (2.47), directly connected to the power system. The areas that were aggregated can be seen in fig. 4.1.

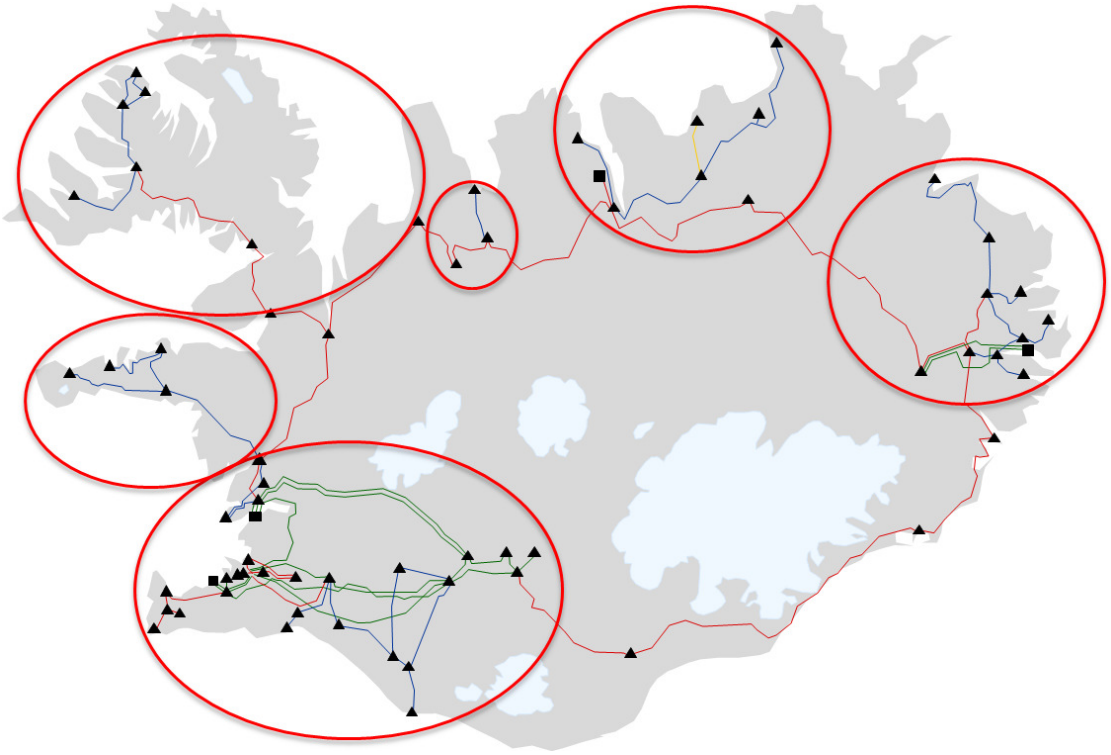

Figure 4.1: Aggregated area of the power system

For the aggregate generators the model of choice is the 5th order generator model as described by eq. (2.38) to (2.42). Hydro generators in the Icelandic transmission system are modelled as a 5th order model in PSS/E but the geothermal units are modelled as a 6th order generators. Since the Icelandic Power System is hydro dominant this is approximation is acceptable. Equivalent generation units were aggregated using REI-equivalents as described in section (2.8). The assumption is made that south west area is lossless and the voltage is 1 p.u. This simplifies the equation so the equivalent base power of each area is

$$S_{eq} = \sum_{i=1}^{N} S_i \tag{4.1}$$

where N is the generator number in that area. Generator ratings are summed up, based on their participation in the most dominant mode for the system without the PSS's active. When

eq. (2.52) was used to calculate the equivalent parameters, the result was not reasonable when compared to other generators p.u. values. However if the parameters were calculated using the weighted short circuit power the results was more ”reasonable” as compared to [19]. For example the subsynchronous reactance was then calculated as follows

$$x_{dg}^{''} = \frac{1}{S_{eq_g}} \sum_{i=1}^{N} x_{di}^{''} S_i. \tag{4.2}$$

The resulting parameters for the generators were then calculated and can be seen in table 4.1.

Table 4.1: Parameters for the aggregated generators

Generator	Southwest Gen	East Gen	Blanda
Sbase	1864 MVA	1097 MVA	162 MVA
$T_{d0}^{'}$	6.32 p.u.	8.6 p.u.	5.3 p.u.
$T_{d0}^{''}$	0.061 p.u.	0.037 p.u.	0.06 p.u.
$T_{d0}^{''}$	0.63 p.u.	0.258 p.u.	0.17 p.u.
H	4.29 p.u.	3.52 p.u.	2.75 p.u.
D	0	0	0
X_d	1.38 p.u.	1.1 p.u.	0.931 p.u.
X_q	1.11 p.u.	0.72 p.u.	0.5500 p.u.
$X_d^{'}$	0.255 p.u.	0.292 p.u.	0.23 p.u.
$X_d^{''} = X_q^{''}$	0.2087 p.u.	0.195 p.u.	0.17 p.u.
X_t	0.1 p.u.	0.1 p.u.	0.1 p.u.

For the control system as described in sections 2.6.1 and 2.6.2, the control parameters for the equivalent were selected. For the AVR the excitation systems of the areas were observed and a average time constant evaluated. In table 4.2 the control parameters for the south west generator can be seen.

Table 4.2: Parameters for excitation,PSS and governor system for the south west generator

AVR		**PSS**		**Governor**	
K	100	Kstab	1	w_{ref}	1
Tr	0.025	Tw	10	Pm_{max}	1.05
Efmax	7	T1	0.05	Pm_{min}	0
Efmin	0	T2	0.02	R_{dyn}	0.8
		T3	3	R_{stat}	0.0.4
		T4	5.4	T_r	5
		vsmax	0.2	T_w	1
		vsmin	-0.2	$Gate_{Max}$	0.95
				$Gate_{Min}$	0

The PSS parameters were adopted from the two area Kundur system since it has the same frequency of oscillations [19]. However the gain of the PSS in the south system was changed to 1 due to the fact that only the AVR control at Hrauneyjar is accompanied by a PSS. Furthermore too high gain on the PSS in the Southwest area made the damping to good compared to the full system. The governor parameters were adopted from the Nordic 32 system. However the governor parameters are not of great interest since there is loss of load or generation during the simulations and the governor system is usually much slower than the excitation system.

Table 4.3: Parameters for excitation, PSS and governor system for the east generator

AVR		**PSS**		**Governor**	
K	100	Kstab	10	w_{ref}	1
Tr	0.05	Tw	10	Pm_{max}	1.05
Efmax	7	T1	0.05	Pm_{min}	0
Efmin	0	T2	0.02	R_{dyn}	0.8
		T3	3	R_{stat}	0.0.4
		T4	5.4	T_r	5
		vsmax	0.2	T_w	1
		vsmin	-0.2	$GateMax$	0.95
				$GateMin$	0

The parameters for the generator in Blanda were adopted from the PSS/E case, however it was not equipped with an PSS due to the fact that it showed some stability problems in the initialisation when it was implemented. Furthermore the tuning of the PSS is outside of the scope of this thesis. In fig. 4.2 the simplified model can be seen implemented in Dymola.

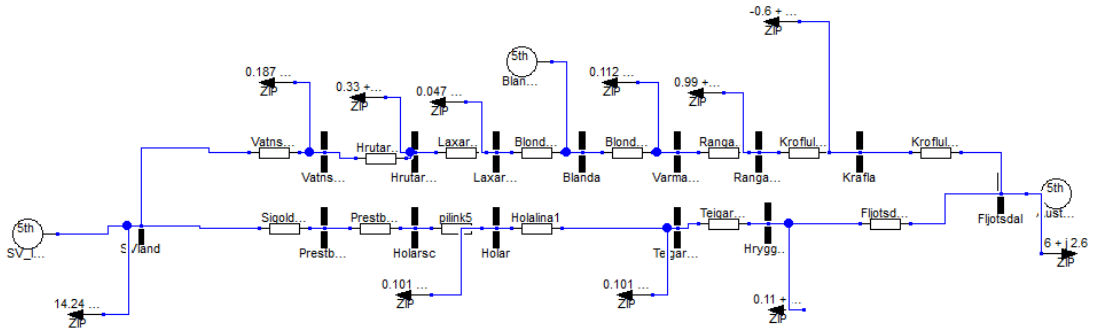

Figure 4.2: Simplified power system in Dymola

Three generators are connected to the simplified system to the southwest bus, to the bus Blanda and to the east bus. The loads were modelled as a ZIP loads where the real part of the load was 80 % constant impedance and 20 % constant admittance, and the reactive part was 20 % constant impedance and 80 % constant admittance, as described by (2.46) and (2.47).

4.2 Comparison

First the system was simulated without the PSS's active and a fault in the south west area analysed. In fig. 4.3. the oscillations over the stability cut can be seen for the full system in PSS/E as shown in Chapter 3.

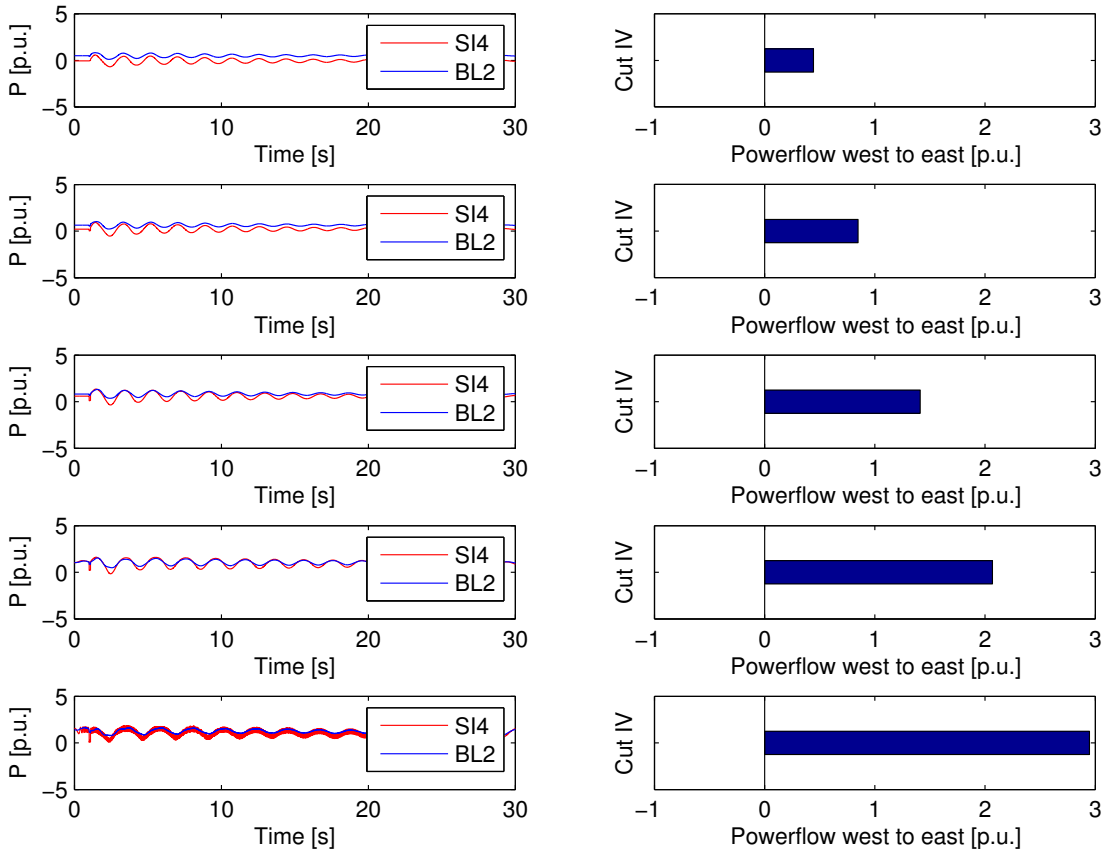

Figure 4.3: Load 560 MW and generation varied, active power flow over stability cut IV for the full system in PSS/E

Although the oscillations are poorly damped they do not grow in magnitude and seem to be a bit damped.

In fig. 4.4 the oscillations over the stability cut can be seen for the simplified system.

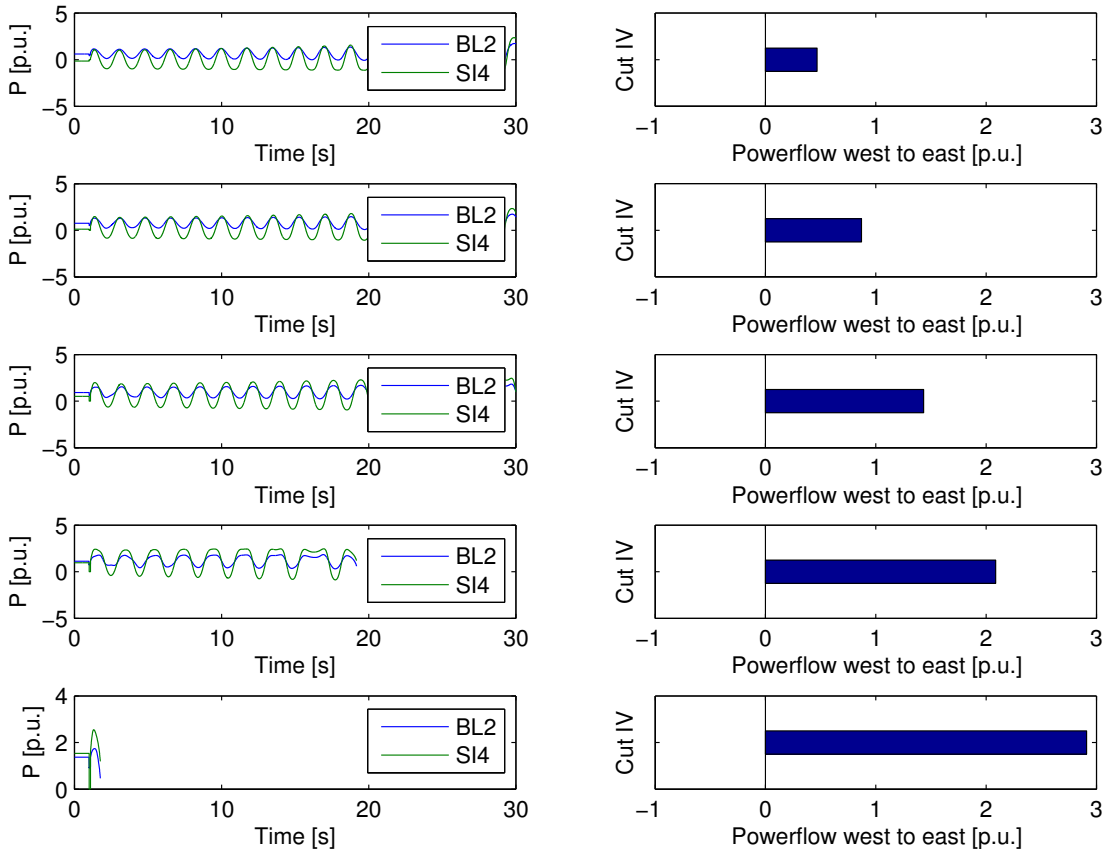

Figure 4.4: Load 560 MW and generation varied, active power flow over stability cut IV

Following this disturbance the system is experiencing oscillations that are undamped. In the last case the oscillations cause pole slip which ends the simulation. For the full system as seen in fig. 4.3 the inter-area oscillations are damped. The purpose of the AVR is to control the terminal voltage. Fast AVR action will improve the synchronising torque following faults by raising the terminal voltage beyond 1 p.u. However the inherit lag of phase of a fast AVR causes the excitation system to amplify low frequency oscillations as can be seen in fig. 4.7. Furthermore, the AVR that is used in Dymola is a rather simple one as seen in fig. 2.11 compared to all the excitation systems in the Southwest area [20].

In fig. 4.5 the oscillations over the stability cut can be seen for the full system in PSS/E with the PSS's active.

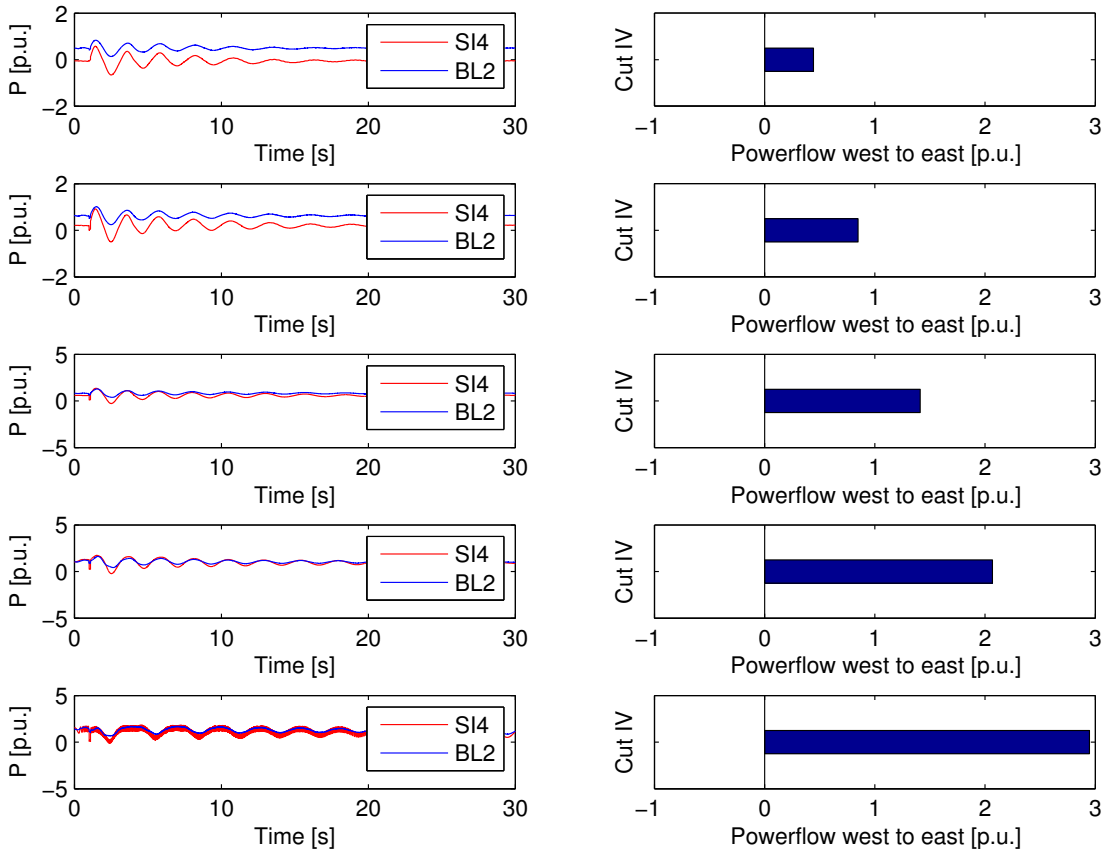

Figure 4.5: Load 560 MW and generation varied, active power flow over stability cut IV for the full system in PSS/E with PSS's active

The PSS's were then actived in dymola and simulation run again. As can be seen in fig. 4.6 when the PSS's are actived the damping of the oscillations has been improved compared to fig. 4.4.

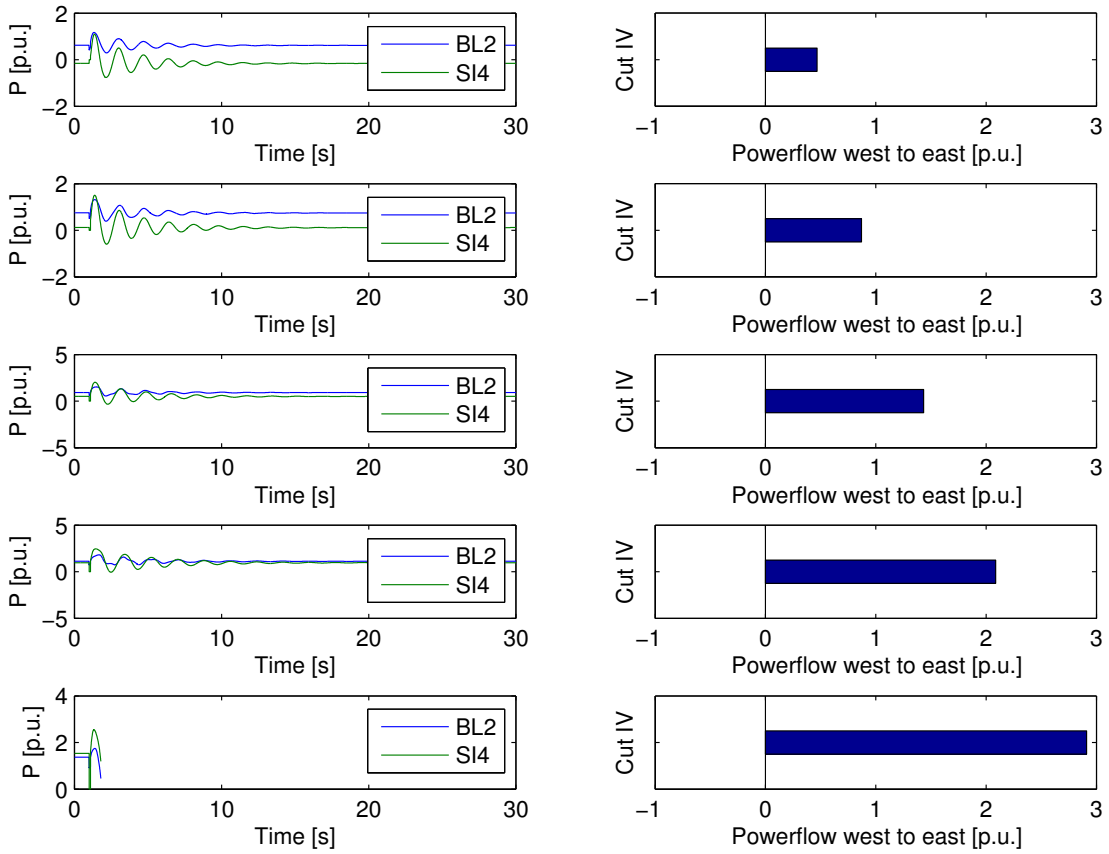

Figure 4.6: Load 560 MW and generation varied, real power flow over the stability cut IV with PSS's active

In the last case the power transfer between the areas is so high that after the fault a pole slip is detected and the simulation is terminated. The power oscillations are now similar to what can be seen in fig. 4.5. The damping is better for the simplified system, however our main interest are the first swings so this is acceptable.

In fig. 4.7 the field voltage, terminal voltage, generator speed for the south generator can be seen. Although the variation of the field voltage is very small it is able to stabilise the angular oscillations.

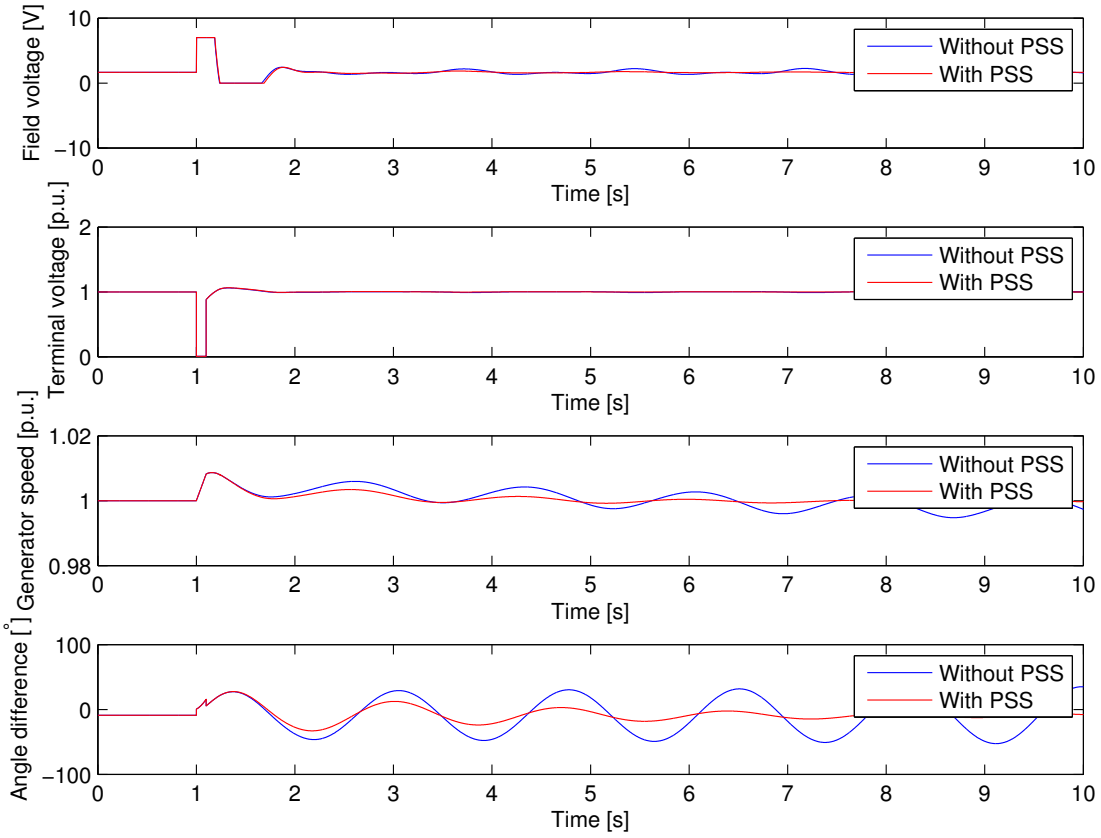

Figure 4.7: Basecase with and without pss installed

4.2.1 Critical clearing time

The critical clearing time of the different fault cases was then calculated using simulations when the angle deviation was greater than 180 degree. In fig. 4.8 the critical clearing time of the faults can be observed.

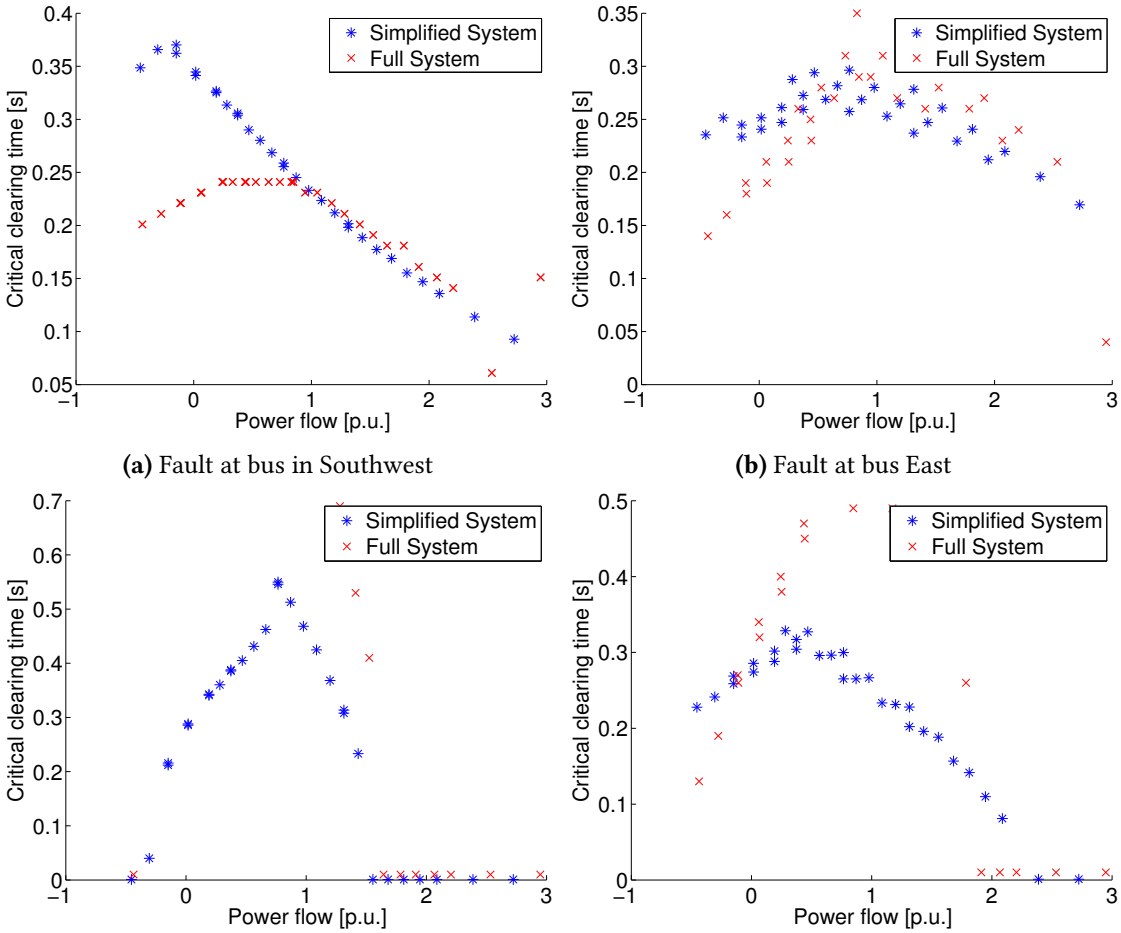

(a) Fault at bus in Southwest

(b) Fault at bus East

(c) Fault at Sigöldulina 4

(d) Fault at Kröflulína 2

Figure 4.8: critical clearing time of different faults

For the first case when there is a fault in the Southwest area as seen in fig. 4.8a, when powerflow to the East is increasing the critical clearing times are similar but however deviate as the power flow is varied to the south. It is very likely that this is caused by the over simplification of the system in the Southwest. When a fault is applied in the East as seen in fig. 4.8b both magnitude and critical clearing times are of similar magnitude except when power flow to the Southwest area is increased. For faults which should mimic faults in the 132 kV a higher fault impedance was applied. The limits when the system crashes are similar to the full system for both cases. In fig. 4.8c the fault that should mimic fault on Sigöldulína 4 is seen. The critical clearing time for the full system is very high compared to the low critical clearing times of the simplified systems. For fault impedance mimic faults on Kröflulína 2 the cases are similar although the full system shows higher clearing time than the simplified one. However this is beleaved to be sufficient for simulation of fault at Kröflulína 2.

In general the simplification of the power system is thought to be sufficient when studying faults in the east and wind power integration there.

4.3 Summary

In this chapter the system has been simplified into two area systems, but the transmission lines are kept between the areas. It was important to keep the generators in Blanda so the loadability of the system was similar to the original case. The frequency of oscillations was the same due to the same reactance between the areas. For faults within the strong parts the fault reactance was set very low so the voltage dropped close to zero. For simulating faults in the 132 kV grid a higher fault reactance was applied. Faults in the east, in the simplified model showed similar characteristic as for the full system. For faults in the south when considering power flow to the east, showed similar behaviour although the critical clearing angle for fault on the 132 kV with loss of line gave lower critical clearing time than for the full system. The conclusion was that the model was sufficient for the study of inter-area oscillations but aggregating the whole south system is a rather rough approximation. However it is assumed to be sufficient when working power import into the east part of the system and faults in that area.

5

Wind integration into the eastern part of the Icelandic Power System

In this chapter wind generation is connected to the eastern part of the Icelandic Transmission System. Different levels of wind generation are analysed as well as different scenarios for power flow over the stability cut.

5.1 Description

In the last years there has been an increase in the demand of electricity in the eastern part of Iceland. This is mainly due to local fishing industries have switched from using oil to generate electricity, to be directly connected to the grid [1]. In some areas of Iceland, this can easily be done due to local strong grid, but in many areas the possibilities are limited due to system constraints and these industries need to be curtailed during unfavorable reservoir levels of hydro power plants etc. This has been the case for the eastern part of Iceland and therefore it is of great interest to increase the generation in that area in order to meet the increasing demand. Additional generation in that area can delay transmission system expansions and therefore reduce the total system cost. The National Power Company has in recent years, been working on analysing the wind conditions in Iceland and the location shown in fig. 5.1 has shown promising results [21].

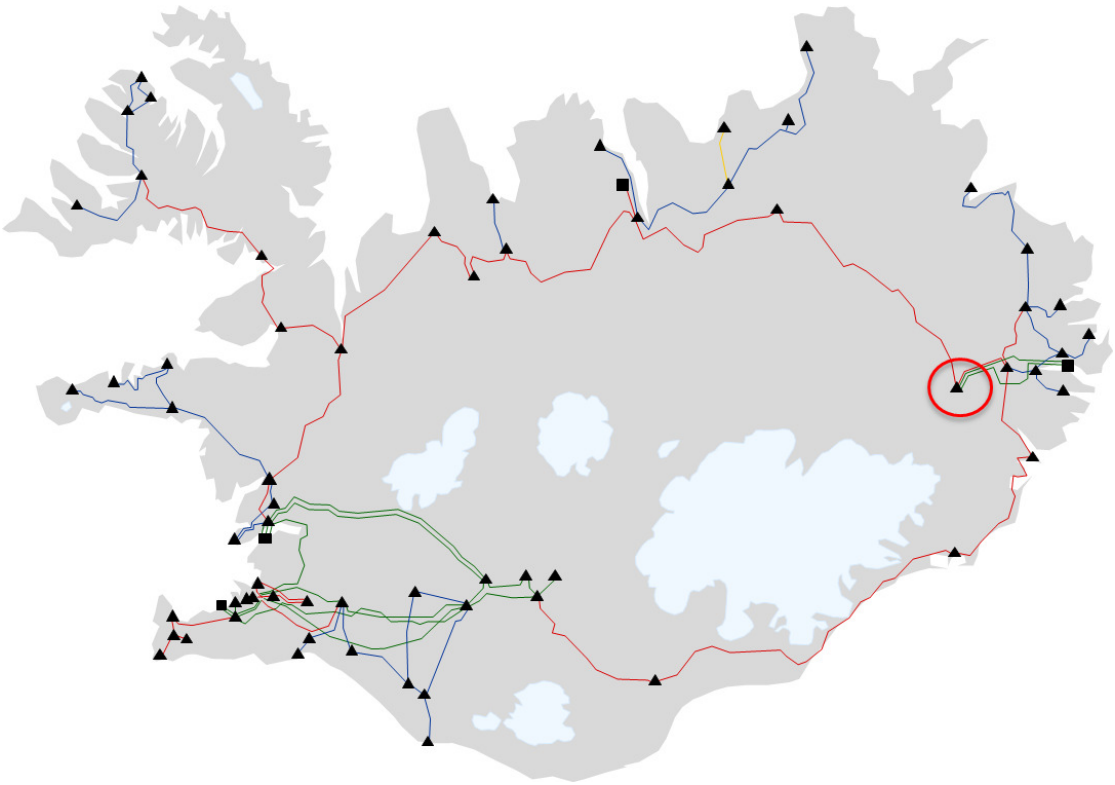

Figure 5.1: Location for integration of wind power into the Icelandic Power System in this study

The benefit of that location is that there is a large hydro power plant with a large reservoir nearby, which can be used to store electricity when the wind is blowing and can compensate during low wind periods. However, power flow into this area depends on the stability of the system as has been shown in previous chapter. If such wind integration is to be carried out it is of utmost importance to realise whether it will affect the stability limits of the system. Two different sizes of wind generation are simulated, 100 MW and 200 MW. Both the cases of full generation and no generation with the wind farm connected are considered. For 100 MW windfarm the increase of load in the east area is 50 MW. The hydro generation is reduced by 50 MW for full generation of the wind farm and increased by 50 MW for no generation. When considering 200 MW windfarm the additional load is set to 100 MW and the hydro generation decreased by 100 MW for full wind generation and increase by 100 MW for low wind conditions. In fig. 2.17 the limit of the VSC converter can be seen. In this thesis the limit which depends on the grid voltage is not considered. The reason for that is during faults with large clearing times, after the fault the voltage of the grid rises due to the fact that the simple excitation system accumulates a large error for long fault times. This leads to such a high voltage levels that block the converter for the reactance that was used. For such cases the output of the model became unreasonable as the converter was uncontrollable. Furthermore a rather simple model of the excitation system is used so the voltage rise following the fault can be higher than expected. This makes it very hard to compare the basecase with the wind cases.

The maximum converter voltage would have to be increased in order to withstand faults with a very long clearing time. In reality this is a question about optimising the cost and the security of the system. In fig. 5.2 the model implementation in dymola can be seen. The parameters for the windfarm can be seen in table 5.1.

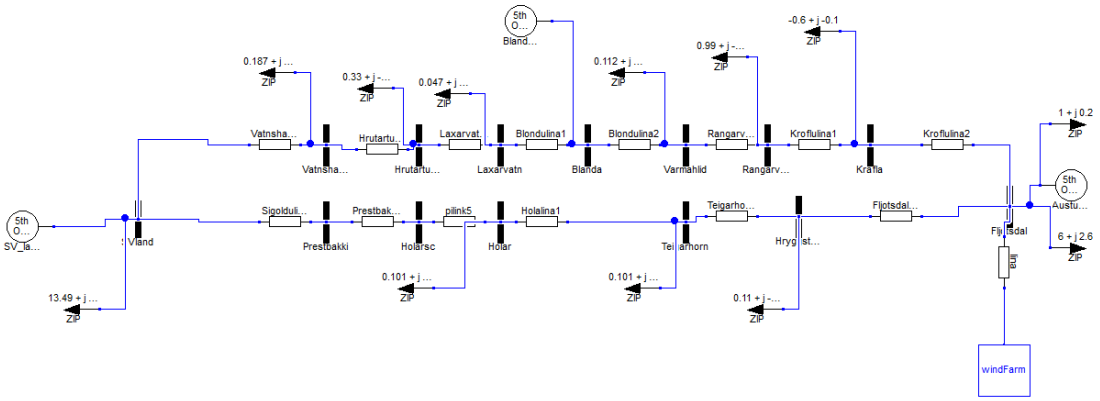

Figure 5.2: Implementation in Dymola

Table 5.1: Parameters for the windfarm

Parameter	Value	explanation
U_{dc}	1 p.u.	DC voltage
$U_{ac_{nom}}$	1 p.u.	Nominal ac voltage
R_t	0 $p.u.$	Transformer Restance
X_t	0.10 $p.u.$	Transformer Reactance
n_t	1 $p.u.$	Transformer Ratio
X_r	5 $\%$	Phase reactor inductance
C_{filter}	0.0015 p.u.	Filter Capacitor
K_0	1.235163	Modulation constant
K_{pI}	0.4727	Inner current controller proportional gain
K_{pQ}	0.4	Reactive power controller proportional gain
K_{iQ}	70	Reactive power controller integral gain
K_{pU}	11.66248	U_{pcc} controller integral gain
K_{iU}	5.831238	U_{pcc} controller integral gain
K_{pd}	2.33356	DC voltage controller integral gain
K_{id}	49.5	DC voltage controller integral gain
K_{iP}	49.5	Active power controller integral gain
m_{max}	1	maximum modulation ratio
m_{min}	0	minimum modulation ratio
$I_{r_{max}}$	1 p.u.	maximum real current
I_{max}	1.1 p.u.	maximum current
X_{line}	0.1 p.u.	Reactance of transmission line

The same fault cases as applied for the full system were analysed for the wind integration for different power flow and different clearing time. For the scenarios two different conventional control methods for the wind farm were simulated, voltage control and reactive control.

5.2 Voltage Control

The voltage control uses a PI controller to calculate the Q_{ref} needed to achieve a certain V_{ref} at the point of connection of the grid. The stability of the system was analysed for four different faults. The critical clearing time for each case was then calculated.

The critical clearing time for the system was also calculated for varying power flow between areas and different fault cases.

5.2.1 Fault at the Southwest equivalent

Three phase fault is applied at the bus for the Southwest equivalent which represents the aggregated system in the Southwest Iceland. The voltages in the east and in the southwest, the real and reactive power injected by the converter and the angle difference between the areas p.u. As shown by (2.4) oscillations in the angle difference will determine the power oscillations that will occur between the areas. In fig. 5.3 the voltages at the east bus and the Southwest bus can be seen for two different fault clearing times.

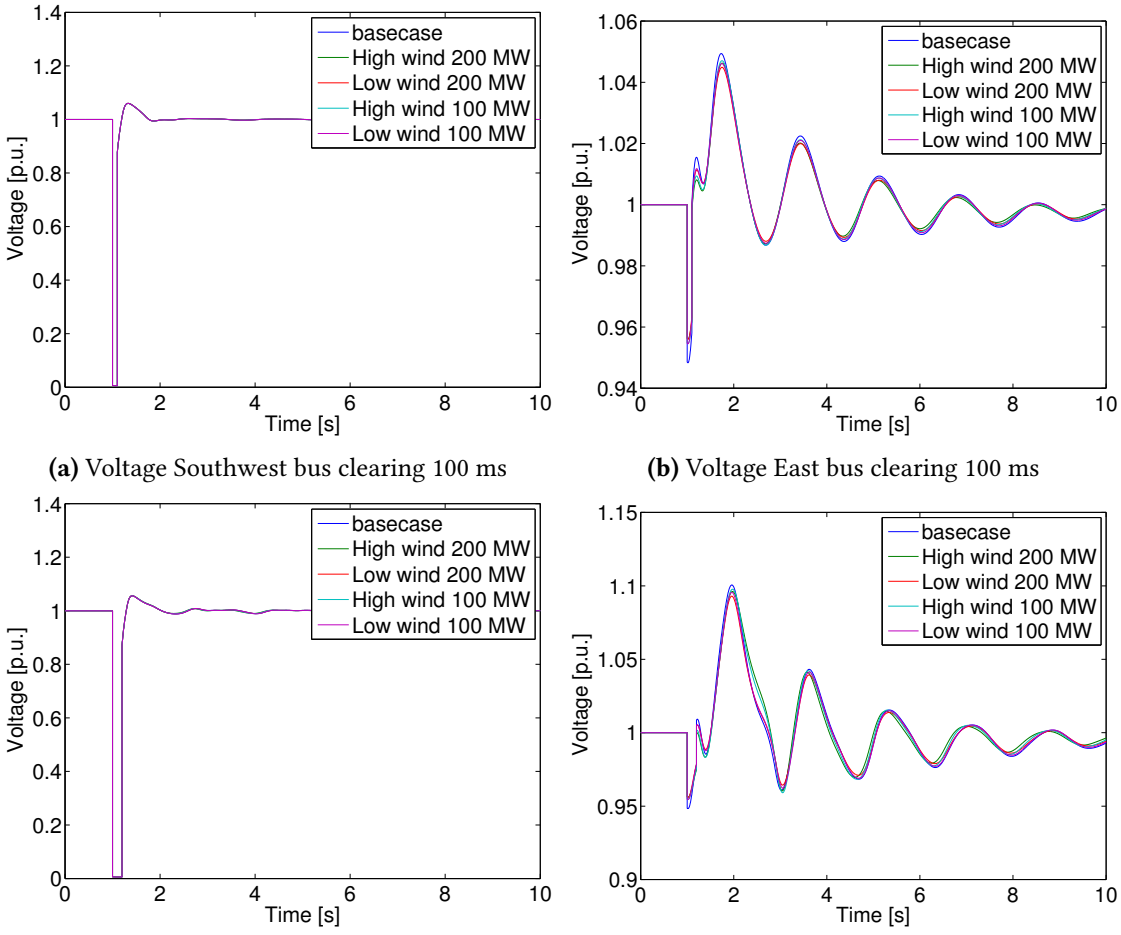

(a) Voltage Southwest bus clearing 100 ms

(b) Voltage East bus clearing 100 ms

(c) Voltage Southwest bus clearing 200 ms

(d) Voltage East bus clearing 200 ms

Figure 5.3: Voltages in the system following fault

When observing the fault in the south west part of the system there is not much difference between the cases. Since the fault is in the other end of the system the voltage deviation close

to the wind farm is not that great. The voltage control can though be seen in fig. 5.3d in action. For the base case the voltage varies more than with the windfarm since the windfarm tries to control the voltage at the point it is measured, at the terminals of the transformer. However that indirectly influences the voltage at the PCC, where the hydro power plant and the wind power plant are connected. Since there is more reactive capability when the windfarm is not producing power, in low wind scenario the wind farm has better capability of controlling the voltage. As the clearing time of the fault is increased the voltage rise following the fault is increased. This is because of more angle variations following longer clearing time.

In fig. 5.4 the real and reactive power injection of the windfarm can be seen.

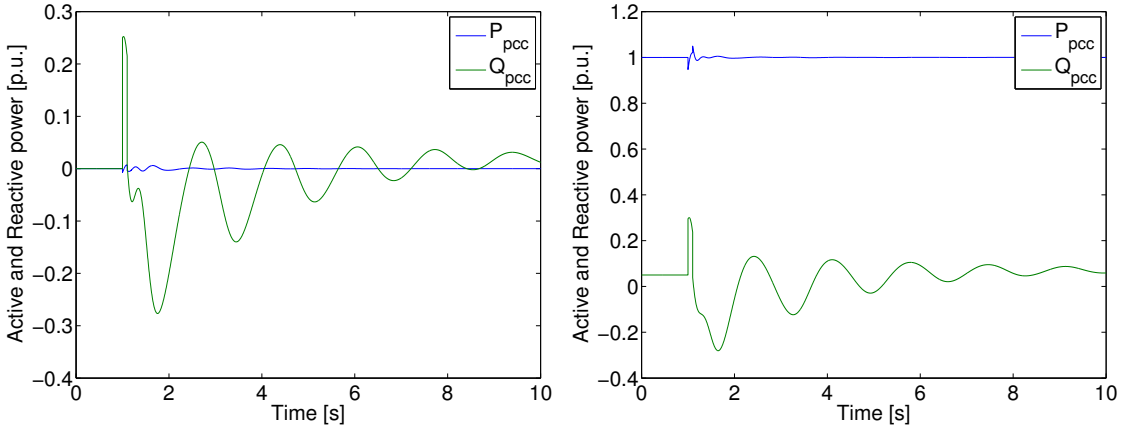

(a) Low wind scenario

(b) High wind scenario

Figure 5.4: Real and reactive power with 100 MW windfarm

The injection of reactive power into the system is very similar with slight deviation though which can be seen when focusing on the response just after the fault. After the fault the voltage rises at the PCC and the windfarm tries to control it by absorbing reactive power. As seen in fig. 5.4b the rating of the converter at full power is above 1 p.u., otherwise it would not contribute any reactive power to the grid during oscillations. In fig. 5.5 the angle difference between the generators in the East and the west can be seen following the fault for 100 ms and 200 ms clearing time.

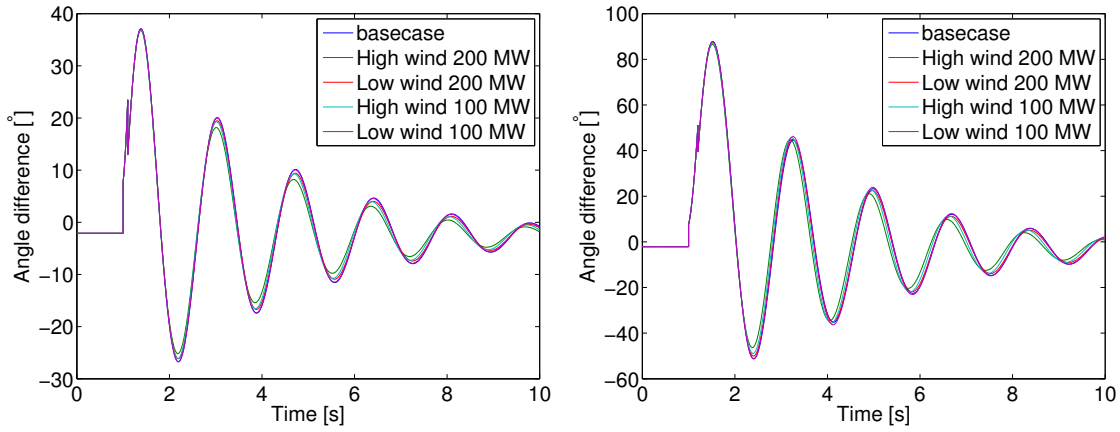

(a) Fault clearing time 100 ms

(b) Fault clearing time 200 ms

Figure 5.5: Angle difference in the system following faults with different clearing times

For this fault there is a minor difference and the wind farm does not have significant impact on the inter-area oscillations, however high wind does have positive impact on the damping of the system. It can also be seen that as the clearing time increases that the angle difference after the fault is increased. The reason for the small difference is that the generation in the east is varied. The voltage drop in the east area, following a fault in the Southwest, is quite low as can be seen in fig. 5.3d. Since the voltage drop in the east is low the generators where the generation is varied do not accelerate that much following a fault as seen in (2.27).

5.2.2 Fault at the East equivalent

A fault was applied to the bus at the East equivalent, which is where the hydro power plant and the wind farm are connected. Voltages in both end of the system, real and reactive power and the angle difference following a fault observed.

In fig. 5.6 the impact of the wind farm is much clearer since the fault is very close the connection point, therefore the voltage controller of the converter acts more trying to reset the voltages to it's reference.

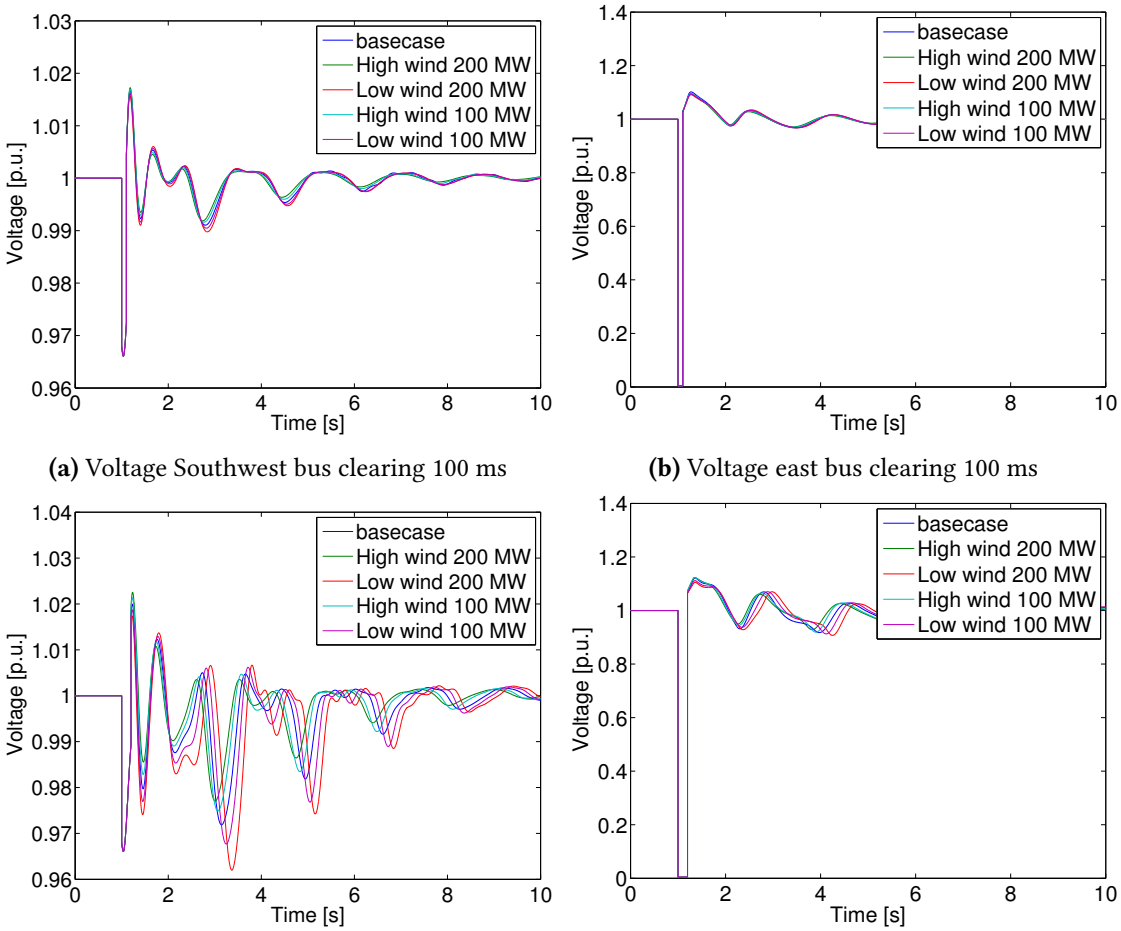

(a) Voltage Southwest bus clearing 100 ms

(b) Voltage east bus clearing 100 ms

(c) Voltage Southwest bus clearing 200 ms

(d) Voltage east bus clearing 200 ms

Figure 5.6: Voltages in the system following a fault

For high wind generation we reduce the apparent power coming from the hydro power plant in the east. Therefore the hydro power plant has more reactive capability following the fault. In fig. 5.6d it can be seen how during high wind that the voltage is boosted the most. This is mainly due to the automatic voltage control of the hydro generation.

As seen in fig. 5.7 the reactive injection to the system varies more than before.

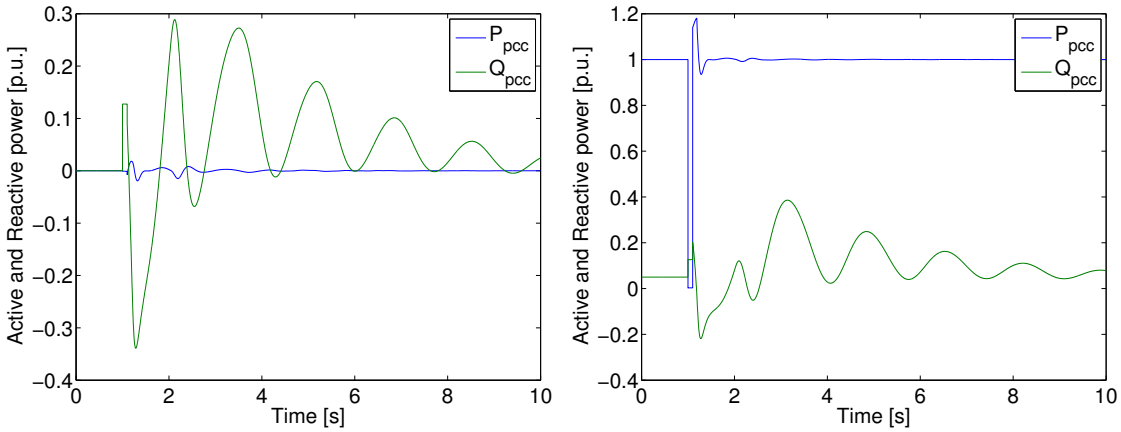

(a) Low wind scenario **(b)** High wind scenario

Figure 5.7: Real and reactive power with 100 MW windfarm

The converter is trying its best to control the voltage at the PCC and since during low wind scenarios the reactive capability of the hydro power plant is more constrained than for high wind scenarios it can be seen how the converter varies it reactive power input more, as seen in fig. 5.7a compared to fig. 5.7b.

The impact of a wind generation on the angle difference following a fault at East equivalent is quite evident as seen in fig. 5.8.

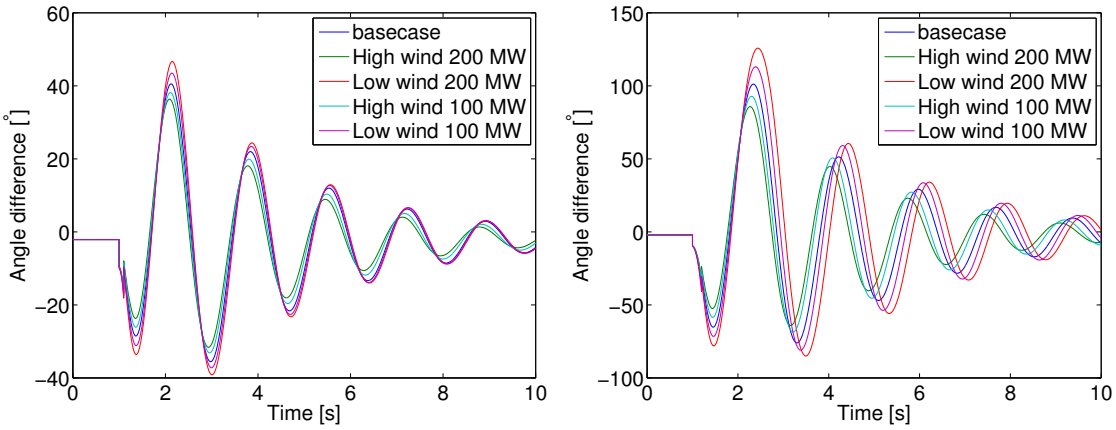

(a) Fault clearing time 100 ms **(b)** Fault clearing time 200 ms

Figure 5.8: Angle difference in the system following faults with different clearing times

During a high wind scenario the generation of the hydro power plant is reduced so its acceleration is slower during the fault which leads to lower angle difference. The opposite holds for low wind scenarios since then the hydro generation output has to be increased and the acceleration constant is higher. As the clearing time is increased this angle difference becomes clearer. The angle increase with low wind is much higher as expected according to

(2.26), as the mechanical power of the hydro generation is lower.

5.2.3 Fault at transmission line Sigöldulína 4

A fault is now applied at the Southwest bus with a reactance that simulates a fault on the 132 kV bus and the transmission line Sigöldulína 4 is disconnected. The fault reactance is lower then in the fault before to simulate the response of the system to a fault in the 132 kV interconnection.

In fig. 5.9 the voltage drop at the Southwest bus and the East bus can be seen.

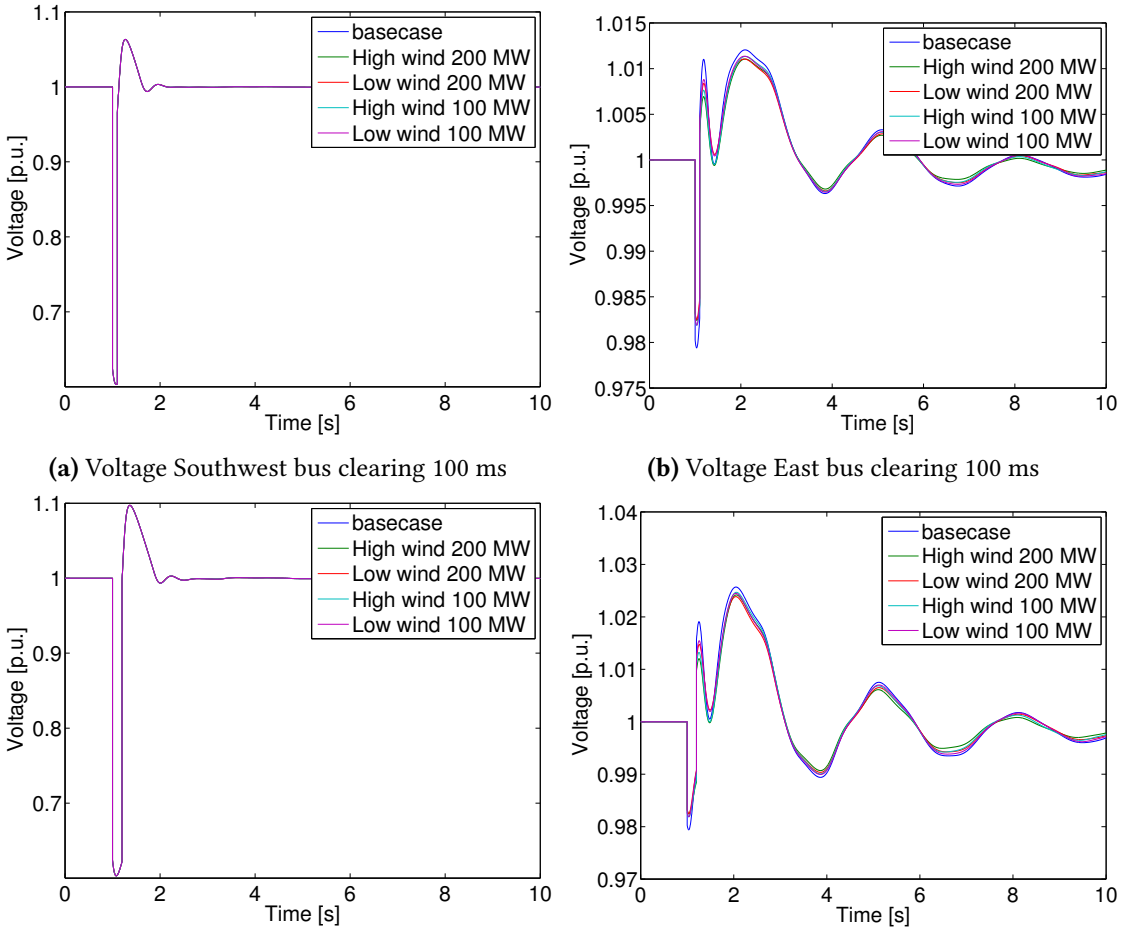

(a) Voltage Southwest bus clearing 100 ms

(b) Voltage East bus clearing 100 ms

(c) Voltage Southwest bus clearing 200 ms

(d) Voltage East bus clearing 200 ms

Figure 5.9: Voltages in the East and the Southwest following a fault

As seen in fig. 5.9 the voltage drop at the bus is reduced compared to fig. 5.3. This is due to the fact that when simulating the fault, a higher fault reactance was implemented, which leads to lower voltage drop during the fault. However due to the loss of a transmission line between the two areas the voltage will oscillate more than when the reactance was lower. That means that the wind up of the excitation will be less and we will have less voltage deviations

following the fault. This can be seen on fig. 5.9d and fig. 5.9b where the base case gives the most voltage variation. Since the converter does not need so much reactive capacity to control the voltage deviations both high and low wind case give better voltage control.

In fig. 5.10 the response of the wind farm to a fault in the Southwest part and disconnection of a transmission line can be seen.

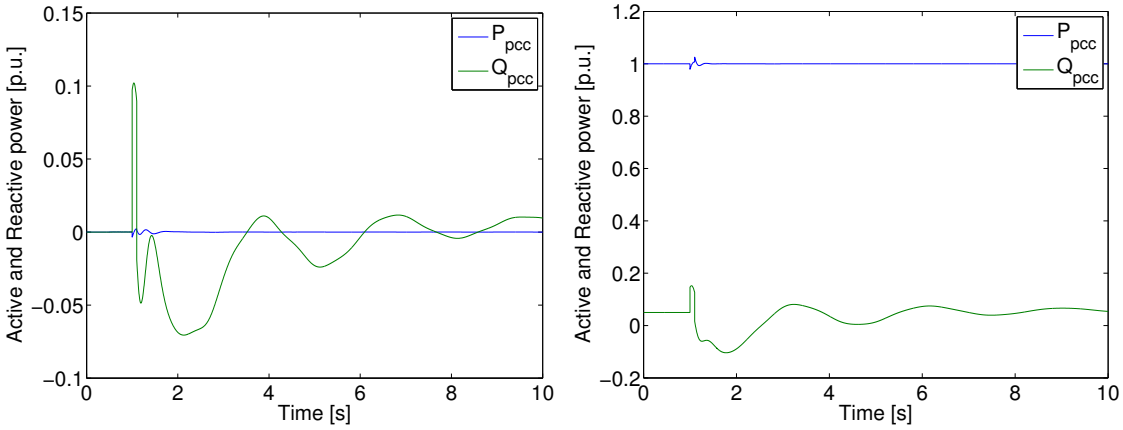

(a) Low wind scenario **(b)** High wind scenario

Figure 5.10: Real and reactive power with 100 MW windfarm

Since the fault is applied at the Southwest bus, and the voltage drop is lower than direct fault on the bus itself, the converter does not react as strongly to the fault as seen in fig. 5.4.

In fig. 5.11 it is seen how the angle does not increase as much due to lower voltage drop compared to fig. 5.5.

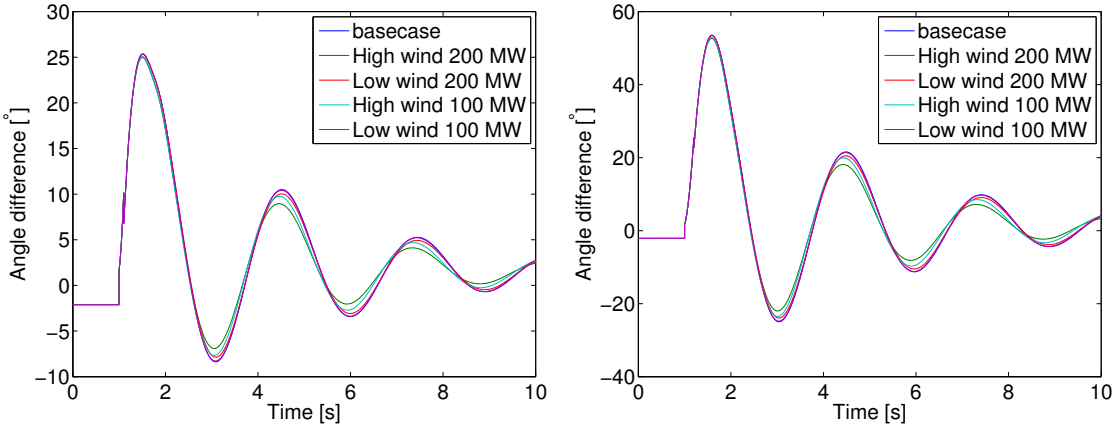

(a) Fault clearing time 100 ms **(b)** Fault clearing time 200 ms

Figure 5.11: Angle difference in the system following faults with different clearing times

There is not a major difference between the cases although the first and second swings

are slightly reduced for high wind scenarios. This is as before because of lower acceleration constant. The damping of the system is better for most of the wind cases.

5.2.4 Fault at tranmission line Kröflulína 2

Fault is now applied at the East bus with a fault reactance to imitate a fault in the 132 kV network. After the fault the transmission line Kröflulína 2 is disconnected. In fig. 5.12 the voltage for two clearing times, 100 and 200 ms, can be observed.

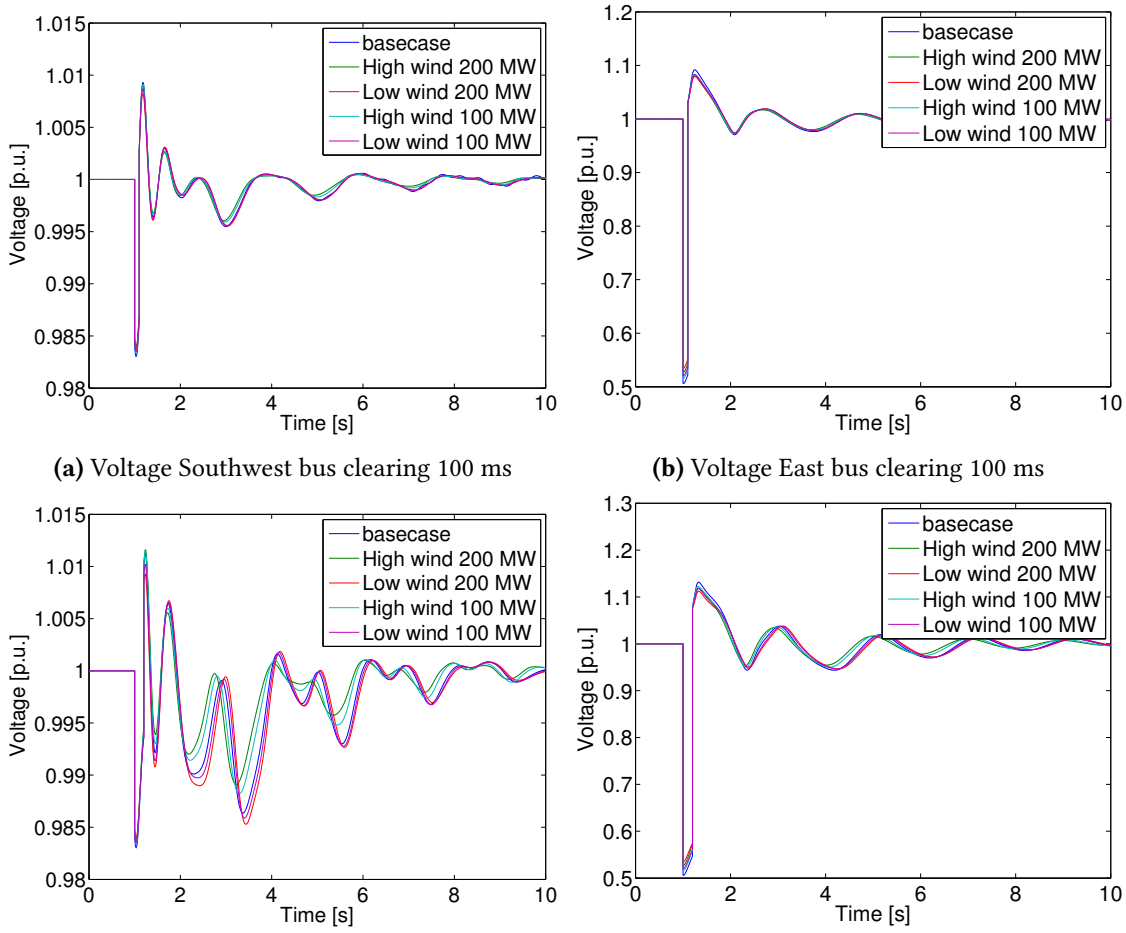

(a) Voltage Southwest bus clearing 100 ms

(b) Voltage East bus clearing 100 ms

(c) Voltage Southwest bus clearing 200 ms

(d) Voltage East bus clearing 200 ms

Figure 5.12: Voltages in the system following a fault

If fig. 5.12 and 5.9 are compared it can be seen that the voltage drop is greater for a fault close to the generator close to the generator in the east although the fault reactance is the same. The reason is that the short circuit power of the generators close to that fault is much lower than in the other end of the system so the voltage drop is greater. In fig. 5.12d and in fig. 5.12b the voltage drop is lower for the cases when we have the wind farm since the wind farm

provides reactive power support during the fault and raises the voltage level at the bus.

In fig. 5.13 the real and reactive power injection following a fault can be seen for 100 MW windfarm.

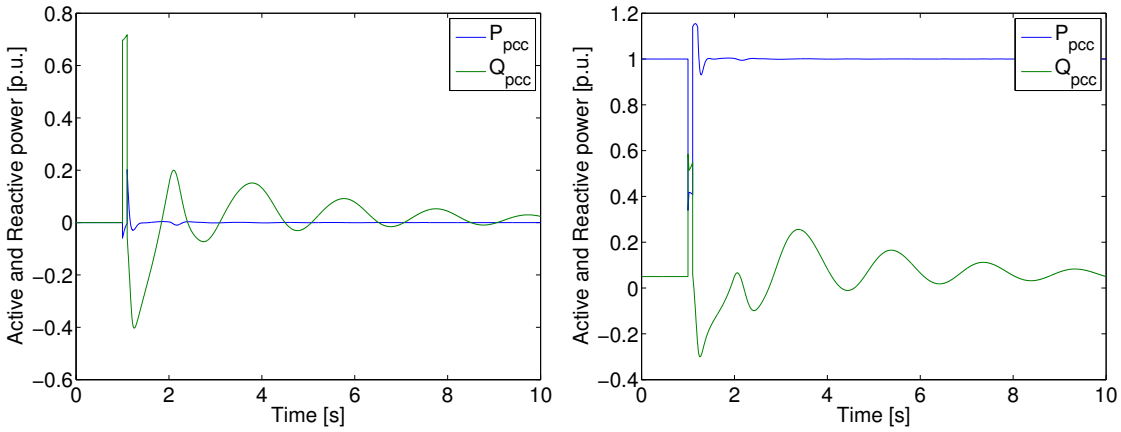

(a) Low wind generation **(b)** High wind generation

Figure 5.13: Real and reactive power injection with 100 MW windfarm

During the fault the voltage drop does not limit the operation of the converter that much so it can inject 0.7 p.u. of reactive power as seen in fig. 5.13a and to -0.4 p.u. when the excitation system of the generator tries to raise the voltage.

In fig. 5.14 the angle deviation following a fault can be seen.

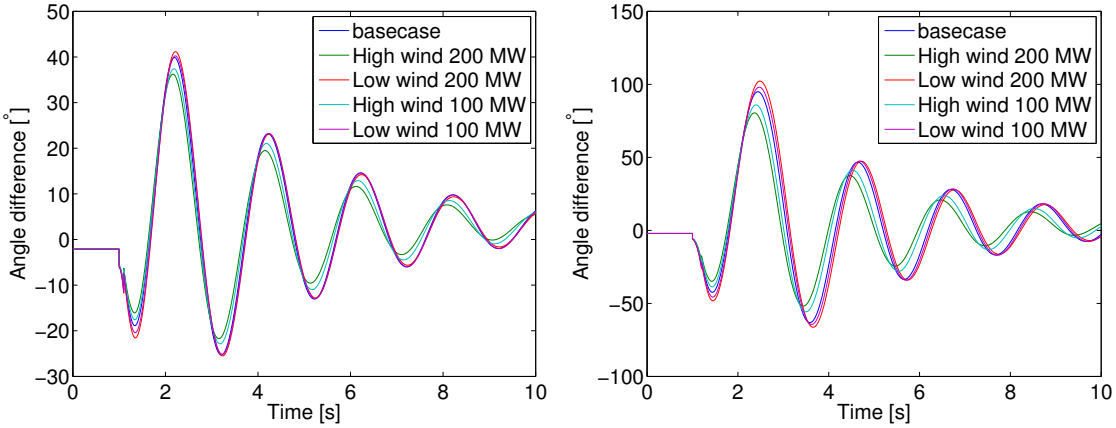

(a) Angle difference clearing 100 ms **(b)** Angle difference clearing 200 ms

Figure 5.14: Angle difference in the system following faults with different clearing times

If faults at Sigöldulinu 4 and Kröflulina 2 are compared again it can be seen that the angle difference deviates more for a fault at Kröflulínu 2, if fig. 5.14 and fig. 5.11 are compared. Similar to a fault in the east end of the system the second swing of angle difference is larger.

There is also a big difference between high and low wind scenarios in angle deviation following a fault.

5.2.5 Critical clearing time

In the previous section the angle difference and voltage have been observed for different faults. However it is of great interest to calculate the critical clearing time of the system with respect to the power transfer. The critical clearing time will vary based on the power transfer and based on the generator set points. The case with 200 MW wind farm will be displayed since that size give the most deviation in clearing time and there was not a significant difference between the 100 MW and 200 MW wind farm. The only difference was that the clearing time varied more for a larger wind farm. For a fault in the southwest area as seen in fig. 5.15a different wind scenarios do not impact the critical clearing time.

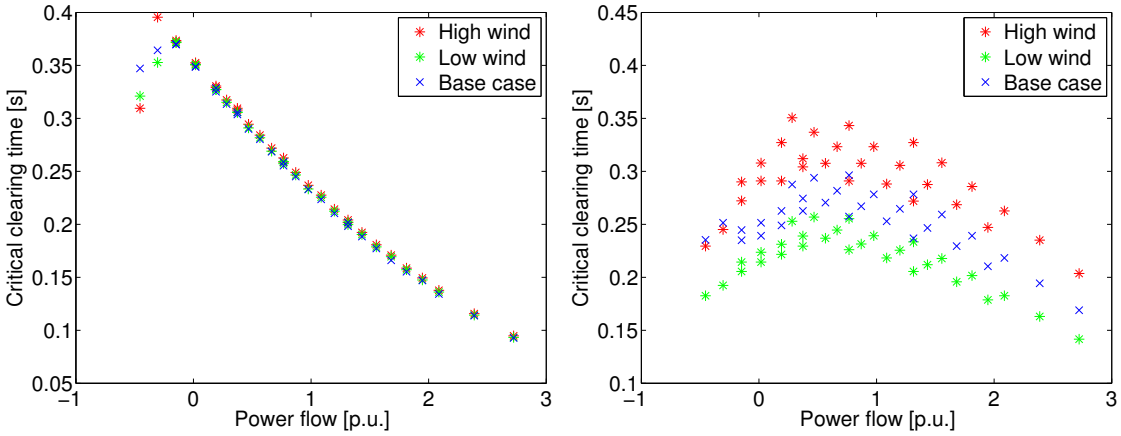

(a) Fault in the Southwest area

(b) Fault in the East area

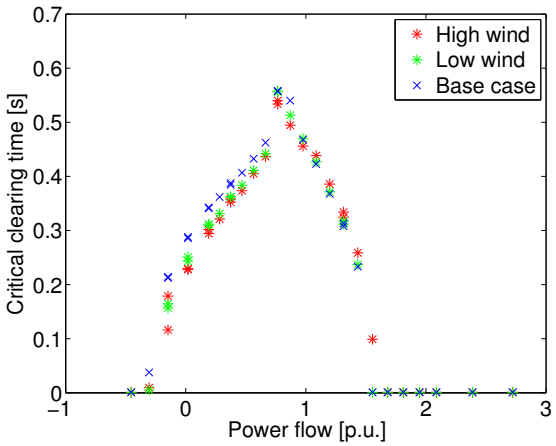

(c) Fault at transmission line Sigöldulina 4

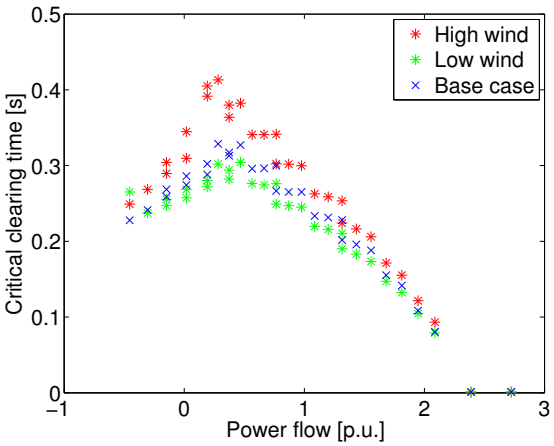

(d) Fault at transmission line Kröflulina 2

Figure 5.15: Critical clearing time of different faults

However there is a slight difference when the power flow towards the west system increases. For a fault at Sigöldulína 4 the impact of wind generation is not that great as seen in fig. 5.15c. For a fault on Sigöldulína 4 the critical clearing time is reduced slightly when considering more flow towards the south west part of the system and improves a bit when the power flow is increased towards the east. In fig. 5.15b and 5.15d there is more variation of the critical clearing time due to the fact that the faults are closer to the generation that is being varied. However the critical clearing time becomes more scattered than in the cases when the fault were in the other end of the system. The reason for this scatter is that many set points of generation are visualised. This impacts the acceleration factor which will lead to different clearing times. The low wind cases generally reduce the critical clearing time for these fault case. While high wind scenarios increase the critical clearing time for faults in the east. When fig. 5.15a and fig. 5.15b are compared it can be seen how variation in power transfer affects much more the faults in the south system. For faults in the south system the first swing is the most determining one while for the east the second swing is the most determental. Since in fig. 5.15b and fig. 5.15d it is hard to clearly see the impact a scenario with fixed P_m was plotted as seen in fig. 5.15.

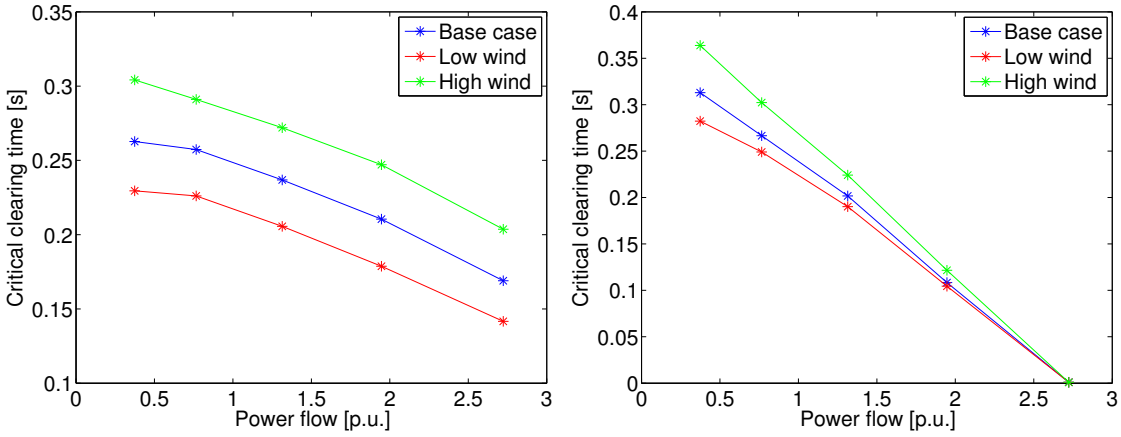

(a) Fault in the east area

(b) Fault in the east area disconnection of line

Figure 5.16: critical clearing time of different faults

The positive effect that high wind generation and the negative effect that low wind scenarios have on the critical clearing time is clearly visible in fig. 5.16. Since the wind farm has no inertia it indirectly affects the critical clearing time of the generators in the east, since that generator group has to vary its generation to compensate for different wind scenarios.

5.3 Reactive power control

In this section reactive power control is compared with the voltage control. The Q_{ref} is set to zero to keep the power factor at unity. This is important because it is critical to analyse how much the voltage control impacts the stability of the system for different faults compared with

constant power factor. Low wind scenarios will only be visualised since it is for those cases when the biggest difference between reactive and voltage control can be seen. The size of the windfarm was assumed to be 200 MW.

5.3.1 Fault at the Southwest equivalent

A fault was applied at the Southwest bus and then the fault cleared after 200 ms. In fig. 5.17 the impact on the voltage in the each end of the system can be seen following a fault at the Southwest bus.

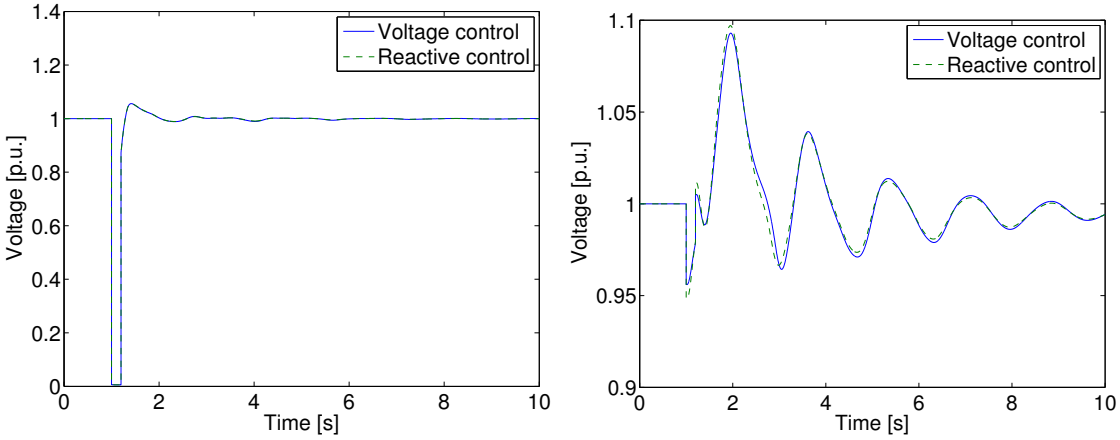

(a) Voltage Southwest bus clearing 200 ms

(b) Voltage east bus clearing 200 ms

Figure 5.17: Voltage in the system following of different faults

In fig. 5.17b the difference can be seen between the different control strategies. The voltage control reduces the voltage variation following the fault by reducing the voltage drop by injecting reactive power and by absorbing when the voltage is high, however the difference is not big.

In fig. 5.18 the comparison between the two control strategies on the angular difference can be seen.

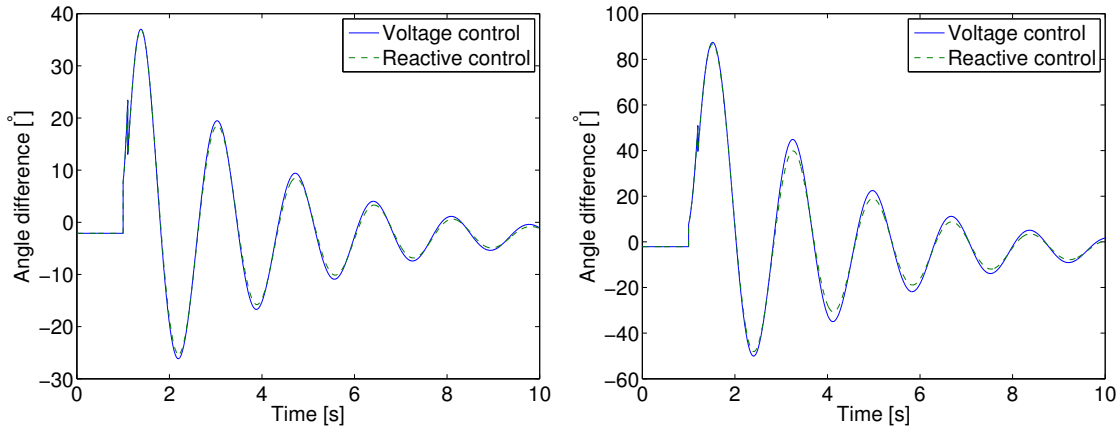

(a) Angle difference clearing 100 ms **(b)** Angle difference clearing 200 ms

Figure 5.18: Angle difference following a fault

Since the voltage control is trying to reduce the voltage it affects the electric power injected into the network. There is not a significant difference between the control strategies for the first swing. However the damping is reduced sligthly when considering voltage control as seen in fig. 5.18b.

5.3.2 Fault at Fljótsdalur

Fault was applied in the east part of the system and the control strategies compared.

In fig. 5.19 the voltages in the east and south can be seen.

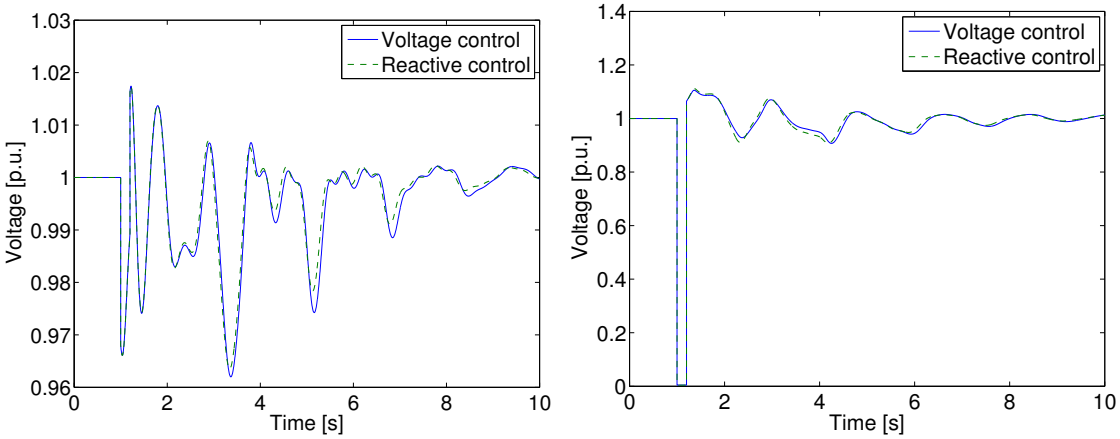

(a) Voltage Southwest bus clearing 200 ms **(b)** Voltage east bus clearing 200 ms

Figure 5.19: Voltages in the system following a fault in Fljótsdalur

As expected the voltage variation is reduced with the voltage control method when a fault is applied at the East bus.

In fig. 5.20 comparison of angle deviation for the two control stragies can be seen

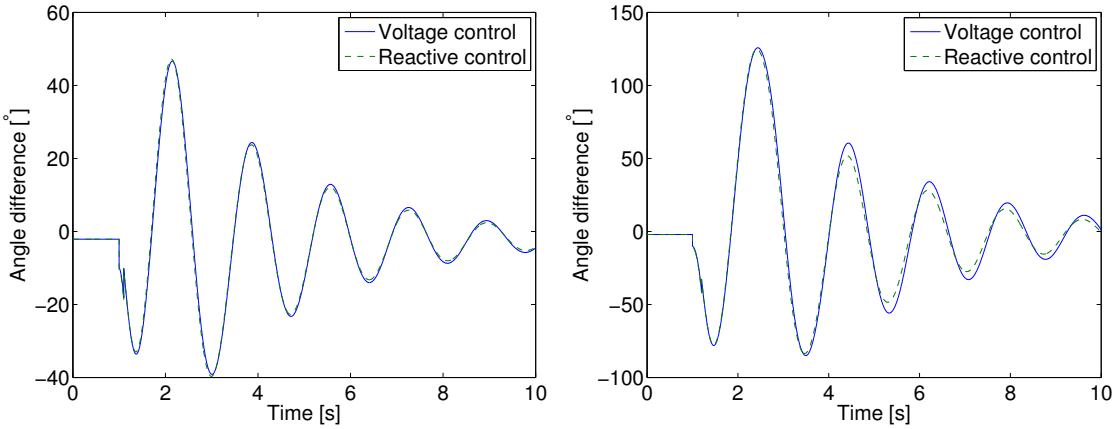

(a) Angle difference clearing 100 ms **(b)** Angle difference clearing 200 ms

Figure 5.20: Angle difference following a fault

Now the fault is applied close to the wind farm and the voltage drop is significant as seen in fig. 5.19. As for the fault case in the south the damping of the oscillations is reduced for voltage control as seen in fig. 5.20.

5.3.3 Fault at transmission line Sigöldulína 4

A fault is applied at the south west part of the system with a fault reactance to imitate a fault on the 132 kV bus and then a line is disconnected.

In fig. 5.21 the impact on voltage can be seen.

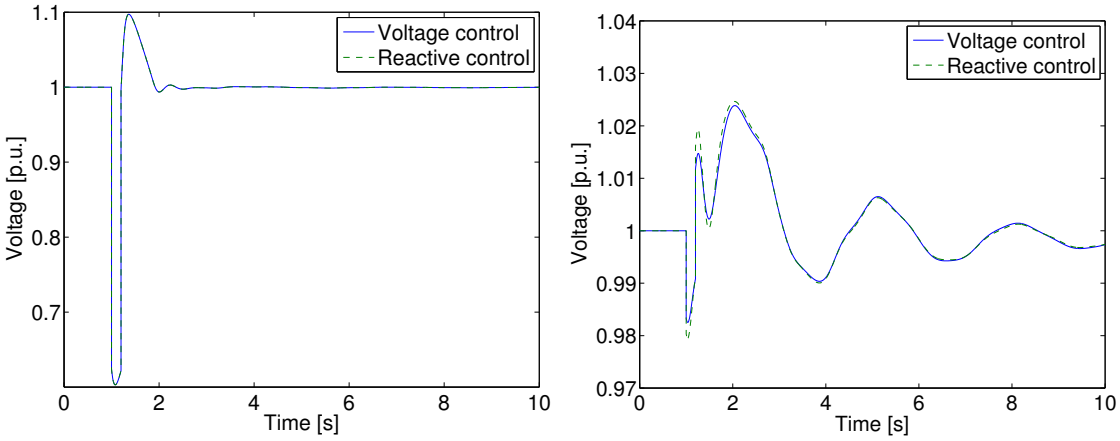

(a) Voltage Southwest bus clearing 200 ms **(b)** Voltage east bus clearing 200 ms

Figure 5.21: Voltages in the system following a fault at Sigöldulina 4

The voltage control tries to control the voltage variation after the fault as can be seen in fig. 5.21b. The voltage control reduces the voltage drop after the drop and then the rise following the fault.

In fig. 5.22 it is seen how the first swing is almost identical but the voltage control has worse damping as before.

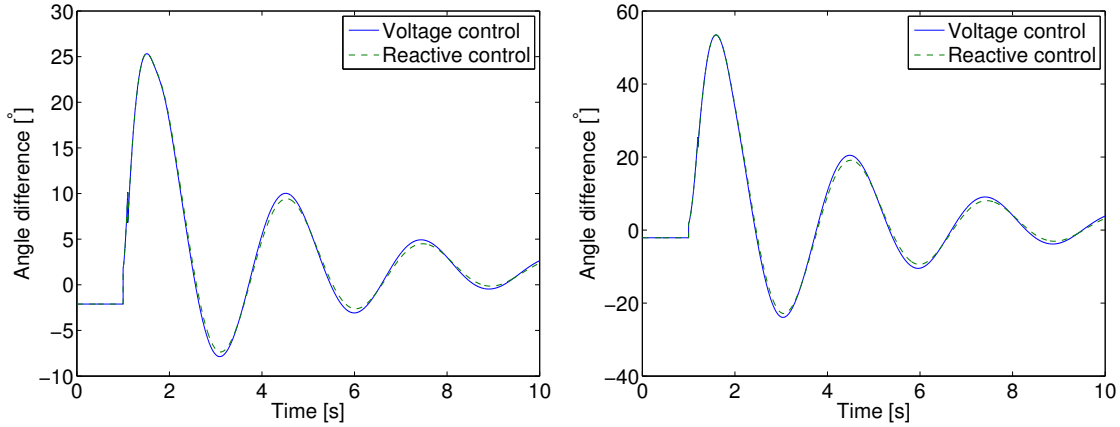

(a) Angle difference clearing 100 ms **(b)** Angle difference clearing 200 ms

Figure 5.22: Angle difference following a fault at Sigöldulina 4

5.3.4 Fault at tranmission line Kröflulína 2

Fault was applied in the East to imitate a fault in the 132 kV grid and the transmission line in the northern interconnection next to the Eastern part of the system disconnected. The impact on the voltages in the Southwest and the East can be seen in fig. 5.23.

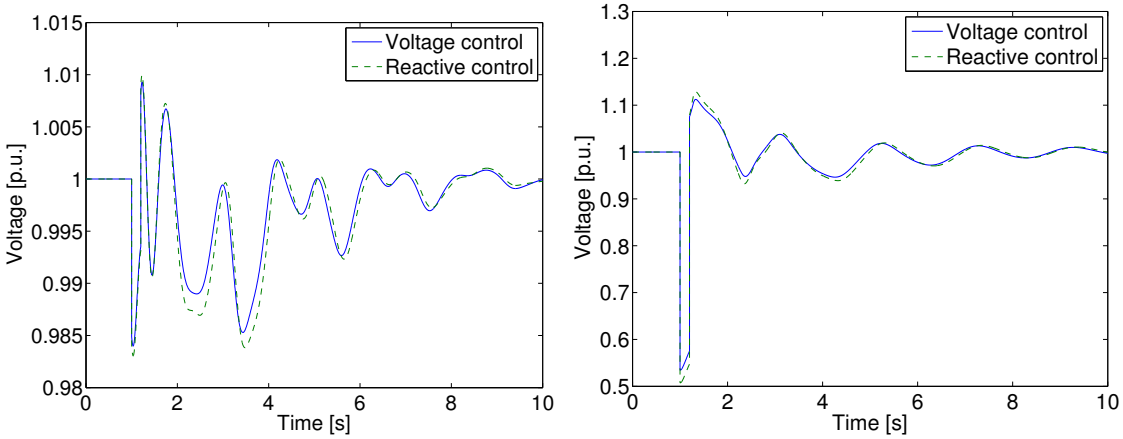

(a) Voltage Southwest bus clearing 200 ms **(b)** Voltage East bus clearing 200 ms

Figure 5.23: Voltage in the system following fault at Kröflulina 2

As for the fault in the East the voltage control, reduces the voltage variations following a fault compared to the Reactive control. In fig. 5.24 the impact on the angle deviation can be seen.

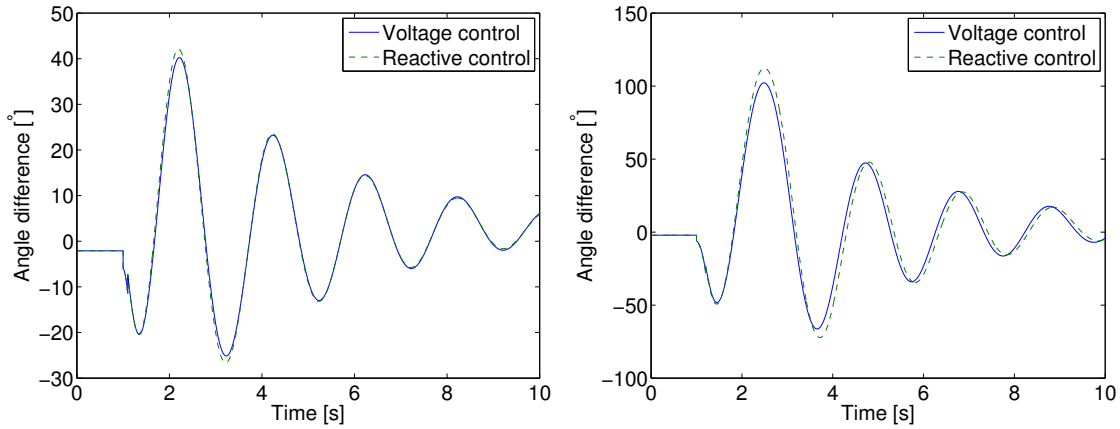

(a) Angle difference clearing 100 ms low **(b)** Angle difference clearing 200 ms high

Figure 5.24: Angle difference following a fault

This case acts as the other simulations, however one interesting thing is that following the voltage variations the first swings of the angle difference are actually reduced when using the voltage control, as seen in fig. 5.24. However as before the damping is better when reactive control is implemented. So for this certain case the voltage control is actually beneficial since the second swing is the large one, which can cause the system to go unstable.

5.3.5 Critical Clearing time

The critical clearing time for the reactive control and the voltage control was computed and compared together. In fig. 5.25 the critical clearing angle for the four fault cases can be seen.

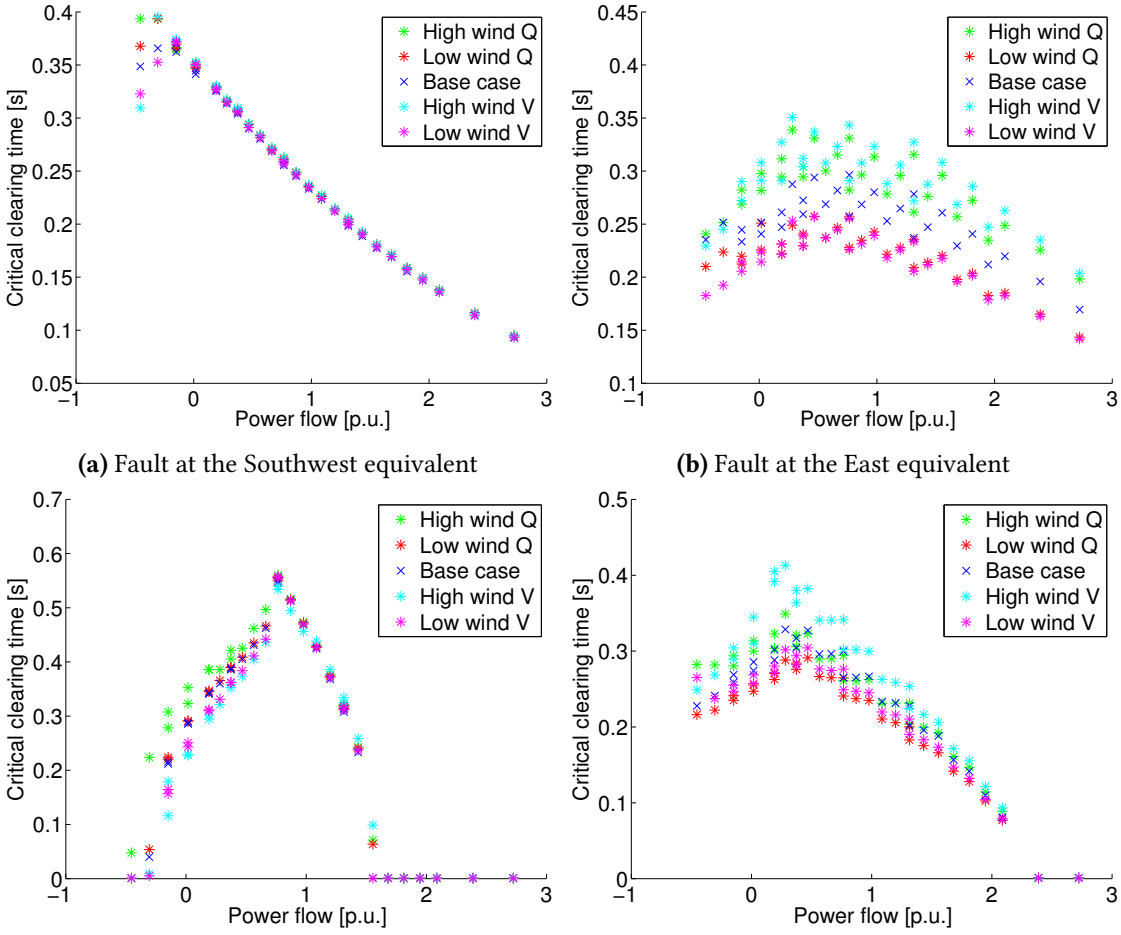

(a) Fault at the Southwest equivalent

(b) Fault at the East equivalent

(c) Fault at tranmission line Sigöldulina 4

(d) Fault at tranmission line Kröflulína 2

Figure 5.25: Critical clearing time of different faults

As seen in fig. 5.25a and 5.25c the impact is not that great when faults are in the other end of the system. However the reactive control gives high clearing time when the transfer is to the west. As seen in fig. 5.25b and fig. 5.25d. The impact is much greater. It seems that the voltage control with high wind aids the critical clearing time more than high wind with constant power factor. For the low wind scenarios voltage control gives lower critical clearing time than reactive control. In fig. 5.26 this difference become more evident.

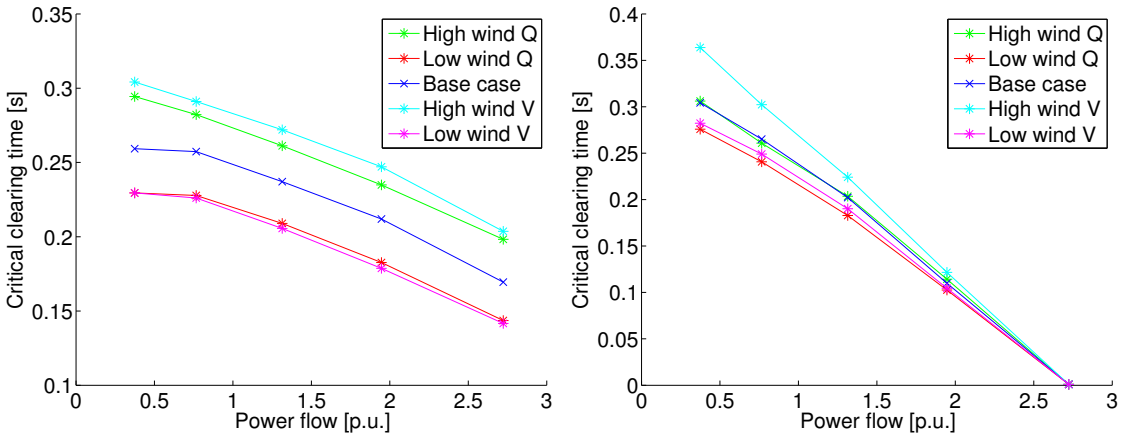

(a) Fault at the East equivalent

(b) Fault at tranmission line Kröflulína 2

Figure 5.26: critical clearing time of different faults

The general assumption is still valid that voltage control aids in the high wind scenarios while reactive power control is more beneficial for low wind scenarios.

5.4 Summary

Wind integration with full converter wind turbines in the east part of the system indirectly affects the stability of the system. The impact is biggest for faults close to the generators which compensate the intermittency of the wind. In this study the big generators in the east compensated for low wind scenarios and as their generated power was increased it decreased the critical clearing time of the system. Decreasing their generation, in high wind scenarios, increased the critical clearing time of the system. When the generation of the wind farm is decreased, the generation of the hydro power plant has to be increased which increases their acceleration constant. The windfarm does not contribute any inertia to the system as it is ”hidden” behind the converters. When the two control methods of the wind turbines were investigated, voltage and reactive control, reactive control showed more promise in low wind scenarios while voltage control improved the critical clearing time for high wind generation scenarios. Low wind scenarios in general decreased the critical clearing time for faults close to the wind farm and the compensating generation. This is counterproductive, as in these cases more power is needed to be transferred to the wind generation area.

6

Supplementary control schemes

In this chapter supplementary control strategies will be implemented in order to improve the transient stability of the system during low wind scenarios. A ”bang bang” or ”big bang” strategy will be implemented as describe in [22]. In the Icelandic system there are several PMU's [23] which provide wide area measurements and in this thesis measurements in the east and the southwest are used for control purposes. As seen in the chapter 5, the control strategies investigated do not necessarily aid the transient stability and the inter area oscillations. Unfavorable voltage control or constant power control can in some cases reduce the critical clearing time. The angle variation determines the oscillations between the areas and if the angle trajectory can be influenced. If the voltage magnitude close to the generator oscillations is varied it will impact the trajectory of the angle following the fault.

6.1 Controller description

Two versions of the controller were implemented. One which used the derivative of the local angle of the east generator and another which used the angle difference between the areas to inject power. The derivative of the angle is the speed of the generator. A certain dead band is implemented from 0.1 p.u. to -0.1 p.u. speed difference. Furthermore a 100 ms time delay was added on the input signal to the control in order to take into account the communications.

$$Q_{ref} = \begin{cases} 1\ p.u. & \dot{\delta} > 0.1 \text{ p.u.} \\ -1\ p.u. & \dot{\delta} < -0.1 \text{ p.u.} \end{cases} \tag{6.1}$$

During simulations 1 p.u. reactive power was injected gave approximately 1.1 p.u voltage at the east bus during faults close that point. Injecting reactive power will have the effect that the synchronizing torque is increased when the angle increasing. Injecting reactive power will have the impact at in the east that the voltage will rise and if reactive power is absorbed the voltage will lower. This will change the power curve which will decrease or increase the angle variation depending on the goal. The control scheme using the angle difference between the

area is referred to as ”WA control” and the one using local measurements is referred to as ”L control”. The control scheme was simulated for the same fault cases as before.

6.1.1 Fault at the Southwest equivalent

Fault was simulated at the Southwest bus and the impact on the voltages and angle observed. In fig. 6.1 the voltages in the south west and the east can be seen.

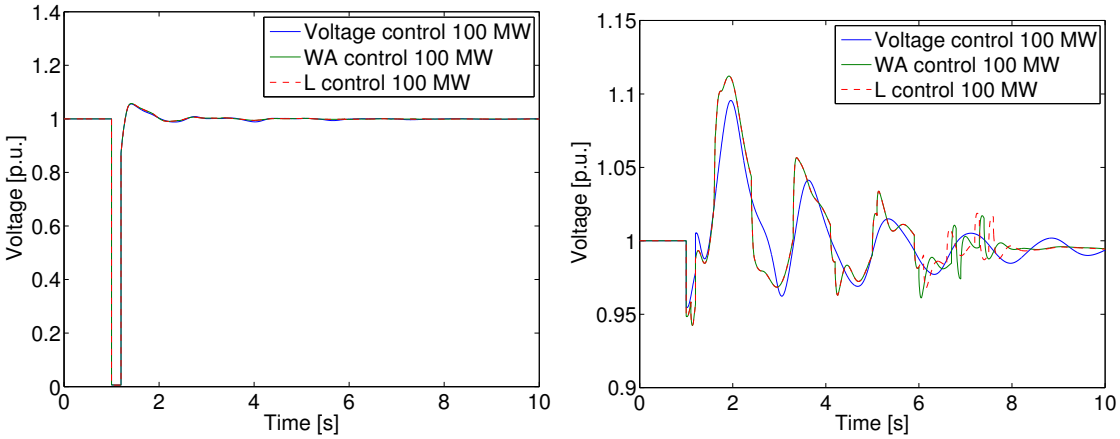

(a) Voltage Southwest bus clearing 200 ms

(b) Voltage East bus clearing 200 ms

Figure 6.1: Voltages in the system following fault

The voltage varies quite significantly when comparing the WA and L control with the voltage control. The difference between WA and L control is quite insignificant. The voltages after the fault at the east bus is increased which has impact on the synchronizing torque between the areas. Since the local angle in the east is not affected as greatly as the angle in the south west following a fault, the angle difference between the busses WA control should be more effective here. In fig. 6.2 the response of the wind farm, when it’s subjected to a fault can be seen.

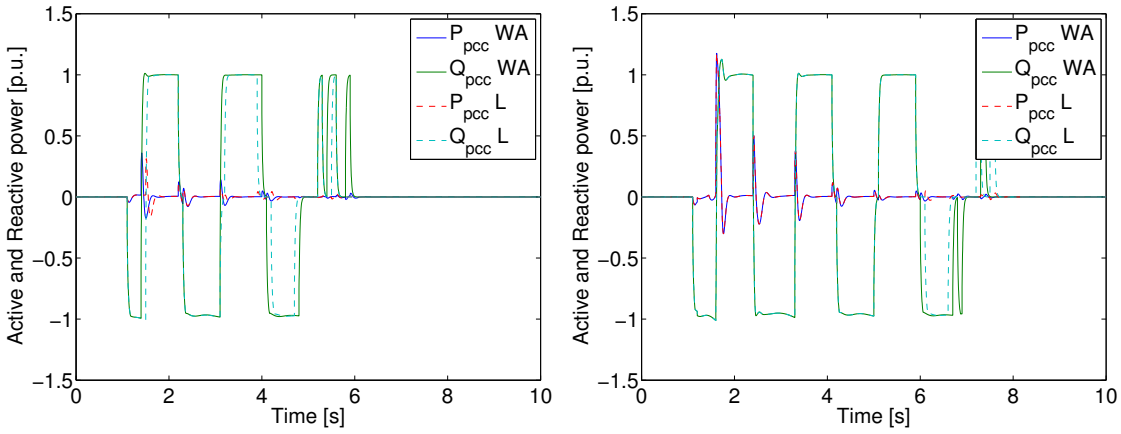

(a) Clearing time 100 ms, 100 MW Windfarm **(b)** Clearing time 200 ms, 100 MW Windfarm

Figure 6.2: Active and Reactive power injected by the wind farm following a fault

There is a slight difference between the control methods since the angle difference is not the same as the angle deviation at the bus Fljótsdalur as seen in fig. 6.3.

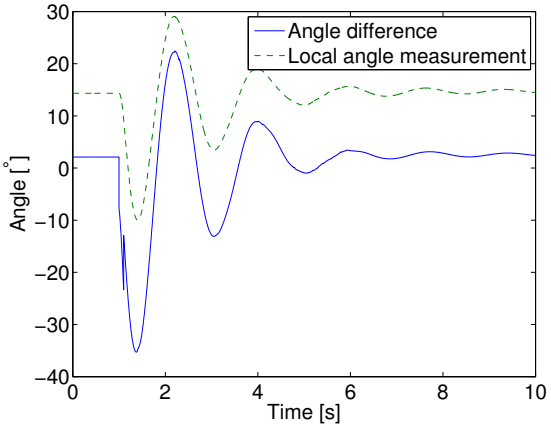

Figure 6.3: Local angle and angle difference measured for control

The reactive power controller is much faster then the active power control of the converter and therefore a spike in the active power can be seen. This is due to active and reactive controllers measures the power injected and compensates the error by changing the voltage vector ordered at the converter terminals. As Q_{ref} is changed the reactive controller sees an error and starts to change the imaginary part of the voltage. However there is a change in voltage and angle during this period and the converter injects a little amount of active power as the active power controllers is to slow to compensate for the changes due to reverse of reactive power reference.

The positive impact of the increased synchronizing torque can be seen in fig. 6.4 as the first swing and second swing are reduced compared to the case for voltage control.

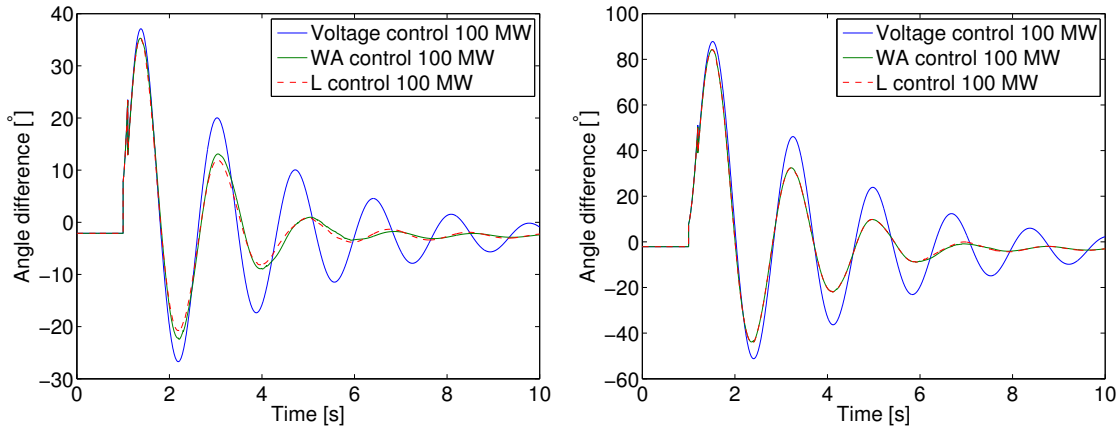

(a) Angle difference clearing 100 ms **(b)** Angle difference clearing 200 ms

Figure 6.4: Angle difference between areas following a fault

An additional improvement is that the damping of the system has been increased. Although the damping is not the main aim of this method it is greatly improved with this control strategy.

6.1.2 Fault at the East equivalent

Now a fault in the east is simlated and the voltage and angle deviation following a fault observed. Now a fault is applied close to the wind farm and the voltages observed. As seen in fig. 6.5 the control strategies influences the voltages quite significantly.

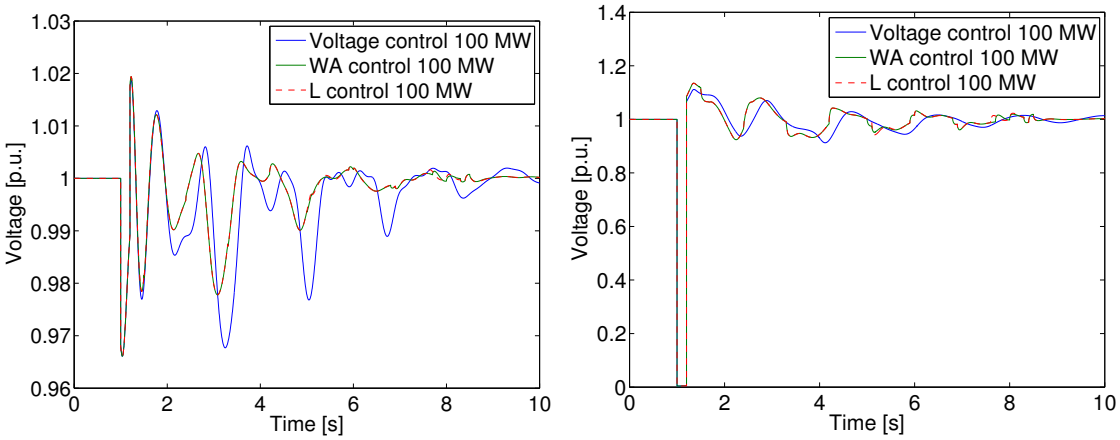

(a) Voltage Southwest bus clearing 200 ms **(b)** Voltage east bus clearing 200 ms

Figure 6.5: Voltages in the system following fault

The WA control and L control influence the voltage in a very similar manner since the angle deviation between the busses and the local measurements should be very similar as seen in fig. 6.6.

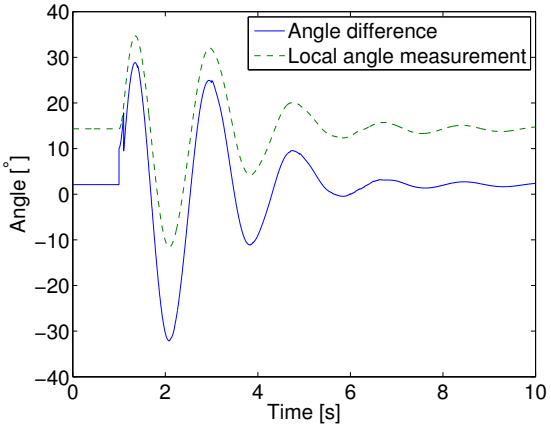

Figure 6.6: Local angle and angle difference measured for control

The south west area has a high short circuit capacity so the generators there will not accelerate as much as the east generator when the fault was applied in the south west area.

In fig. 6.7 the response of the wind farm can be seen, when it's subjected to a fault.

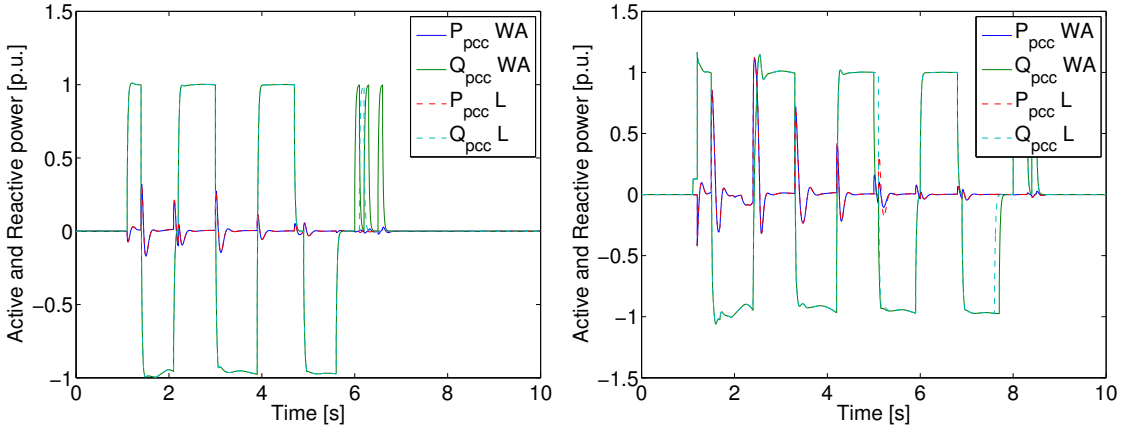

(a) Clearing time 100 ms, 100 MW Windfarm **(b)** Clearing time 200 ms, 100 MW Windfarm

Figure 6.7: Active and Reactive power injected by the wind farm following a fault

If fig. 6.7 is compared to fig. 6.2 the response has now opposite sign and it is due to the fact the angle difference has a positive derative so we inject power. As seen in fig. 6.8 the angle devation is reduced by using the wide area measurements.

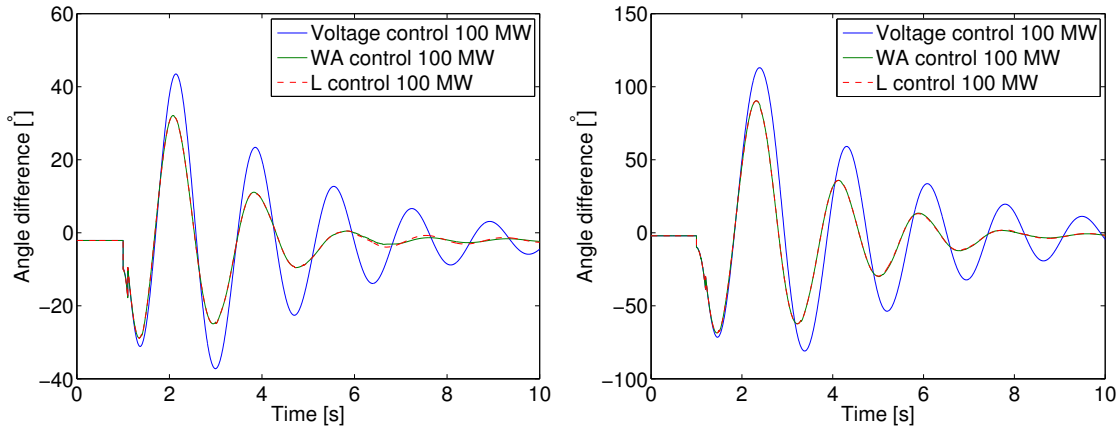

(a) Angle difference clearing 100 ms **(b)** Angle difference clearing 200 ms

Figure 6.8: Angle difference following a fault

Specially for the second swing which is important since that swing is the most important for the transient stability as it is bigger than first swing. As before the damping is significantly improved.

6.1.3 Fault at tranmission line Sigöldulína 4

A fault with a reactance in order to simulate a fault in the 132 kV transmission network in the south west and a transmission line in the southern interconnection was disconnected. As seen in fig. 6.9 the voltage drop following a fault in the south west is not that significant.

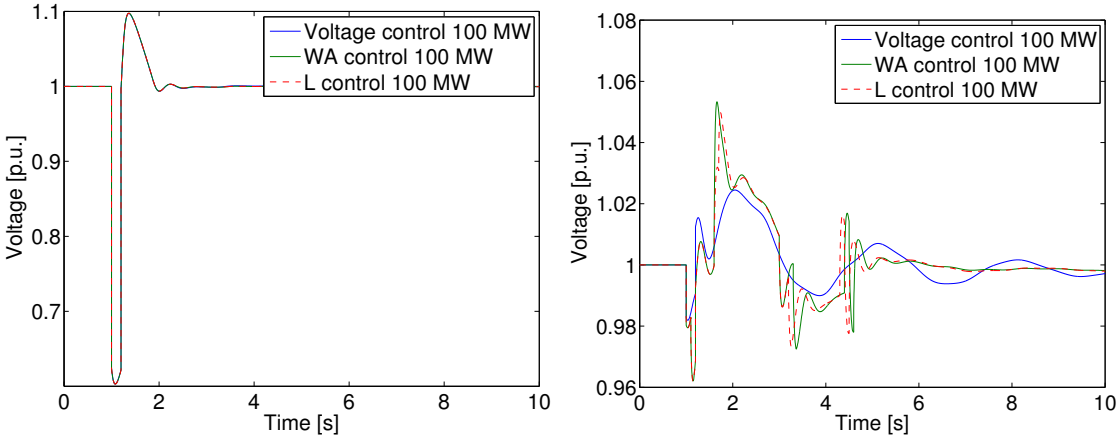

(a) Voltage Southwest bus clearing 200 ms **(b)** Voltage East bus clearing 200 ms

Figure 6.9: Voltages in the system following fault

The impact of the converter can be seen in fig. 6.9b with the control method. The voltage variation is less than in fig. 6.1b

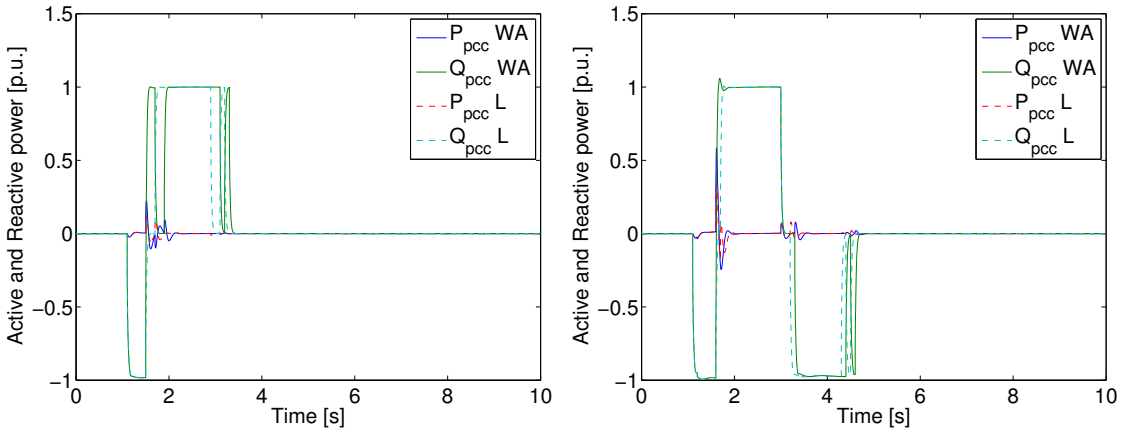

(a) Clearing time 100 ms, 100 MW Windfarm **(b)** Clearing time 200 ms, 100 MW Windfarm

Figure 6.10: Active and Reactive power injected by the wind farm following a fault

The response of the converter subjected to a fault at Sigöldulína 4 can be seen in fig. 6.10. Now the response of the controller is reduced compared to fig. 6.2 due to less deviation of angle difference and the oscillations are damped pretty quickly.

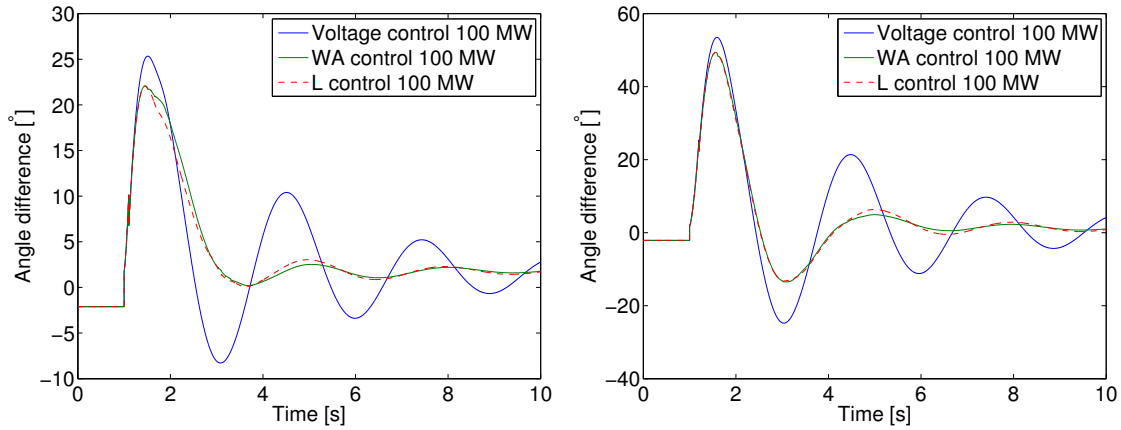

(a) Angle difference clearing 100 ms **(b)** Angle difference clearing 200 ms

Figure 6.11: Angle difference between areas following a fault

The small variation has a big impact on the angle deviation between the areas and also increases the damping significantly. As in the case for fault in the south west there is a deviation between the WA and L control, since the angle difference between the areas will deviate more than the local angle in the east.

6.1.4 Fault at tranmission line Kröflulína 2

A fault was applied at the east bus with a fault reactance to simulate a fault in the 132 kV transmission network and transmission line in the northern interconnection disconnected.

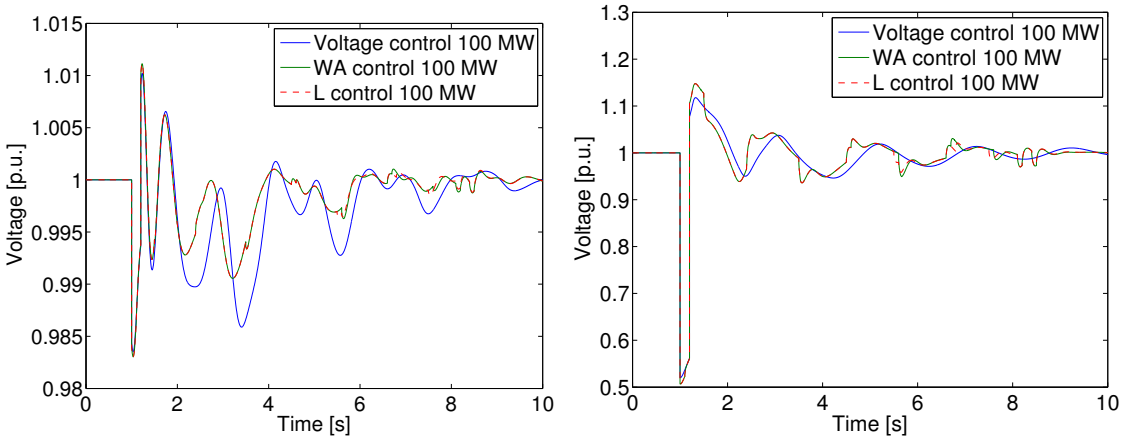

(a) Voltage Southwest bus clearing 200 ms **(b)** Voltage east bus clearing 200 ms

Figure 6.12: Voltages in the system following fault

In fig. 6.12 the voltages in the system are observed following a fault on Kröflulína 2. Now there is not a much difference between local and WA measurements as for the case when we had a fault in the east part of the system.

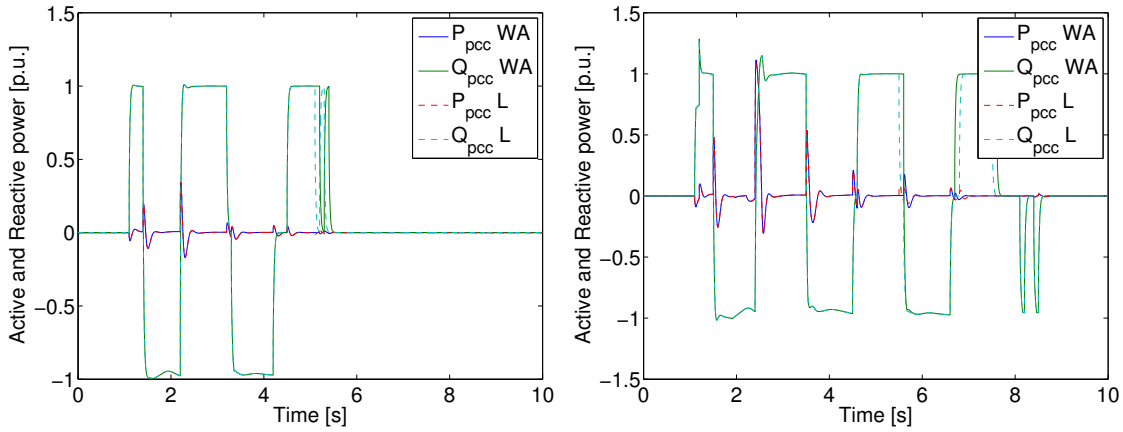

(a) Clearing time 100 ms, 100 MW Windfarm **(b)** Clearing time 200 ms, 100 MW Windfarm

Figure 6.13: Active and Reactive power injected by the wind farm following a fault

The response of the converter to a fault at Kröflulína 2 can be seen in fig. 6.13. The sign of the injected reactive power has changed signs if compared to fig. 6.10. The response of the converter is also prolonged due to more angle variations than if compared to fig. 6.10.

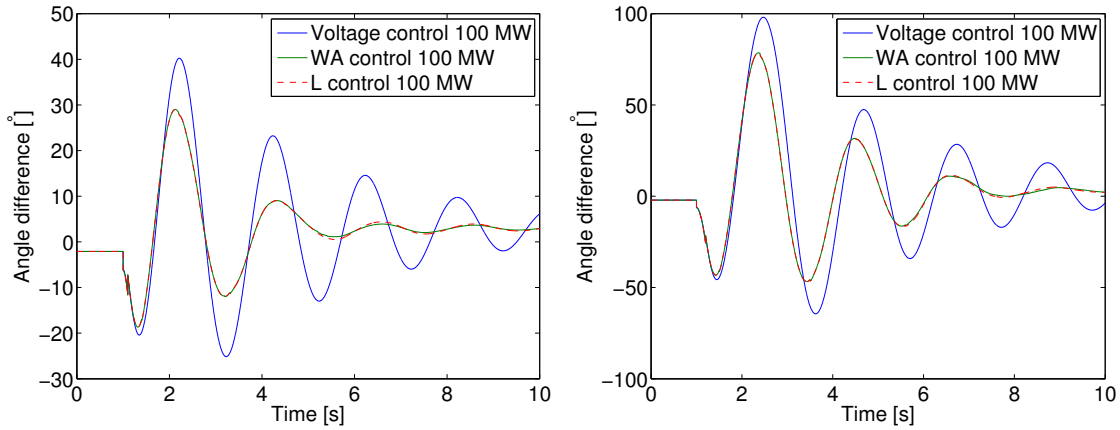

(a) Angle difference clearing 100 ms **(b)** Angle difference clearing 200 ms

Figure 6.14: Angle difference following a fault

The angle deviation following fault as seen in fig. 6.14 is reduced and also the damping improved. It is seen that the angle deviation for the second swing is reduced more than for a fault where the voltage at the east bus drops to zero as in fig. 6.8.

6.1.5 Critical Clearing time

In this chapter the critical clearing times for the cases with low wind generation are compared to the base case. The case with the voltage control is compared to WA and L control.

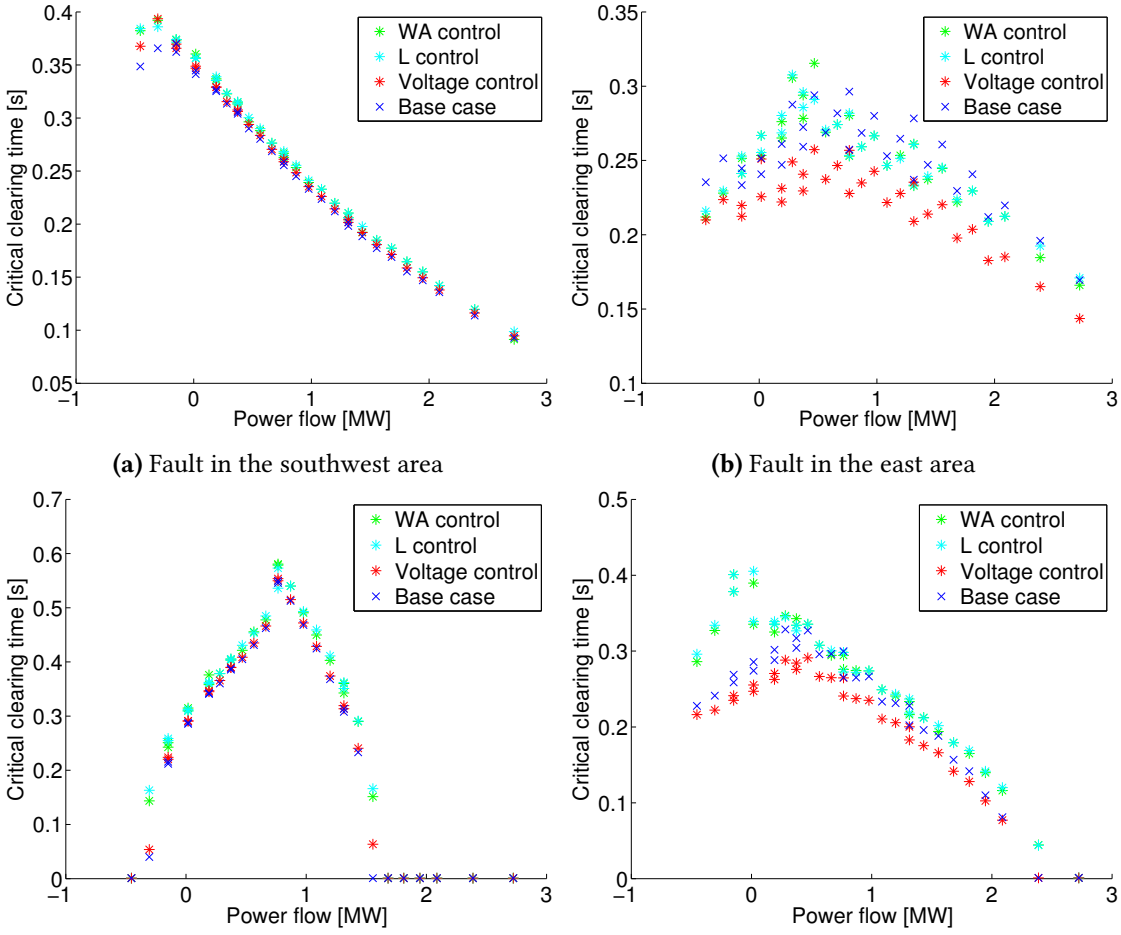

(a) Fault in the southwest area

(b) Fault in the east area

(c) Fault at Sigöldulína 4

(d) Fault at Kröflulína 2

Figure 6.15: Critical clearing time of different faults

As seen in fig. 6.15 the ”bang-bang” control strategy improves the critical clearing time dramatically, compared to the voltage control. In fig. 6.15a and fig. 6.15c the critical clearing time is displayed for a fault in the south west part of the system. All the simulated control methods for the wind farm improve the critical clearing time although L control and WA control improve the clearing time more than voltage control. In fig. 6.15b the critical clearing time for a fault with a low reactance in the east is displayed. By implementing the proposed control strategy the critical clearing time is improved compared to the voltage control strategy. However it does not improve the critical clearing time to what the base case values. In fig. 6.15d it can be seen how the critical clearing time is improved beyond the base case without, wind generation, for a fault with higher fault reactance. How much reactive power the converter can inject during faults, depends on the voltage drop during the fault, as can be seen when viewing fig. 6.15b and fig. 6.15d.

In order to visualize the impact of the wind power on the critical clearing time in the east 5 points with constant P_m are plotted.

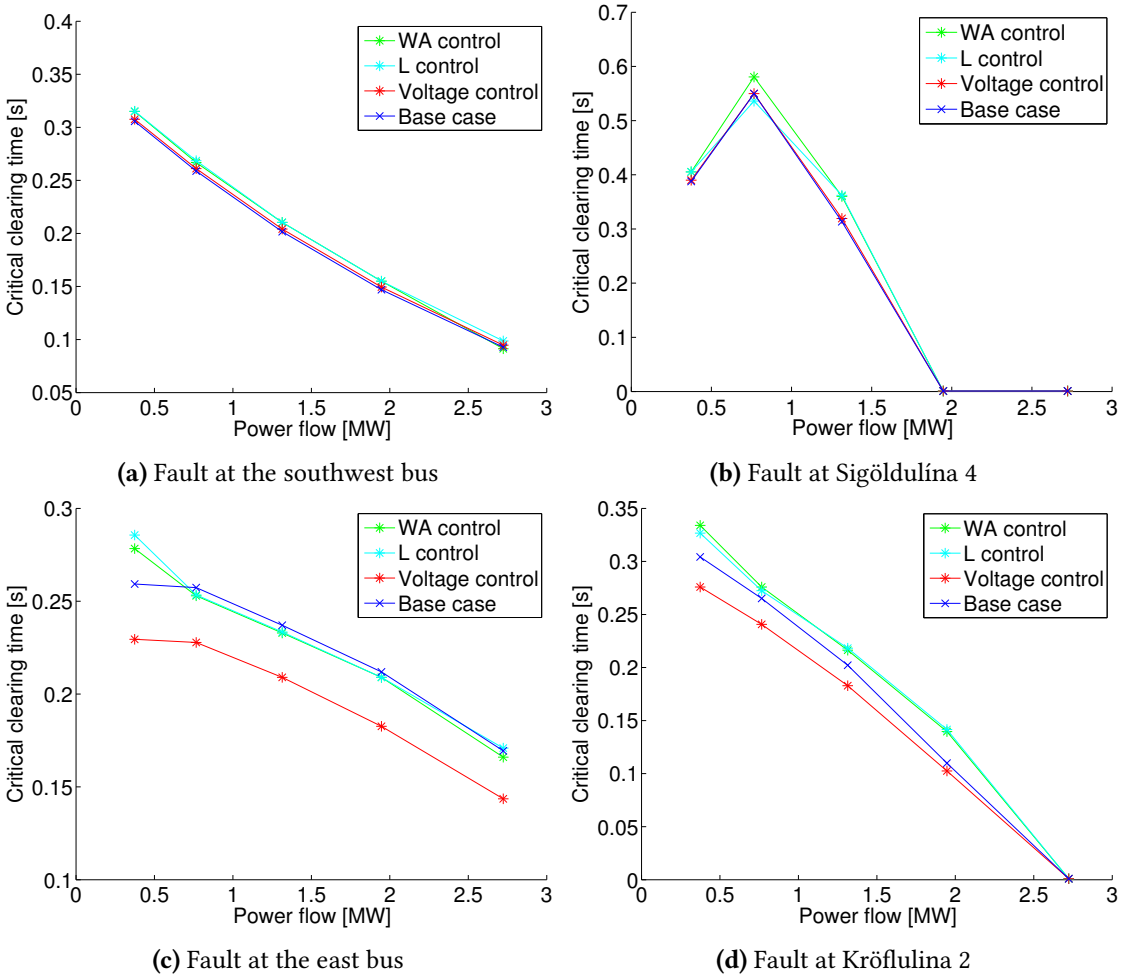

(a) Fault at the southwest bus

(b) Fault at Sigöldulína 4

(c) Fault at the east bus

(d) Fault at Kröflulina 2

Figure 6.16: Critical clearing time of different faults

In fig. 6.16 the impact of the control strategies can clearly be seen. There is not much difference between the performance of the strategies depending on wether the input signal is just from one generator or the angle difference. However this control strategy improves the critical clearing time for the low wind generation so the critical clearing time is improved to be better or equal to the base case.

6.2 Summary

By influencing the voltage at the point of common connection for the wind farm and the hydro generation in the east the acceleration and deacceleration of the hydro generator can be altered. Although the wind farm does not contribute any rotating mass to the system it can be used for voltage control. The potential of the voltage control is highest for low wind scenarios and that is also when the impact on the critical clearing time was highest. By implementing sup-

plementary control based on wide area measurements the critical clearing time was increased to a level, which was close to the previous critical clearing time. For faults when the voltage dropped to zero it was a little bit lower than for the base case, however for faults where the voltage did not completely drop to zero it improved the critical clearing time beyond the base case. The reason for this was that if the voltage does not drop to zero the capability curve of the converter is big enough to be able to improve the voltage during the fault.

7

Conclusions and Future work

7.1 Conclusions

In this thesis the transient and oscillatory stability limits of the Icelandic Power System have been analysed. A simplified model of the Icelandic Power System, based on that analysis, was derived where the strong parts of the system were aggregated. A model of a windfarm was implemented based on the full converter wind turbine topology and its impact on the system stability analysed. Finally a supplementary control strategy based on Wide Area Measurements was derived and its impact on the stability of the Power System was analysed.

7.1.1 Transient stability Analysis of the Icelandic System

As shown in Chapter 3 the power transfer between areas is limited by transient stability.

- Faults within the 220 kV system caused the largest acceleration of the generators and gave lower clearing time but higher damping compared to faults in the 132 kV network following a disconnection of a line.
- Faults on the 132 kV buses close to the 220 kV areas and disconnection of a transmission line, had a higher clearing time when the angle difference was low. However, the critical clearing time declined faster as the power transfer to the East was increased, due to a loss of transmission line.
- It was also shown, how the frequency of oscillations are independent of the fault location but depend rather on the system reactance and power transfer. With a full system the frequency of power oscillations were around 0.5 Hz.
- The peak damping and the critical clearing time was highest when the power transfer was around 75 MW over stability cut IV.

- When the PSS's were active the damping of oscillation was improved, however the initial acceleration of generators was the same as before as expected so the PSS's did not impact the critical clearing time for the cases analysed.
- There were some initial condition issues and a ripple in the response of some generators following a fault with the PSS's active, so their parameters need further investigation.

7.1.2 Simplification of the Icelandic Power System

In Chapter 4 the Icelandic Power System was aggregated into a two area systems, but the transmission lines were kept between the 220 kV parts.

- To calculate the aggregated generator reactances, a weighted mean was used based on the apparent power as the equation given in [7] gave unreasonable p.u. value of those parameters.
- The generators in Blanda were critical to keep the loadability between the Southwest and the East area.
- Frequency of oscillations was similar compared to the full case. However the damping was better in the simplified version but this error was accepted as the main focus was on the transient stability.
- The simplified model gave good results for faults in the Eastern part of the system compared to the full system.
- The simplified system gave good results for the critical clearing time of faults in the Southwest for a full system, when the power transfer was increased to the east. However, it did not give the same results compared to the critical clearing time of the full system when the power transfer was increased towards the Southwest part. Since the scope of this thesis is on power transfer to the Eastern area this error was accepted.
- The simplified system gave lower critical clearing time for faults close to the Southwest on the 132 kV network and disconnection of a line, compared to the original case. As before the main interest is in the faults in the Eastern area so this error was accepted.
- The conclusion is that the simplified model is sufficient when working with wind power integration and faults in the eastern part of the Power System.

7.1.3 Wind integration

In Chapter 5 the wind integration into the simplified system was investigated.

- Wind generation indirectly impacts the critical clearing time in the Eastern part of the system. As the hydro generation is varied to compensate for different wind scenarios and the wind generation does not contribute any additional inertia to the Eastern part of the power system.

- Wind integration in the Eastern part has a minimal impact on the critical clearing time of faults in the Southwest part of the Power System.
- Low wind scenarios, where generation was increased in the Eastern part, reduced the critical clearing time when faults were applied in the East.
- High wind scenarios, where the generation was decreased in the Eastern part ,improved the critical clearing time of the system when faults were applied in the East.
- When comparing voltage control and constant power factor control, the voltage control gave higher critical clearing time for high wind scenarios while the constant power factor control gave higher clearing time for low wind scenarios.
- Low wind scenarios lead to a lower critical clearing time for faults in the Eastern part which is counter productive as more power import is needed for those scenarios.

7.1.4 Supplementary control schemes

In Chapter 6 a supplementary control method is derived based on Wide Area Measurements.

- The supplementary control of the Wind Farm increased the critical clearing time for low wind scenarios.
- The supplementary control increased the damping of the inter area oscillations as well.
- The effect of the supplementary control was greater when the voltage drop was reduced, since during the fault it could boost the voltage.
- The critical clearing time was increased close to the base case values.
- There is not a significant improvement when angle difference between the areas is used as an input compared to using the local voltage angle in the East.

7.2 Future Work

For weak Transmission Systems, variation in generation and the economic dispatch can have significant impact on the stability of the system. Suggested future work concerning the stability of the Power System following wind integration is:

- The impact on the transient stability using other wind generation topologies has to be investigated.
- Transient stability analysis of more wide spread wind integration needs to be analysed since coordinated control of such wind generation pattern should improve the system stability.
- Verfication of the Wide Area Control scheme with the full system is needed.

- Impact of controlling the active power output of the wind farms for transient stability enhancement for different wind scenarios should also be investigated.
- Analysis of the impact of additional hydro generation units following wind generation should be investigated, furthermore a variation of the economic dispatch to compensate for low wind scenarios should also be investigated.
- A three phase model of the wind farm is needed to investigate how much the voltage limit at the converter will limit the improvement of the critical clearing with the Wide Area Control scheme.

7.3 Suggestion for wind integration in Iceland

As shown in this thesis the variation of the hydro generation in the Icelandic Power System impacts the critical clearing angle. Therefore before the wind integration is carried out, an acceptable value for the critical clearing time for certain power transfer between the areas has to be determined. This is important as it will limit how much the Generating Companies can vary their hydro generation until there is a need for additional generating units in order to decrease the acceleration constant of the existing generation. Furthermore for wind integration in the Eastern part of Iceland, Wide Area Control scheme should be implemented as it is an cheap method to increase the critical clearing time for faults in that region. Since the second swing in the angle deviation between the areas is larger than the first swing, for faults in the east area, the Wide Area Control scheme using reactive power, is very efficient to improve the largest angle deviation. However this specific control scheme may not apply for all locations of wind integration, so each wind integration site has to be analysed in order to determine which control scheme should be used based on Wide Area Measurements.

Bibliography

[1] Samorka, "Flutningskerfi raforku mætir ekki eðlilegum kröfum," Feb. 2013.

[2] Landsnet, *Kerfisáætlun Fimm ára áætlun 2013-2017 // Langtímaáætlun til árs 2017*. Landsnet, 2013.

[3] P. Kundur, J. Paserba, V. Ajjarapu, G. Andersson, A. Bose, C. Canizares, N. Hatziargyriou, D. Hill, A. Stankovic, C. Taylor, T. Van Cutsem, and V. Vittal, "Definition and classification of power system stability ieee/cigre joint task force on stability terms and definitions," *Power Systems, IEEE Transactions on*, vol. 19, pp. 1387 – 1401, aug. 2004.

[4] J. R. B. Jan Machowski, Janusz W. Bialek, *Power System Dynamics and Stability*. John Wiley & Sons, 2008.

[5] IEEE, "Ieee recommended practice for excitation system models for power system stability studies," *IEEE Std 421.5-1992*, pp. 0–1, 1992.

[6] Y. Chompoobutrgool, W. Lo, and L. Vanfretti, "Development and implementation of a nordic grid model for power system small-signal and transient stability studies in a free and open source software," in *IEEE PES General Meeting Conference*, (California,USA), pp. 1–8, July 2012.

[7] F. Milano and K. Srivastava, "Dynamic rei equivalents for short circuit and transient stability analyses," *Electric Power Systems Research*, vol. 79, no. 6, pp. 878 – 887, 2009.

[8] T. Ackermann, *Wind Power in Power Systems*. John Wiley and Sons, Ltd, 2005.

[9] G. M. A.D Hansen, "Multi-pole permanent magnet synchronous generator wind turbines grid support capability in uninterrupted operation during grid faults," *IET Renewable Power Generation*, vol. 3, no. 3, pp. 333–348, 2009.

[10] A. Perdana, *Dynamic Models of Wind Turbines*. PhD thesis, Chalmers University of Technology, Göteborg Sweden, 2008.

[11] N. R. Ullah, *Wind Power - Added Value for Network Operation*. PhD thesis, Chalmers University of Technology, Göteborg Sweden, 2008.

[12] Digisilent, *DIgSilent Technical Documentation: PWM Converter.* DIgSILENT GmbH Germany, 2007.

[13] S. Cole, *Steady-State and Dynamic Modelling of VSC HVDC Systems for Power System Simulation.* PhD thesis, Katholieke Universiteit Leuven, Leuven-Heverlee Belgium, 2010.

[14] J. Hauer, "Application of prony analysis to the determination of modal content and equivalent models for measured power system response," *Power Systems, IEEE Transactions on*, vol. 6, no. 3, pp. 1062–1068, 1991.

[15] S. PTI, *PSSE 32.0.5 Online Documentation.* Siemens, 2010.

[16] B. Persson, "Affärsverket svenska kraftnäts författningssamling," tech. rep., Svenska Kraftnäts, 2005.

[17] D. S. AB, *Dymola Dynamic Modeling Laboratory User Manual Volume 1.* Dassault Systèmes AB, 2012.

[18] M. Larsson, "Objectstab—an educational tool for power system stability studies," *IEEE TRANSACTIONS ON POWER SYSTEMS*, vol. 19, pp. 56 – 63, February. 2004.

[19] M. Klein, G. Rogers, and P. Kundur, "A fundamental study of inter-area oscillations in power systems," *Power Systems, IEEE Transactions on*, vol. 6, no. 3, pp. 914–921, 1991.

[20] R. F. Bragason, "Damping in the icelandic power system- small signal stability analysis and solutions," Master's thesis, Lund University, Lund Sweden, 2005.

[21] J. Blöndal, T. Birgisson, H. Björnsson, K. Jónasson, and G. N. Peterson, "Vindhraðamælingar og sambreytni vinds," Tech. Rep. 14, Icelandic Meteorological Office, 2011.

[22] M. Beza, *Control of Energy Storage Equipped Shunt-connected Converter for Electric Power System Stability Enhancement.* PhD thesis, Chalmers University of Technology, Göteborg Sweden, 2012.

[23] D. Wilson, K. Hay, P. McNamm, J. Bialek, Z. Lubosny, N. Gustavsson, and R. Gudmannsson, "Identifying sources of damping issues in the icelandic power system," in *16th PSCC*, (Glasgow,Scotland), pp. 1–8, July 2008.